Research on inhibition of gas hydrate formation in pipelines and armatures using surface active substances

Dissertation

zur Erlangung des akademischen Grades eines
Doktors der Naturwissenschaften
– Dr. rer. nat. –

vorgelegt von

Florian Stephan Merkel

geboren in Trier

Fakultät Chemie
der
Universität Duisburg-Essen

2016

Die vorliegende Arbeit wurde im Zeitraum von April 2013 bis März 2016 im Arbeitskreis von Prof. Dr.-Ing. Schultz am Institut für Lacke und Oberflächenchemie (ILOC) der Hochschule Niederrhein sowie im Arbeitskreis von Prof. Dr. Schmuck am Institut für Supramolekulare Chemie der Universität Duisburg-Essen durchgeführt.

Tag der Disputation: 29.03.2017

Gutachter:	Prof. Dr. Carsten Schmuck
	Prof. Dr.-Ing. Heyko Jürgen Schultz
Vorsitzender:	Prof. Dr. Mathias Ulbricht

“And yet their wills did not yield, and they struggled on.”

— J.R.R. Tolkien, The Return of the King, 6, III.

Abstract

Clathrate hydrates of natural gases, also called gas hydrates, have gained in importance over the last decades, mainly because of their potential as energetic resource. But hydrates are not only beneficial as energetic resource or in gas storage, they also cause problems in oil and gas industry: during the transport of gases in pipelines, unwanted hydrates can form, which can reduce flow rates and even lead to blockage of the whole pipeline. This phenomenon is called *plugging* and its prevention, the so-called *inhibition*, occupies scientists and engineers since the 1930s. Today, plugging can be prevented physically and by means of chemicals, but only at high cost and with high environmental impact, since e. g. the chemicals have to be dosed in the pipeline permanently and separated again after transport.

In this work, steps have been taken to investigate new hydrophobic and hydrophilic inhibitor candidates under pipeline-like conditions.

Goal of the investigations was the development of a functional inhibitive coating that shall be applied in pipelines permanently and thus inhibit hydrate formation without the above-mentioned disadvantages.

Numerous substances were investigated regarding their inhibition potential in different reaction systems with methods developed in-house, inhibitor candidates were custom-tailored and investigated, hydrate formation kinetics were analyzed using different mathematical models.

Finally, the proof of concept for fixating an inhibitor candidate on a model substrate surface has been established successfully.

Kurzfassung

Clathrate natürlicher Gase, auch “Gashydrate” genannt, haben in den letzten Jahrzehnten stark an Bedeutung gewonnen, hauptsächlich wegen ihres Potentials als Energieressource. Aber Hydrate haben nicht nur Potential als Energielieferant oder für die Gasspeicherung, sie verursachen auch große Probleme in der Öl- und Gasindustrie: während des Transports von Gasen in Pipelines kann es zu einer unerwünschten Hydratbildung kommen, die die Durchflussraten verringern und sogar zur Blockade der gesamten Pipeline führen kann. Dieses Phänomen wird als *plugging* bezeichnet und die Verhinderung der Plugbildung, die sogenannte *Inhibierung*, beschäftigt Wissenschaftler und Ingenieure seit den 1930er Jahren. Heutzutage kann plugging sowohl mit physikalischen, als auch mit chemischen Methoden verhindert werden, aber nur unter hohen Kosten und starker Umweltbelastung, da bspw. inhibierende Chemikalien der Pipeline permanent zugesetzt und nach dem Transport wieder abgetrennt werden müssen.

Im Rahmen dieser Arbeit wurden daher Schritte zur Untersuchung neuer hydrophober und hydrophiler Inhibitor-“Kandidaten” unter pipeline-ähnlichen Bedingungen unternommen.

Ziel der Untersuchungen war die Entwicklung einer funktionellen inhibierenden Beschichtung, die permanent in einer Pipeline fixiert werden und so die Hydratbildung ohne die o. g. Nachteile verhindern soll.

Zahlreiche Substanzen wurden in verschiedenen Reaktorsystemen mit eigens entwickelten Methoden in Hinblick auf ihr Inhibierungspotential untersucht; Inhibitorkandidaten wurden hergestellt und untersucht, Betrachtungen der Hydratbildungskinetik wurden mittels verschiedener mathematischer Modelle durchgeführt.

Schlussendlich wurde der Beweis erbracht, dass es möglich ist, einen Inhibitorkandidaten erfolgreich auf einem Modellsubstrat zu fixieren.

Contents

Figures

Tables

1 Introduction

Clathrates of natural gases, also called “gas hydrates” or “burning ice”, have gained greatly in importance over the last few decades, mainly because of their potential as an energetic resource. They are solid, ice-like inclusion compounds, which form at high pressures and low temperatures and are made up of a hydrogen-bonded water network with guest compounds trapped in cages of water molecules. Estimates state that the amount of carbon stored inside of gas hydrates is higher than that of all other fossil energy carriers combined [1]. Gas hydrates also show great potential in gas storage and transport since 1 m^3 of gas hydrate can store up to 164 m^3 of gas under standard conditions [2].

But this promising energy carrier also causes problems in the industry since the 1930s, when they were first discovered in pipelines [3]. The phenomenon of gas hydrate formation in pipelines, which can lead to blocking of the whole pipeline, is referred to as “plugging”.

The prevention of plugging, the so-called “inhibition”, causes industry substantial operating expenditure every year and also uses a lot of chemicals, e. g. methanol, which may pose risks to the environment.

These problems gain in importance with oil and gas production moving to more extreme (deeper, colder) conditions over the last decades, since higher pressures (when getting to deeper water regions) greatly increase the probability of hydrate formation.

The current methods of inhibition are either very energy intensive, like heating of pipelines to prevent hydrate plugging, or they use chemicals that have to be dosed into pipelines continually and separated again after transport. Also, these chemicals are usually pollutants and hence detrimental to the environment.

Therefore, focus of this work was on the investigation of new, customized hydrate inhibitors, that can be applied as a permanent coating in the pipeline wall and thus eliminate the aforementioned disadvantages.

1.1 Motivation and objectives

The objective of this project is the qualitative and quantitative determination of the influence of hydrophobic and hydrophilic as well as ionic substances on gas hydrate formation in critical regions of pipelines and the development of functionalized surfaces to inhibit gas hydrate formation in technical processes.

On the one hand, the acting mechanisms of hydrate inhibition shall be characterized further. On the other hand, due to the gained knowledge, a better understanding of hydrate inhibition shall lead to the development of “better”, customized inhibitors as well as functional inhibitive coatings.

The most important thing to mention is that up to the start of this work, there was no hydrate inhibitive coating to be found in literature or patents (start of this project was in April 2013).
Hence, developing methods to test the mentioned substances and later on developed coatings in a repeatable and reliable way was integral part of this thesis.

Therefore, the first goal of this work was the development of different methods for measuring and evaluating substances regarding their influence on gas hydrate formation in the different reactor systems, especially their inhibitive potential.

After the development of the methods, screenings for inhibition suitability with several potential inhibitors shall be conducted. A focus of these screenings shall also be on evaluation of the influence of certain functional molecular groups on the formation of gas hydrates and based on those results promising candidates for coating applications shall be chosen.

The most promising inhibitor candidates shall be applied on a model substrate as a functional coating and the influence of this coating on gas hydrate formation shall be determined.

Also, the promising substances shall act as “role model” for the production of custom-tailored inhibitor candidates.

In parallel, a kinetic model to predict gas hydrate formation in a model system shall be developed using and comparing different methods of mathematic modeling.

With this, the goal of a functional inhibitive coating shall be realized. At any rate, the conducted experiments shall help to gain deeper insights into the formation of gas hydrates in pipelines and the factors influencing it.

2 Theoretical background

In this chapter, the theoretical background for understanding hydrate experiments as well as the performed calculations is described.

2.1 Gas hydrate structures / comparison between structures[1]

Figure 1 shows a pipeline that has been plugged by hydrate formation. In this chapter, the theoretical background on gas hydrates as well as the known hydrate structures is given.

Figure 1: Picture of a blocked pipeline. Reprinted with permission from [5]. Copyright (2010) John Wiley and Sons.

Gas hydrates belong to the substance group of “clathrates”. The word is derived from the Latin word “clatratus”, which means “barred”. Clathrates are inclusion compounds made up of “host” and “guest” molecules. They are called “true” clathrates, when there is no covalent bond between host and guest, but solely stabilization via e. g. van-der-Waals-forces. In the case of water clathrates, the host is water; therefore they are also called “hydrates”. [2, 6–8]

[1] Reproduced in part with permission from [1]. Copyright [2016] American Chemical Society. Permanent link to publication: http://pubs.acs.org/doi/full/10.1021/acs.energyfuels.6b01795

The formation of gas hydrates occurs by the scheme illustrated in equation [2.1] and is exothermic.

$$Gas + water \overrightarrow{\leftarrow} Gas\ hydrate \ ; \Delta H < 0 \quad [2.1]$$

Gas hydrates form different structures depending on the size and type of guest molecules as well as ambient / environmental conditions.
According to Jeffrey and McMullan [9], possible guest molecules are sorted into 4 groups:

1. hydrophobic substances
2. acid gases (water-soluble)
3. polar substances (water-soluble)
4. and ternary / quaternary alkylammonium salts (water-soluble). [2]

The two most common clathrate structures in pipelines are the structures s I and s II. A third common structure in nature, but less often occurring in pipelines, is structure *s H*. Therefore, the structures of these three most common natural hydrate structures are described in detail in Table 1. Figure 2 shows the visualization of the cages.

Table 1: Comparison of gas hydrate structures s I and s II [4, 10–13]

	Structure I		**Structure II**		**Structure H**		
Number of water molecules per unit cell	46		136		34		
Cage description / notation	5^{12}	$5^{12}6^{2}$	5^{12}	$5^{12}6^{4}$	5^{12}	$4^{3}5^{6}6^{3}$	$5^{12}6^{8}$
Labeling	U	V	U	W	U	X	Y
Number of cages per unit cell	2	6	16	8	3	2	1
Coordination number z_i	20	24	20	28	20	20	36
Composition (theoretical / ideal)	2 U * 6 V * 46 H_2O		16 U * 8 W *136 H_2O		3 U * 2 X * 1 Y * 34 H_2O		
Hydration number j	5.75		5.67		5.67		

The *hydration number j* in Table 1 describes the number of water molecules per guest and is a measuring factor for the saturation, hence also for the amount of stored gas inside the formed hydrates.

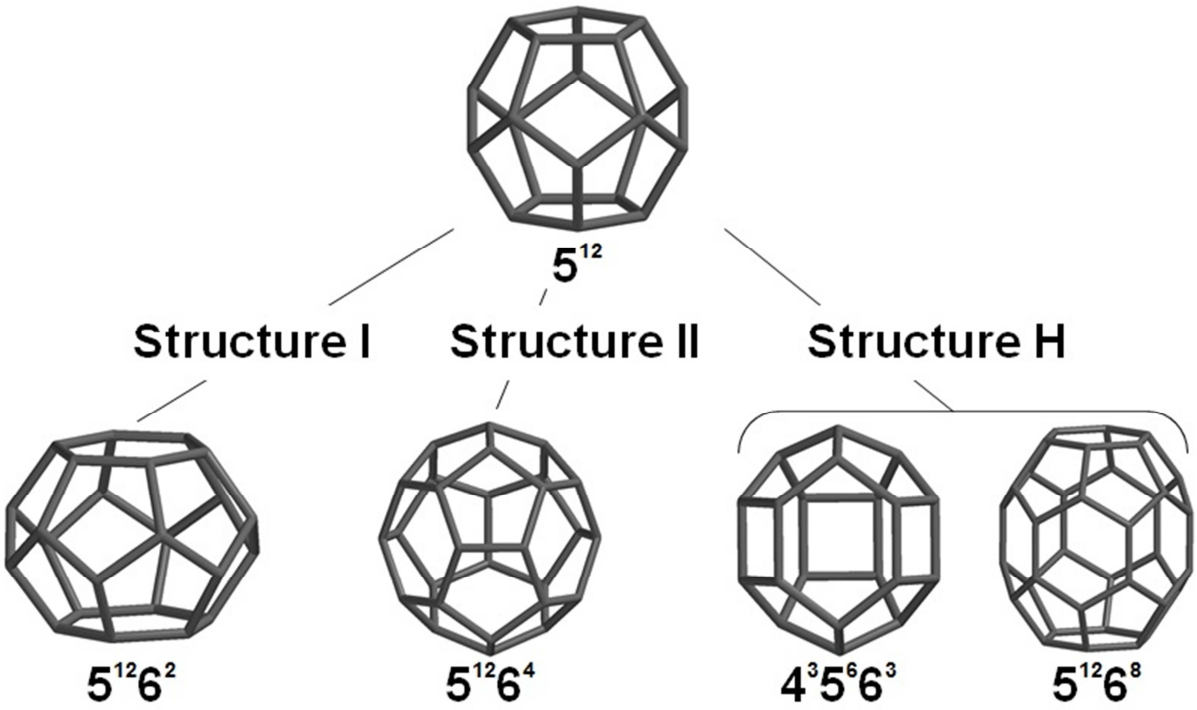

Figure 2: Cages of the three most common natural hydrate structures [10]

Natural gas is a mixture of hydrocarbon gases as well as carbon dioxide, hydrogen sulfide, nitrogen and other components. The composition varies depending on the origin, typical compositions are found in Table 2; since the values were combined from different sources, maximum amounts add up to more than 100 %. Different guest molecules have strong influence on hydrate formation, guest molecule size is the most important factor in determining which structure is formed [2]. Therefore, the type of hydrate structure which the substances usually form is also indicated (when the substance is the only type of guest molecule).

Table 2: Typical composition of natural gas [14–16]

Component	Typical amount [%]	Hydrate structure [2]
Methane	70 – 90	s I
Ethane	1.5 - 7	s I
Propane	0.1 – 1.5	s II
Butane	0.02 – 0.6	s II
Pentane	0 – 0.08	s H (only in mixture with other guests) [17]
Nitrogen	0 – 5.5	s II
Carbon dioxide	0.1 – 1	s I
Oxygen	0 - 0.1	s II
Hydrogen	0 – 0.02	s II (at very high pressure)
Hydrogen sulfide	0 - 5	s I
Rare gases (He, Ne, Ar, Xe)	traces	Xe s I; others s II

Since pentane as the only former of *s H* is only present in very small amounts, structure *s H* is not regarded further in the course of this work.
Because methane is the main component of natural gas (and also of biogas, which will gain in importance in the near future), the main high-pressure research in the course of this work will be done on “pure” methane hydrate, which forms structure *s I*.
However, since mixtures of methane with e. g. propane tend to form structure *s II*, even if only amounts of 1 % propane are present [2, 18], the influence of other possible guests on the formed hydrate structures has to be accounted for, since often, there are other components present in pipelines.
For this, tetrahydrofuran as typical *s II* hydrate former was introduced in some of the experimental series to investigate the influence of possible inhibitors on *s II* hydrate formation.
With this, the most frequent hydrate structures that occur in pipelines have been considered.

2.1.1 Comparison to ice

The structure of gas hydrates is similar to the structure of hexagonal ice Ih. The main difference between ice and hydrates is that ice forms as a pure component, while hydrates are only stable when there is a guest molecule present. This is also caused by the fact, that hydrate cavities are slightly expanded compared to ice and therefore need the guest molecules to stabilize their structure. According to Rodger [19, 20], the repulsion caused by the presence of guest molecules in a cavity as well as in surrounding cavities (repulsion between cavity “walls” and guest molecules) is more important to maintain this cavity expansion than the attraction forces between the water molecules.
The properties of both “substances” (ice and gas hydrates) strongly depend on the formation of hydrogen bonds, since they both form hydrogen-bonded networks of water molecules. Hydrogen bonds in hydrate structures *s I* and *s II* average only 1 % longer than those in ice and the O-O-O angles are also only slightly different.
Hydrates have a higher mechanical stability than ice, meaning that ice will deform significantly faster than e.g. methane hydrate when the same stress is applied. Since ice is known to deform by a coordinated motion of crystalline effects (diffusion-controlled), the higher stability of hydrates is presumably caused by the rate of diffusion of water in hydrates, which is two orders of magnitude slower than in ice (when pure methane hydrate and ice Ih are compared).
Also, the thermal conductivity of hydrates is lower than that of ice but the thermal expansion coefficients are higher. This means that heat is transported slower through hydrates than through ice, but hydrates expand more with temperature than ice does.

All in all it can be said that the differences in ice and hydrate structures are small and seem mostly dependent on the hydrate guest molecules and the structural changes these guests cause. [2, 21–25]

2.1.2 Comparison to other pipeline-blocking phenomena

Pipeline flow is not only reduced by formation of gas hydrates, but also by formation of scale and wax. These two types of pipeline contamination will be discussed shortly to show parallels and to describe important facts that have to be considered for a safe pipeline operation.

2.1.2.1 Scale

Formation of scale is the deposition of inorganic salts with low water solubility from aqueous solutions [7, 26, 27]. The most common scale types in the oil industry are calcium carbonate, sulfate salts, sulfide scales and sodium chloride scales. The most important fact to remember is that some common thermodynamic hydrate inhibitors (see chapter 2.6.2) can promote the formation of scales (e.g. methanol is quite detrimental in this matter [28, 29]). This is another reason for finding new ways of inhibition. Also, it is thinkable to include scale inhibitors in a coating or design a coating that not only inhibits hydrate formation, but acts as a scale inhibitor as well. [7]

2.1.2.2 Wax

Waxes are solids that usually consist of long-chained alkanes (> C18). They do, like gas hydrates (→ chapter 2.2) form by crystallization-like processes. Usually they form, when hot oil from a well is cooled down during transportation. The deposition of waxes is considered to occur by two different mechanisms:

1. If the pipe wall is colder than the *wax appearance temperature* (temperature of first wax precipitation in the system, also called *cloud point*), wax forms at the pipeline wall.
2. Already formed wax close to the pipe wall will move to the pipe wall in regions of lower flow velocity and deposit.

Both mechanisms result in reduction of pipeline diameter and in the long term in pipeline blockage. [7]

The important thing to mention is that since wax deposition starts at the pipe wall it is also thinkable to use a coating to prevent wax deposition from happening. Since waxes also form by crystallization it is even thinkable to create a coating that can inhibit both the

crystallization of waxes and gas hydrates. To our current knowledge, this approach is new and not yet pursued.

2.2 Crystallization phenomena

According to Sloan [2], gas hydrate formation processes are similar to crystallization phenomena, meaning they are divided in a so-called “nucleation phase” of clathrate crystals followed by a (macroscopic) “growth phase”. Also, phenomena like driving forces and equilibria play a critical role in gas hydrate formation. [2, 30, 31]

Figure 3 shows equilibrium lines for crystallization (on the left) and hydrate formation (on the right) with analogies. Both processes do have an equilibrium line (A-B), which is depending on concentration and temperature for “normal” crystallization and, respectively, depending on pressure and temperature for gas hydrate formation. When crossing the equilibrium line (entering the crystallization resp. hydrate formation zone; going from point P in direction of point S in Figure 3 a and b), a metastable region is entered (e. g. in point Q). Here, crystals or hydrates can form from a thermodynamic point of view, but the driving force is low, so that crystals / hydrates “may or may not form” [2]. When a crystal nucleus would be added to the solution (inoculation), crystallization / hydrate formation would take place readily.

When crossing the *thermodynamic spinodal* (line C-D), either by cooling down or by increasing concentration resp. pressure; a high super-saturation is reached and crystal resp. hydrate formation will occur readily. [32]

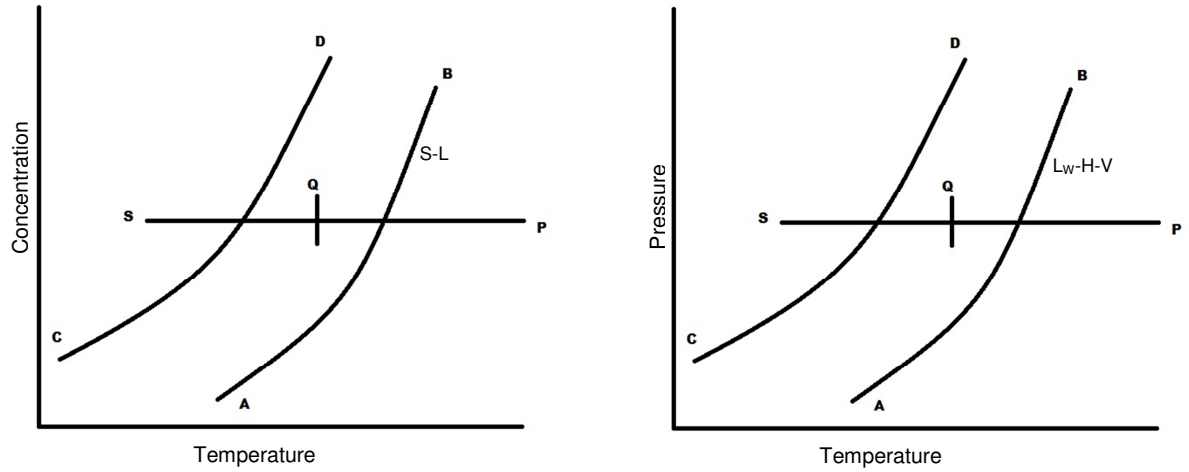

Figure 3: Comparison between hydrate formation on the right (b), and „conventional crystallization“ on the left (a) [2]. A-B: equilibrium line (*S-L: solid-liquid; L_w-H-V: Liquid water-hydrate-vapor*); C-D: thermodynamic spinodal; P: decomposition zone; Q: metastable region; S: crystallization / hydrate formation zone.

2.3 Gas hydrate formation

Gas hydrates can form in a system, when the following conditions are met:

- Occurrence of water (as host) in the system
- Presence of possible guest molecules
- “Suitable” pressure and temperature conditions, meaning high pressures and low temperatures with co-dependence of temperature and pressure (higher pressure in general allows for hydrate formation at higher temperatures).

The actual formation mechanism is not fully explored yet, but similarities to crystallization processes are deemed highly probable (see also chapter 2.2). Hence, all existing theories of formation divide the process in two steps: a “nucleation phase” and a “(macroscopic) growth phase” of hydrates [2, 6, 33–35].

There are currently 4 different theories for gas hydrate formation, which differ mostly in how the nucleation phase is described:

- the *labile cluster theory* [36–38];
- the *nucleation at the interface hypothesis* [39];
- the *local structuring nucleation hypothesis* [40, 41];
- and the *blob theory* [42].

All theories have in common that some kind of reversible step is included in the nucleation phase, which describes the nucleation and dissociation of water molecules to “bigger” particles. When some critical size is reached, the macroscopic growth of hydrates begins. Differences of the theories are described below.

The *labile cluster theory* [36] (see also Figure 4) is divided in four steps. At first, pressure and temperature are in the hydrate formation region, but there are no guest molecules dissolved in the water yet. In the second step, gas is added to the water which results in the immediate formation of the eponymous *labile clusters* that are comprised of (partly) formed hydrate cages with guest molecules. These labile clusters now perform the above-mentioned equilibrium step. They agglomerate by sharing faces and dissociate again, until a *critical cluster size* is reached and macroscopic growth begins in step 4. [2, 36]

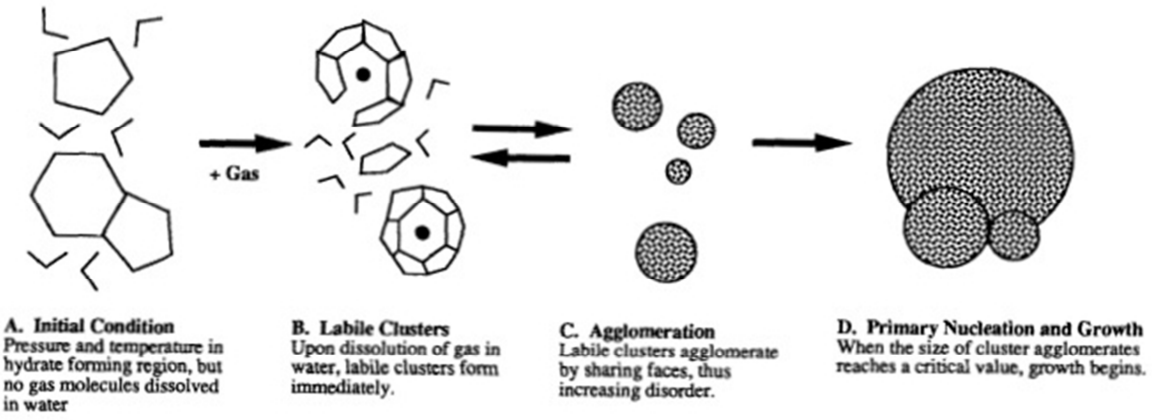

Figure 4: *Labile cluster theory*. Reprinted with permission from [36]. Copyright (1994) John Wiley and Sons.

The *nucleation at the interface hypothesis* postulates that nucleation starts on the vapor side of the gas-liquid interface and hydrate nuclei grow into the vapor phase. This is the biggest difference in comparison to the other theories; otherwise the theory shows great resemblance to the *labile cluster theory* and is again comprised of 4 steps:

- guest molecules are transported to the interface
- guest molecules adsorb on the aqueous surface
- guest molecules migrate to suitable locations for adsorption through surface diffusion; at this location, first partial, then complete cages are formed around the guest molecules
- labile clusters join and grow at the vapor side. [2]

The *local structuring nucleation hypothesis* (see also Figure 5) was first derived by Radhakrishnan and Trout (2002) by free energy calculations for CO_2 hydrate formation. The model is based on local ordering instead of cluster formation for hydrate nucleation. A group of guest molecules takes on a configuration similar to that in the hydrate phase (caused by thermal fluctuations). This causes a perturbance in the structure of nearby water molecules. This reordering proceeds in the area where guest molecules are present, again until a critical size is reached. Then, the order parameters take on values similar to those in the hydrate phase and a critical nucleus is formed. Moon et al. (2003) derived a similar model for methane hydrate formation based on MD simulations. [2]

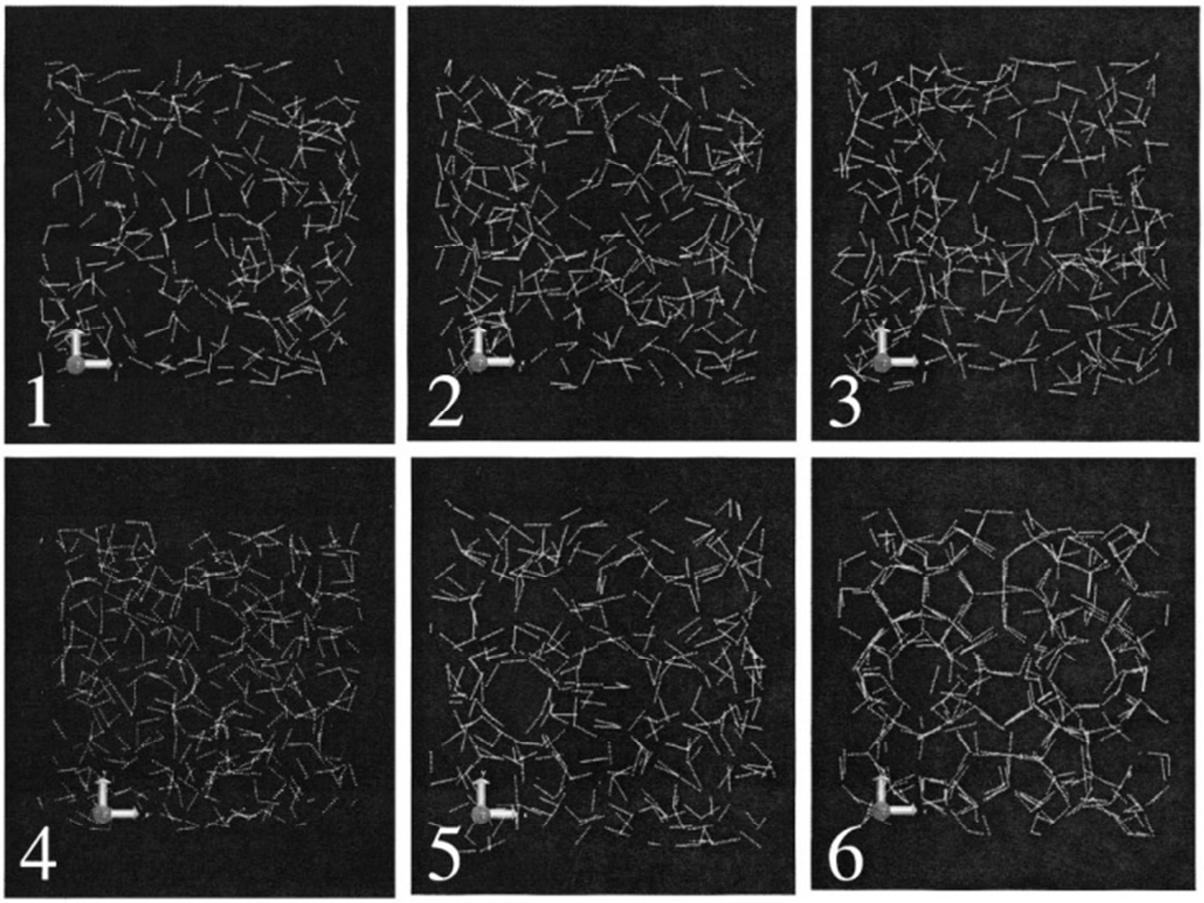

Figure 5: *Local structuring hypothesis*. Reprinted with permission from [40]. Copyright (2002) AIP Publishing LLC. Pictures show the slow transition from a liquid-like (1) to a clathrate-like (6) cluster of molecules caused by thermal fluctuations of guest molecules and resulting reordering processes of the perturbed water molecules.

The *blob theory* (Figure 6) was also found via MD simulation by Jacobson et al. [42–47]. It combines elements of the *local structuring hypothesis* and the *labile cluster theory*. Guest molecules are dissolved in water and concentrate in so-called “blobs”. These blobs are amorphous structures consisting of guest and water molecules, partially formed ring-like structures of hydrogen bonds etc.. They form and dissociate again in an equilibrium process. After the blob reaches a critical size, amorphous clathrates are formed, which then reorganize in a final step to crystalline clathrates. [42]

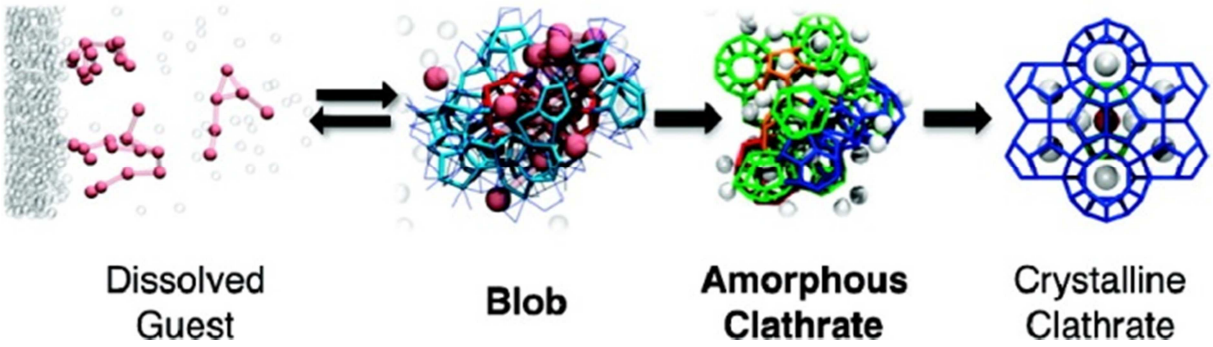

Figure 6: *Blob theory*. Reprinted with permission from [42]. Copyright (2010) American Chemical Society. Guest molecules are dissolved in water and concentrate in *blobs*. After reaching a critical size, amorphous clathrates are formed and reorganize to crystalline clathrate.

All theories include the formation of a “critical nucleus” or similar arrangement of molecules which then leads to macroscopic hydrate formation. It is mandatory to remember that the actual hydrate formation mechanism is not fully explored yet and it is thinkable that different mechanisms can act at different formation conditions. The results of this work will also be discussed in regards to the possible formation mechanism in later chapters.

2.4 Steady-state and transient hydrate formation

In principle, there are two different “ways” for hydrates to form: at steady-state and transient conditions. Steady-state in this case means that the driving force for hydrate formation (influenced mainly by pressure and temperature) is kept constant. Transient conditions in the course of this work mean that temperature and volume are kept constant, with pressure decreasing in the course of hydrate formation.
Although the decreasing of pressure results in a changing driving force of hydrate formation, it can be interesting to investigate hydrate formation at transient conditions, since almost all pipeline transport processes in the field are subject to pressure fluctuations and hence the transferability of results from lab to field is better possible.

In both steady-state and transient experiments, the condition of the water used for hydrate formation is critical for the results. This is caused by the so-called *memory effect* of water. Water that has already formed clathrates can “remember” this clathrate formation and hence forms “new” clathrates much faster compared to “fresh” water, even if it is heated to moderate temperatures after the first hydrate formation. Currently, there are two possible explanations for the *memory effect*:

1. Hydrate structure remains in solution after hydrate dissociation in form of residual structures (partial cages, short-range ordered structures,…) or persistent hydrate crystallites (long-range ordered structures);
2. Dissolved gas remains in solution in higher-than-usual concentrations after hydrate decomposition and thus leads to faster hydrate formation. [2]

To avoid this phenomenon, in the course of this work fresh water was used in every experiment, since the performance of a possible inhibitive coating should be evaluated at pipeline-resembling conditions without memory effect.
In this work, the focus of the investigations was not on determining hydrate phase equilibria, but on determining the time that hydrates took to form, the so-called *induction time* (see also chapter 2.5). Therefore experiments were aborted after hydrates had formed instead of waiting for phase equilibrium to be reached.

2.5 Induction time(s)

In all theories, the so-called *induction time* plays a critical role.

Sloan defines induction time as “the time elapsed until the appearance of a detectable volume of hydrate phase or, equivalently, until the consumption of a detectable number of moles of hydrate former gas” [2]. Following this, the induction time not only describes the nucleation phase but also hydrate growth up to the point where the hydrates can be detected (which of course depends on accuracy of measurements as well as method design). It seems obvious that this type of definition does not yield any exact values but only is a first approximation to somehow quantify hydrate formation times. The measurements are complex and not easy to handle so that quantification of the “real” time when hydrate formation starts on a microscopic level is nearly impossible to realize in a technical process.

Therefore, in this work induction time is defined as the point in the course of an experiment, where a temperature increase with parallel decrease in pressure (even if only small) occurs. In addition, the so-called *plug formation time* was newly established for improved differentiability. Further details are found in chapter 11.1.3.

2.6 Inhibition

In this chapter, an overview on the state-of-the-art regarding the prevention of hydrate formation in pipelines, the so-called *inhibition*, is given.

2.6.1 General aspects

In principle, there are two different methods of hydrate inhibition: physical and chemical inhibition. Figure 7 shows the concepts by means of the equilibrium line of hydrate formation. Physical methods of inhibition contain the removal of water from the pipeline before transportation, the reduction of pipeline pressure (point “A” to point “C” in Figure 7) or heating of the pipeline (point “A” to point “B”).

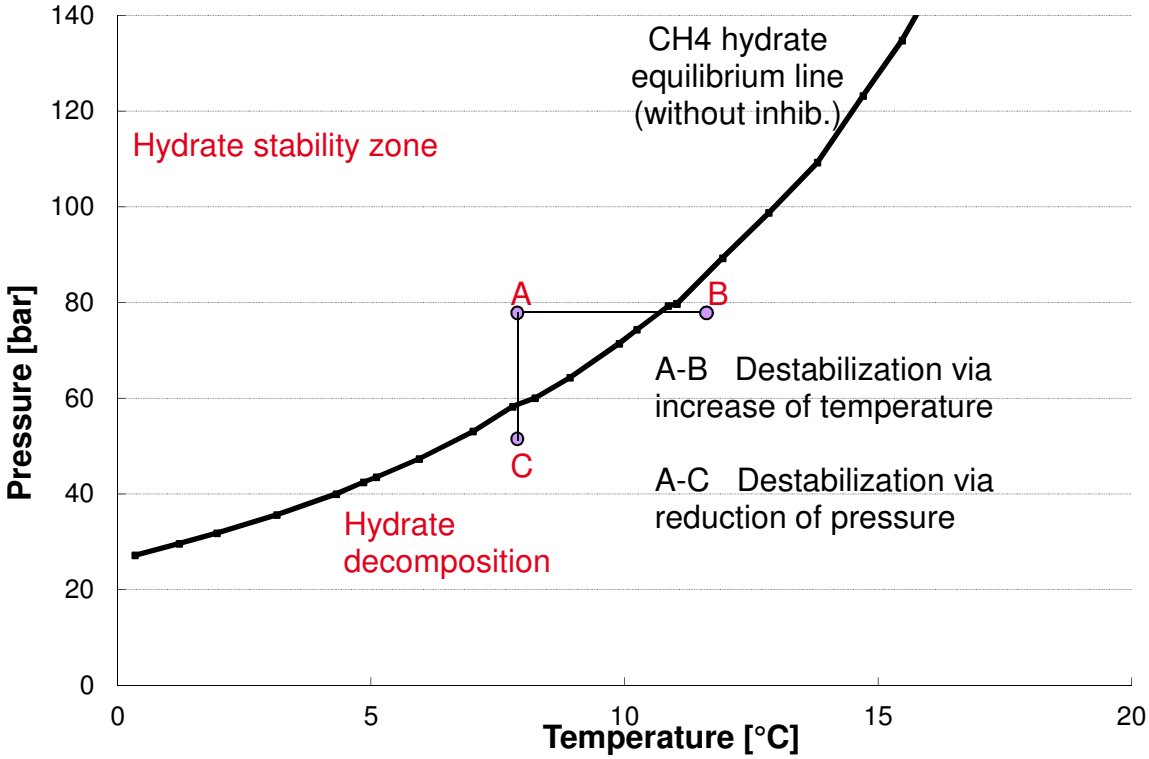

Figure 7: Overview of conventional methods of hydrate inhibition (experimental values for equilibrium line taken from [48])

All those methods bring about high expenditure or are not advisable from a technical point of view. The reduction of pipeline pressure would e. g. result in a lower volume flow of the pipeline and hence in lower transported amounts per time, while removing the water could lead to an increased scale formation [7]. Another method of inhibition uses chemicals. There are different types of inhibiting chemicals, which are described further in the following chapters. [35]

2.6.2 THI

The first group of inhibiting chemicals are the so-called *thermodynamic hydrate inhibitors* (*THI*). They operate by shifting the equilibrium of hydrate formation to higher pressures or lower temperatures (see also Figure 8). They can be used to prevent hydrate formation as well as to "melt" existing hydrates. Commonly used THI are e. g. Methanol, ethylene glycol or electrolytic solvents. They inhibit in a reliable and effective way. However, a permanent surveillance of the pipeline is required, since the THI can even act as promoters (→chapter 2.7) and accelerate hydrate formation, when their concentration is too low ("under-inhibition"). Their biggest disadvantage is that they have to be dosed in the pipeline at very high concentrations ("up to two barrels of THI per barrel of water" [7]), which causes high operating costs and also poses a high risk to the environment. [2, 6, 10, 35, 49–52]
Also, as already mentioned in chapter 2.1.2, they can increase the probability of scale precipitation [7, 28, 29]. If methanol enters the oil phase in a multiphase pipeline, it can also act as a wax precipitant by lowering the wax appearance temperature [7].

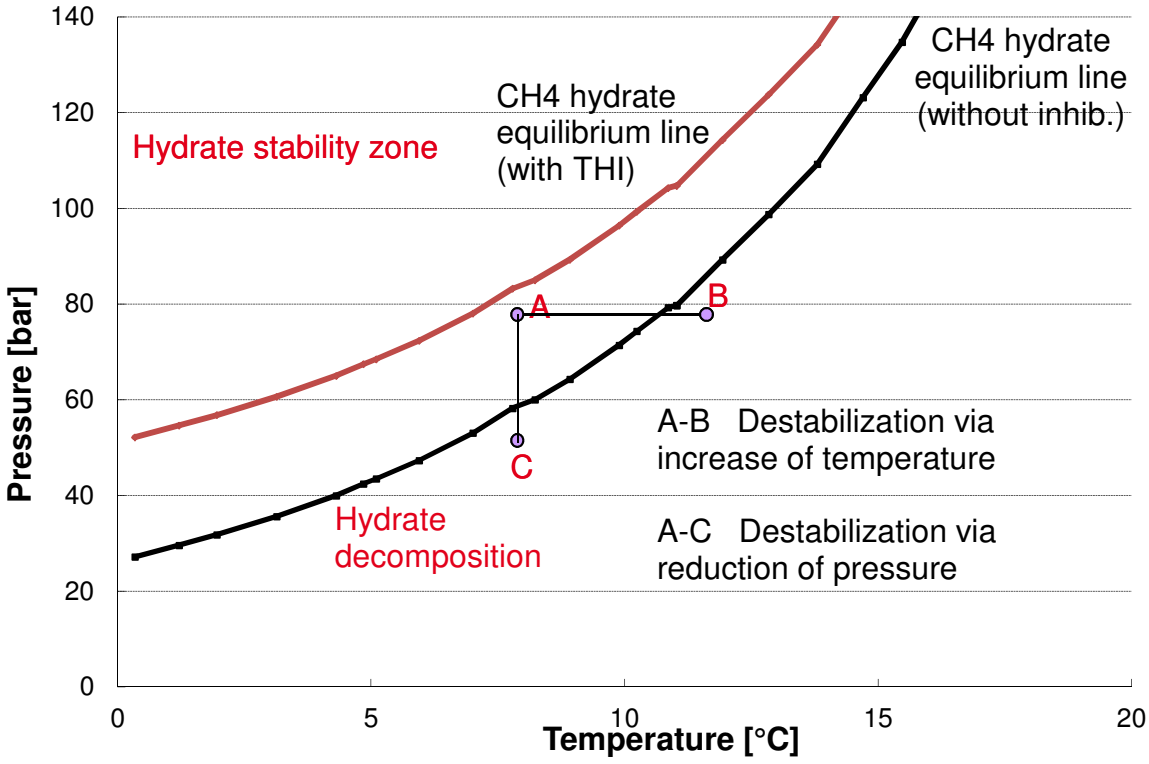

Figure 8: Equilibrium line shifted by thermodynamic hydrate inhibitor (experimental values for underlying equilibrium line taken from [48])

Therefore, the so-called "low-dosage hydrate inhibitors" gain more and more in importance over the last years (→chapter 2.6.3).

2.6.3 LDHI

Low dosage hydrate inhibitors (LDHI) are chemicals which are used in very low concentrations (usually < 1 % wt. active components [7, 8]). They are further divided in two classes: the *kinetic hydrate inhibitors (KHI)* and the *anti-agglomerants* (AA). [6–8, 53–57].

2.6.3.1 KHI

Kinetic hydrate inhibitors are usually water-soluble polymers, amphoteric surfactants or surface-active substances, which are often combined with smaller organic molecules that are added as performance enhancers (synergists) [7, 35].
Typical KHI are e. g. polyvinylpyrrolidone, polyacrylamide or polyvinylcaprolactam, which all have “head” groups and long “tail” molecular chains (see Figure 9). Synergists are e. g. 2-butoxyethanol [58, 59] or 2-isobutoxyethanol [60] as well as certain substituted amines [61] for VCap (vinylcaprolactam) based polymer KHIs (see Figure 10) [7].

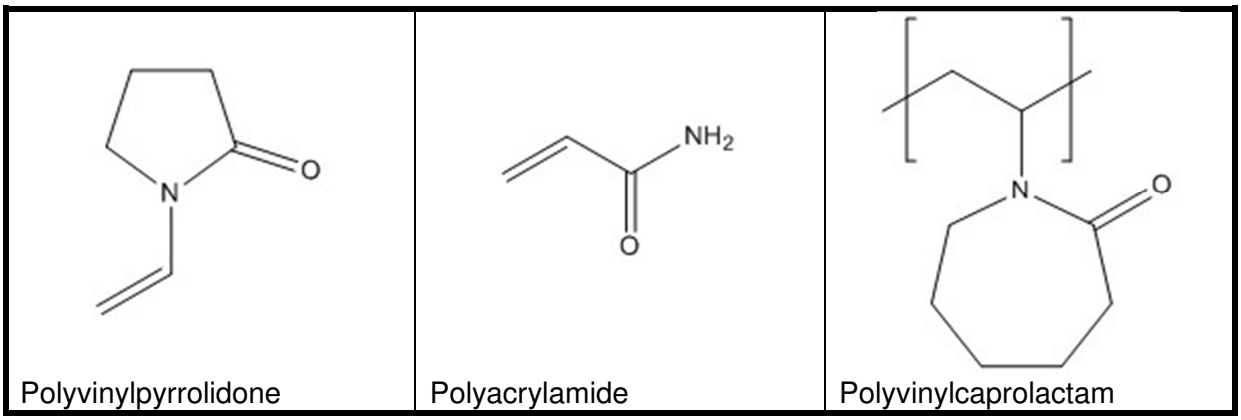

Figure 9: Typical classes of KHIs

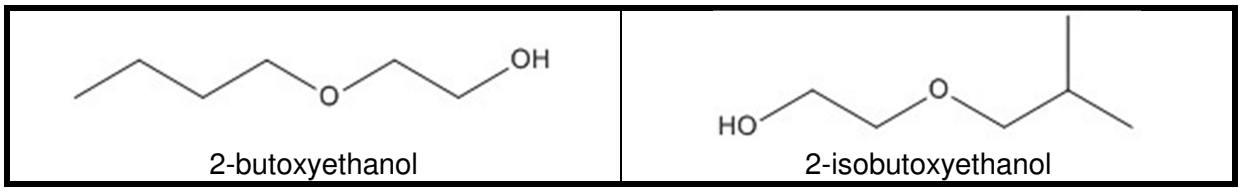

Figure 10: Some enhancers for VCap based polymer KHIs

KHIs do not influence the formation equilibrium of hydrates, but instead they interfere with the kinetics of the process. They act as “anti-nucleates” and slow down hydrate formation. The mechanism by which they work is not yet fully explored; currently there are two major theories, which may also be operating at different conditions or even both at the same time.

One mode of action could be that the KHIs head group fits into the hydrate cages and the tail group causes a steric hindrance so that other hydrate cages cannot “dock” [7, 62–68].

The other one postulates that the KHIs perturb the water structure by hydrophobic interaction to such a degree that gas hydrate particles cannot reach the critical nuclei size and hence that the macroscopic growth phase does not start [7, 8, 69].

KHI can usually only be used at moderate subcoolings, since the KHI performance strongly depends on the driving force for hydrate nucleation; higher subcooling equals higher driving force and hence shortens the time by which KHIs delay hydrate formation. However, they can be used at high pressures in combination with THI that ensure there is only moderate subcooling. [6–8, 70]

2.6.3.2 AA

As the name suggests, *Anti-Agglomerants (AA)* do not prevent hydrate nucleation or formation, but rather they prevent formed hydrates from agglomerating to hydrate plugs.
AA are usually surfactants and are divided into gas-well AAs and pipeline AAs, of which only the pipeline AAs are further described here. [7]
There are two mechanisms by which the AA work in a pipeline. Both usually require a liquid hydrocarbon (or oil) phase to work. One is the addition of a surfactant AA that forms a water-in-oil emulsion. The water droplets then form hydrates and small “hydrate beads” are transported through the pipeline. Examples for emulsion pipeline AAs are e. g. polymeric surfactants based on polyalkylene glycol derivatives of polyalkenyl succinic anhydrides, mixtures of sorbitan monooleate (Span 80) with sodium di-2-ethylhexylsulfosuccinate ([71], see also Figure 11) or carboxylic acid hydroxycarbylamide. [7]

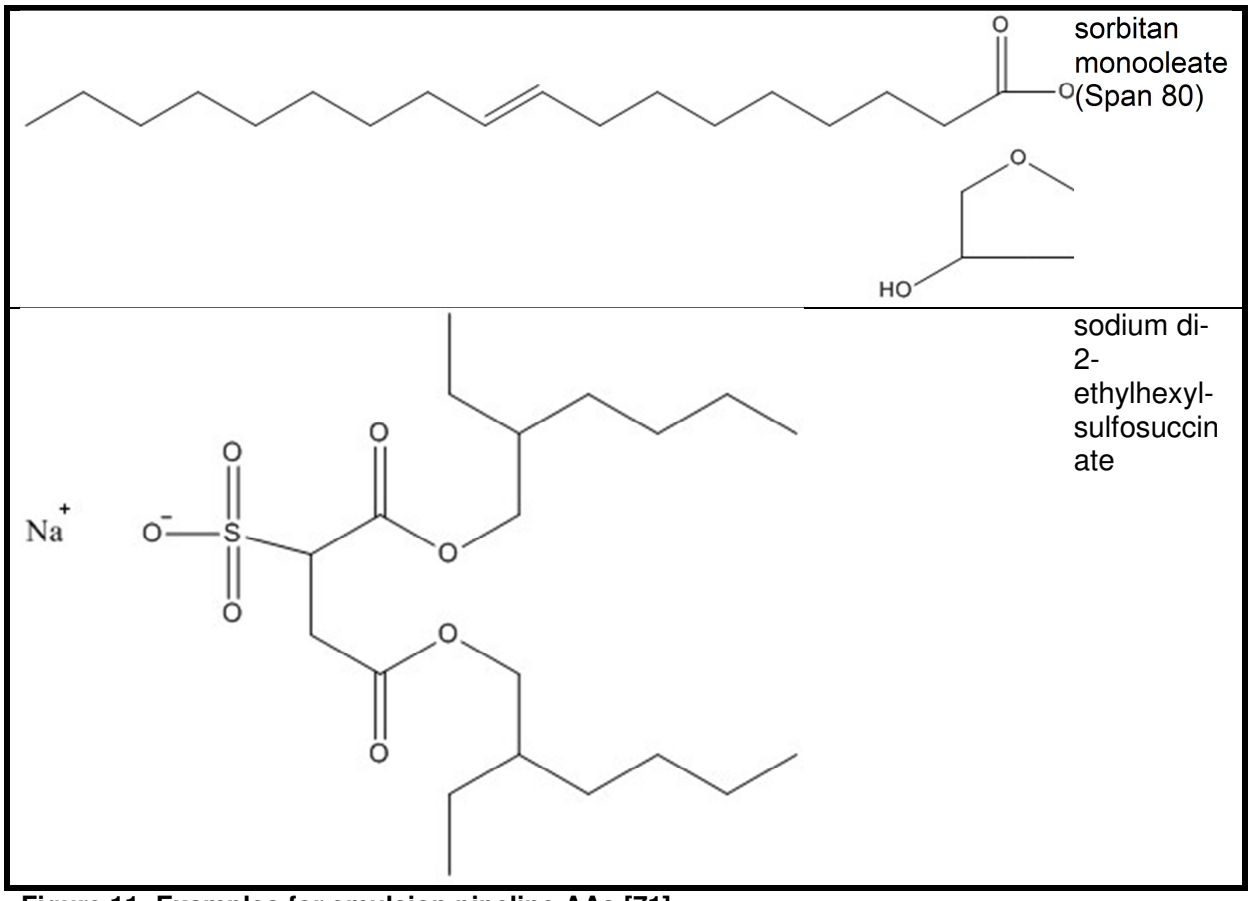

Figure 11: Examples for emulsion pipeline AAs [71]

In the other mechanism, the surfactant molecule has a “hydrate-philic” head and a hydrophobic tail (oil-loving). When enough surfactants bind to a hydrate crystal, it becomes hydrophobic and is then easily dispersed in the liquid hydrocarbon phase. They do not have to form emulsions to work. The most common substance class used in the field are quaternary ammonium and phosphonium surfactants with head groups that contain two or more alkyl groups, e. g. n-butyl groups (see also Figure 12). [7, 8, 72]

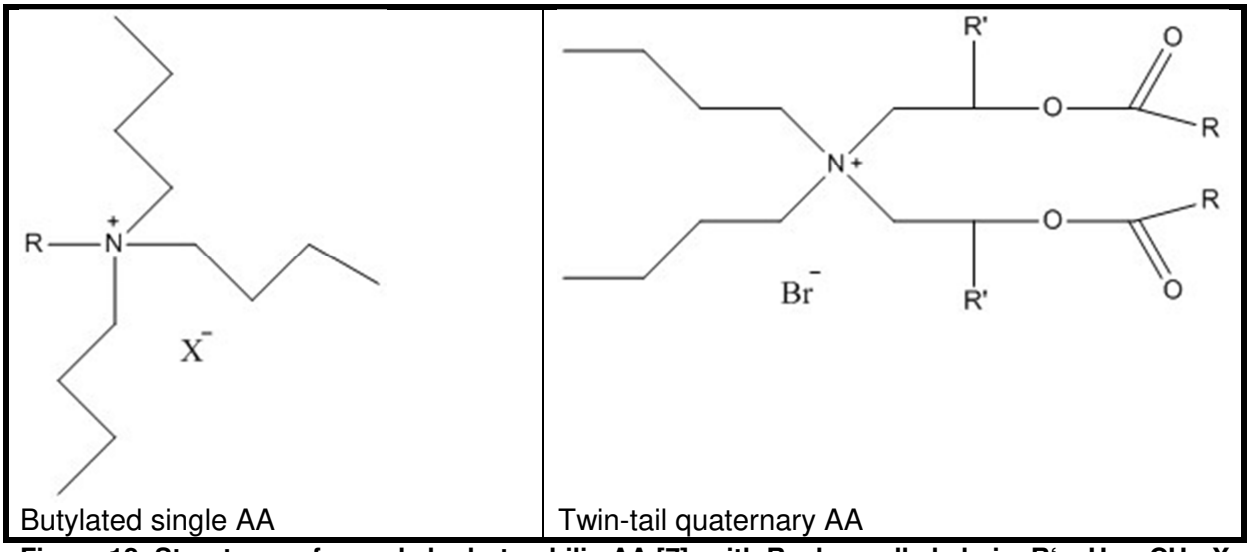

Butylated single AA | Twin-tail quaternary AA

Figure 12: Structures of sample hydrate-philic AA [7]; with R = long alkyl chain, R‘ = H or CH_3, X = counterion.

The effect of AA is strongly influenced by the type of hydrocarbon in the liquid phase, the salinity and the water content in the pipeline. [35]

2.7 Promotion

Next to the above-mentioned inhibitors, there are also chemical substances that facilitate and / or accelerate the formation of gas hydrates. These substances are called *promoters*. The mechanism by which they work is not fully explored yet. For one common promoter, tetrahydrofuran (THF) it is known that THF occupies cages in a formed hydrate and leads to the formation of *s II* hydrates. Since the rate of crystallization strongly depends on the crystals that are formed (see also chapter 2.2), this could already be a cause for the promoting effect. [2]
But there are also other promoters which could act in different ways.
It could also be thinkable that promoters act by influencing the solubility of guest molecules in water (it is e. g. known that some surfactants influence hydrate formation [73], which could be based on solubility effects) or somehow facilitate the nucleation by forming intermediate structures that resemble hydrate cages and therefore lead to a faster nucleation.

2.8 Functional coatings

Functional coatings are used in a variety of processes and for all kinds of purposes, the listing of which would by far exceed the scope of this work.

The most important thing to mention is that up to the start of this work, there was no hydrate inhibitive coating to be found in literature or patents (start of this project was in April 2013).

The only functional coatings remotely related were the usage of “hydrate-phobic” surfaces [74–76], which do not prevent hydrates from forming but instead just facilitate transportation by being “hydrate-repellent” and thus preventing hydrates from sticking to the pipe wall and plugging the pipeline.

The other functional coatings with remote similarity were “anti-ice” coatings [77–79], which shall be used e. g. on rotor blades of wind turbines.

Therefore, with this work, an innovative new idea is being investigated. The future potential of an inhibitive coating that would prevent hydrate formation (as well as further pipeline-blocking phenomena, like scale and wax) is enormous regarding the usage in the field. OPEX of pipeline transport, especially in hydrate-endangered areas, could be significantly reduced. The benefits for the environment, by preventing leakage of conventional inhibitors like methanol, would also be strong.

2.9 Methods of statistical evaluation

In the course of this thesis, statistical analyses of experimental data have been conducted, mainly regarding investigated induction times in all experimental series. Goal of these analyses was testing for normal distribution and outliers. For this, two different statistical tests were used, which shall be explained below.

2.9.1 Shapiro-Wilk test

The Shapiro-Wilk test is a test for normal distribution that was first introduced by S. S. Shapiro and M. B. Wilk in 1965 [80].
The test uses the null hypothesis principle (null hypothesis: data are normally distributed) and is built as follows:

$$W = \frac{(\sum_{i=1}^{n} a_i * x_i)^2}{\sum_{i=1}^{n}(x_i - \bar{x})^2} \quad [2.2]$$

with

$$\bar{x} = \frac{1}{n} * \sum_{i=1}^{n} x_i \quad [2.3]$$

and a_i being a weighting factor that is dependent on the number of samples.

In this work, a modified algorithm by P. Royston came to use [81]. This modified algorithm allows for sample sizes ranging from 3 to 2000

2.9.2 Dixon-Q test

The Dixon-Q test is a test for outliers. It can only be applied to normally distributed data, which is the reason that it was used in combination with the Shapiro-Wilk test in this work.
It was introduced by Dean and Dixon in 1951 [82] and is built as follows:

$$Q = \frac{gap}{range} \quad [2.4]$$

with *gap* being the distance of a doubtful value to its nearest neighbor. The doubtful observation can be the highest or the lowest value that is determined after the data have been sorted in ascending order.
Range is the difference between the highest and the lowest observed value. If the value for *Q* exceeds tabulated data, the doubtful value may be rejected as an outlier with a certain confidence (that was specified before).

3 Experiments and setup

In this chapter, the chemicals and reaction systems used in the course of this thesis are described. Since a major part of this work was development and optimization of equipment and methods, alterations occurred during the processes. Hence, reasons for alteration in the methods as well as changes in equipment are further discussed in chapter 11.

3.1 Chemicals

Table 3 shows all used substances including their purity. If the substance is only mentioned by its trivial name, the column “Comment” gives information on the chemical structure. The molecular structures are shown in Table 4 and Table 5; material safety datasheets are included in the appendices.

Table 3: Used substances

Substance	Manufacturer	Purity	Comment
Methane	Messer Industriegase GmbH	≥ 99.5 %	
Deionized water	In-Lab purification system	Conductivity δ 17 µS / cm	
Milli-Q-water	Millipore Purification system	Conductivity δ 1-3 µS / cm	
Tetrahydrofuran (THF)	Carl Roth; AppliChem; VWR	≥ 99,5 %	
Tylose H20P2 (H20)	SE Tylose	-	Hydroxyethyl cellulose
Glycerol (Gly)	Carl Roth	≥ 99,5 %	
Tylose H300P2 (H300)	SE Tylose		Hydroxyethyl cellulose
Polyvinyl acetate (PVAc)	Carl Roth	purissimum	
Polyvinylpyrrolidone (PVP) K90	Carl Roth	purissimum	
Polyethylene glycol (PEG) 600	Roth (Rotipuran ®)	-	
Potassium thiocyanate (KSCN)	Bernd Kraft	purissimum	
Diboron trioxide (B_2O_3)	Alfa Aesar	≥ 99 %	
Iron(II) sulfate heptahydrate	Roth	≥ 99.5 %	
Ethylene glycol (EG)	Carl Roth	≥ 99 %	
D(+)-Glucose (DGluc)	AppliChem	≥ 99 %	
myo-Inositol (Ino)	Alfa Aesar	≥ 98 %	
Polyvinyl alcohol 72,000 (PVA)	Alfa Aesar	≥ 95 %	

Table 4: Molecular structures of used substances (a)

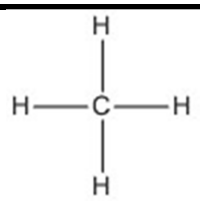 Methane	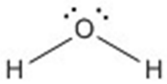 Water
 Tetrahydrofuran (THF)	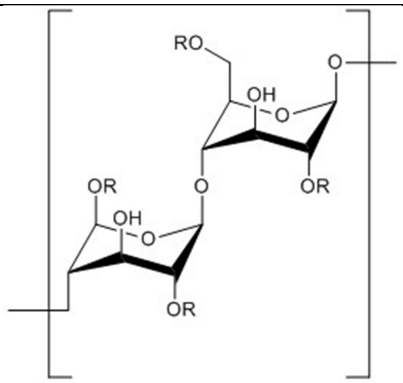 Tylose / Hydroxyethyl cellulose R = H or CH_2CH_2OH
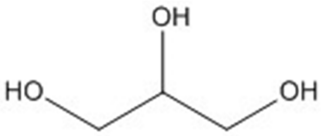 Glycerol	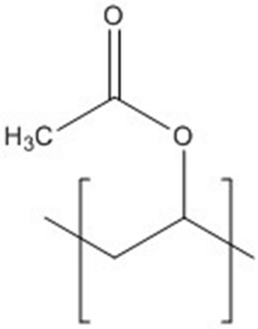 Polyvinyl acetate
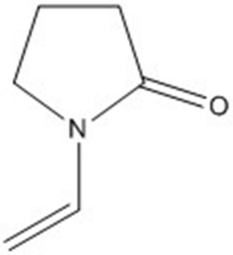 Polyvinylpyrrolidone	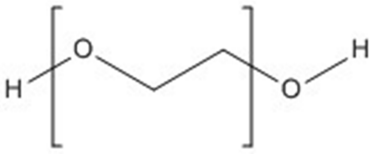 Polyethylene glycol
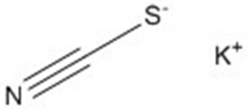 Potassium thiocyanate	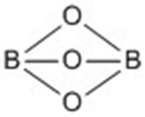 Diboron trioxide
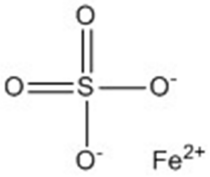 Iron(II) sulfate	

Table 5: Molecular structures of used substances (b)

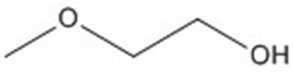 Ethylene glycol	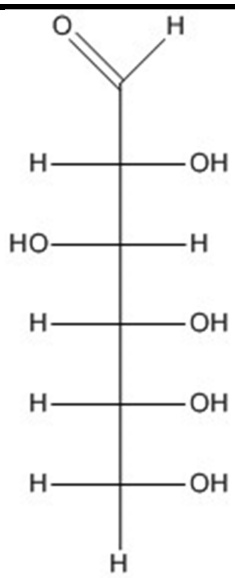 D(+)-Glucose
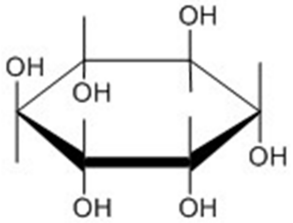 myo-Inositol	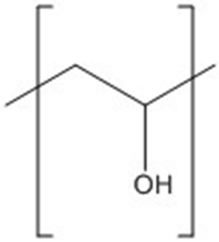 Polyvinyl alcohol

3.2 Reaction systems

This chapter will describe the reaction systems that came to use in the course of this thesis. The conducted experiments will be described in detail throughout the following chapters.

3.2.1 IKA LR 2000

Screening experiments for determining *s II* inhibition suitability were conducted in an "IKA LR 2000" lab reactor system (as seen in Figure 13).

Figure 13: IKA LR 2000 lab reactor system

It can operate at pressures up to 6 bar(g) and at temperatures ranging from -45 to +200 °C. Temperature is controlled by a "Lauda Proline RP 845" thermostat, which has a cooling performance of 0.7 to 0.8 kW at experimental conditions. Accuracy of measurements is shown in Table 6, the corresponding flow scheme of the whole process is shown in Figure 14, the reactor's cross section is shown in Figure 15. The reactor is commercially available, but was modified with an additional pressure transducer (PI 1.04 in Figure 14). Also, the stirrer was modified with different "wiper blade" configurations, as shown in Figure 23.

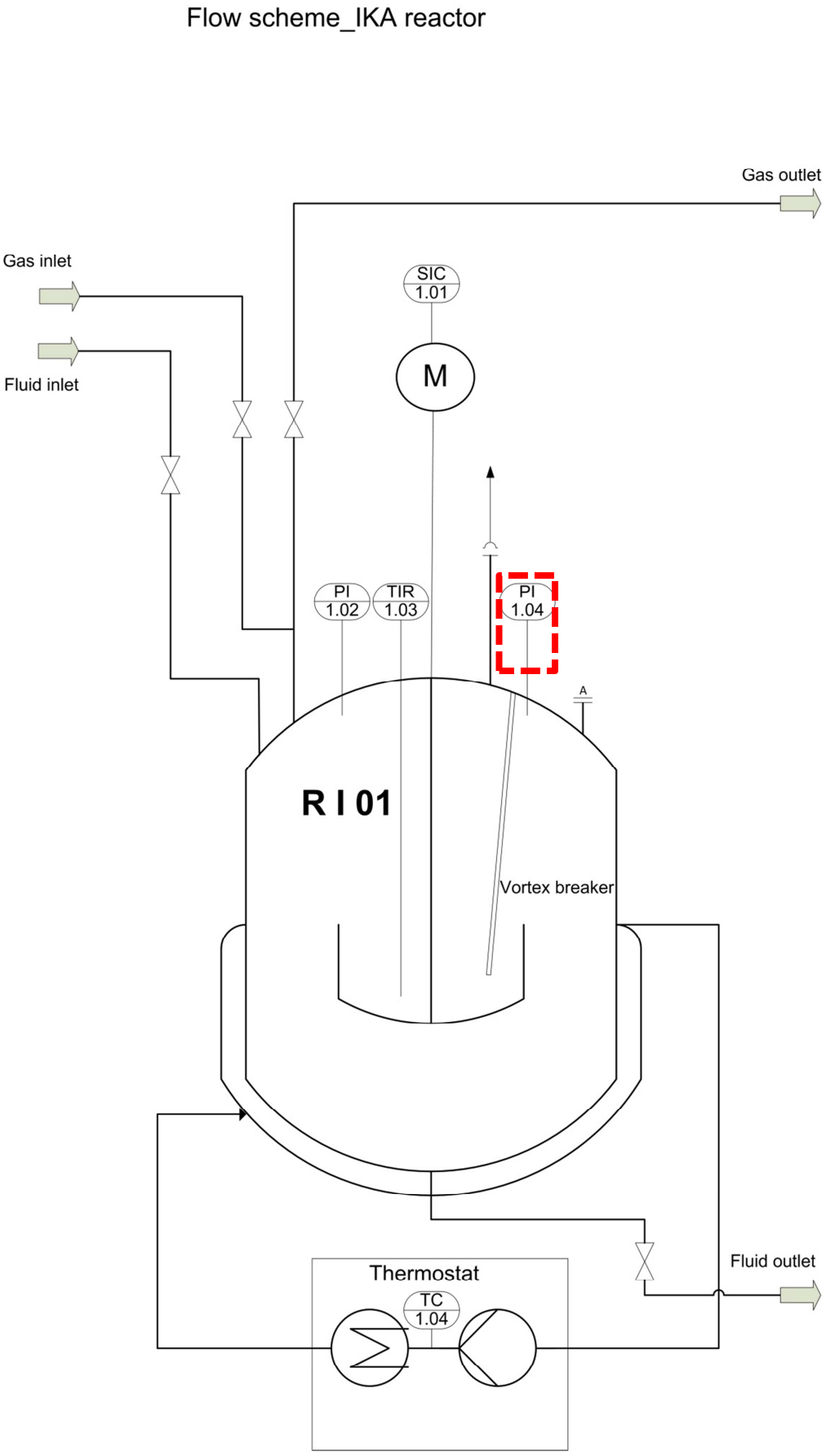

Figure 14: IKA LR 2000 reaction system; flow scheme; modifications made in the course of this thesis are indicated by red dashed lines.

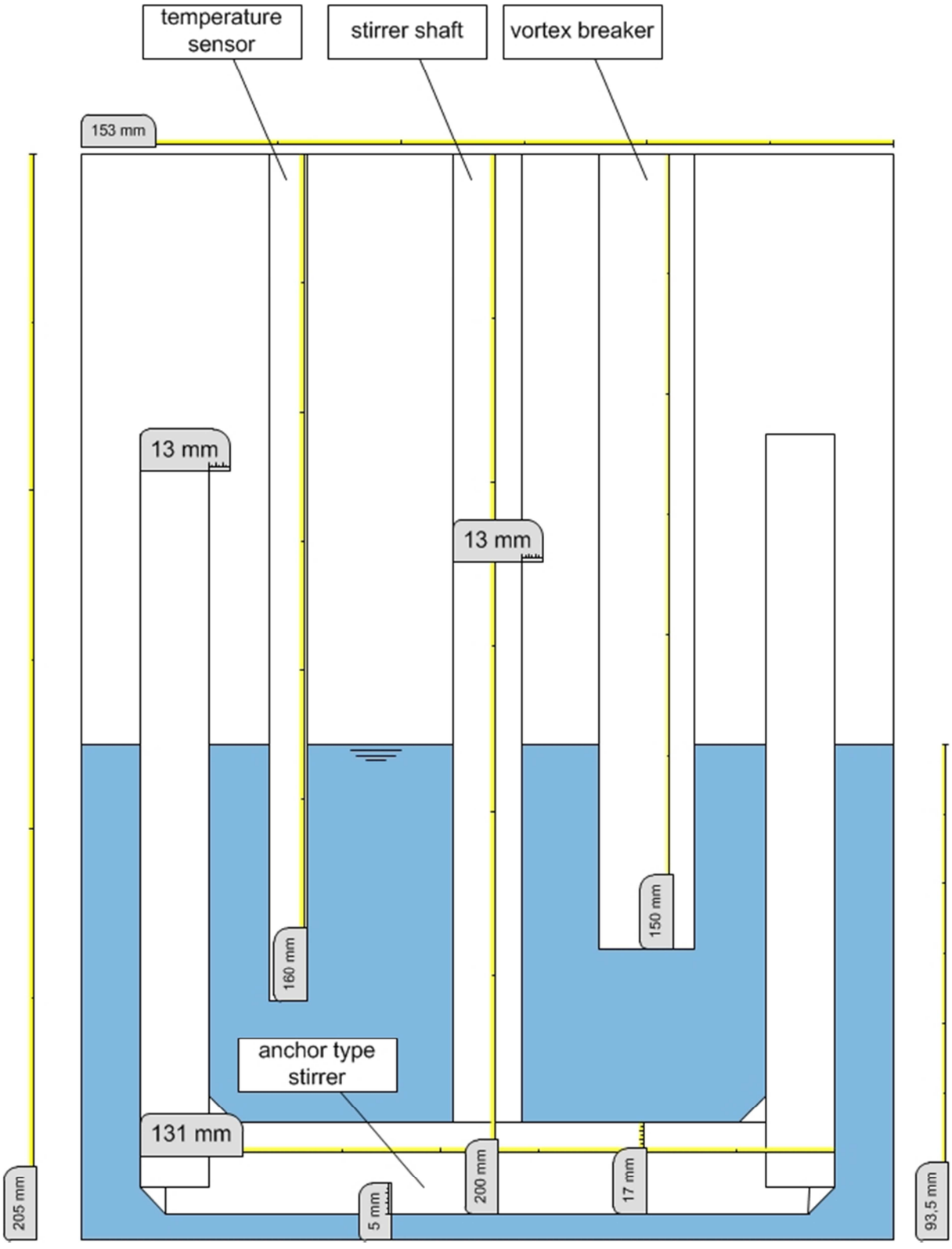

Figure 15: IKA LR 2000 reaction system; cross section

To guarantee the formation of *s II* hydrates and accelerate hydrate formation and the screening procedure, Tetrahydrofuran (THF) was used in all experiments. THF occupies the large cage of *s II*, therefore the formation of *s II* hydrate is guaranteed [2].

Table 6: Accuracy of measurements, IKA LR 2000

Parameter	Sensor	Accuracy
Pressure *p*	WIKA S10 Pressure Transducer	0.25 % of terminal value (± 0.015 bar)
Temperature *T*	PT100	Class A [83] ± 0.15 + 0.002 * ϑ
Mass *m*	Sartorius LE1003s	±0.001g

3.2.2 Parr 4568

In the “high-pressure” experimental series, a pressurized autoclave of the type 4568, manufactured by Parr Instrument (Deutschland) GmbH, was used. The “basic” version of this reactor is shown in Figure 16; chapter 11.1.2 shows the development after several process optimizations and alterations. Figure 17 shows the flow scheme of the whole process, modifications made in the course of this thesis are indicated by red dashed lines. Figure 18 shows the cross section of the reactor after all modifications, e. g. an additional gas phase stirrer, have been completed (see also chapter 11.1.2).

Figure 16: Parr 4568 reaction system, basic version (other versions, see chapter 11.1)

It can operate at pressures ranging from 0 to 200 bar(g) and at temperatures ranging from −10 to +150°C. Heating and cooling were done by a thermostat of the type Presto A40 manufactured by Julabo, which is connected to a PT100-temperature sensor inside the reactor and therefore directly controls the reactor inner temperature. The cooling performance of the thermostat was between 900 and 1200 Watt, the heating performance was 2700 Watt at experimental conditions. The reactor is equipped with a magnetic-controlled stirrer drive and can be equipped with two different stirrers: a hollow shaft stirrer (HSS) for gas input and an oblique blade stirrer (OBS). Pressure [bar(g)], temperature [°C] (measured as voltage signal [V]), rotational frequency [min^{-1}], and stirrer torque [Ncm] are recorded every second. The accuracy of measurements is shown in Table 7. It should be noted that after completion of the “HSS 120 bar(g) 4 °C” measurement series, the pressure

transducer was changed and a more accurate transmitter of type “Emerson Rosemount 2088” was used (see also chapter 11.1.2). In addition, the reactor is equipped with two glass windows for visual observation of the process. [84]

Filling with solids and liquids is done manually by opening the reactor head. Pressurization occurs after closing off the reactor, with simultaneous measurement of gas flow. For this, a Coriolis type mass flow meter manufactured by Bronkhorst Mättig was used. For weighing water, a scale of the type LE1003s, manufactured by Sartorius AG Deutschland, was used.

Pressurization occurs without any additional compressor by using the cylinder pressure of the used gas vessels.

The reactor head is equipped with three manually controlled valves for different purposes. The first one is used to fill the reactor with gas via the above-mentioned coriolis mass-flow meter. The second one can be used to take gas phase samples during experiments. The third one is connected to an immersion tube and can be used to take liquid phase samples.

Table 7: Accuracy of measurements, Parr 4568

Parameter	Sensor	Accuracy
Agitator torque *M*	Parr DR-2500	± 0.1 Ncm
Pressure *p* (old)	Ashcroft OEM-Pressure Transducer G2	1 % of terminal value (± 2 bar)
Pressure *p* (new)	Emerson Rosemount 2088	0.1 % of calibrated terminal value (± 0.18 bar)
Temperature *T*	Juchheim PT100	1/3 class B [83] ± 0.1 + 0.0017 * ϑ
Mass *m*	Sartorius LE1003s	±0.001g
Mass flow	Bronkhorst Mättig mini Cori-flow	≤1.12 % of measured value
Conductivity *δ*	Inolab-cond 740 WTW TetraCon 325	±1% of measured value -.

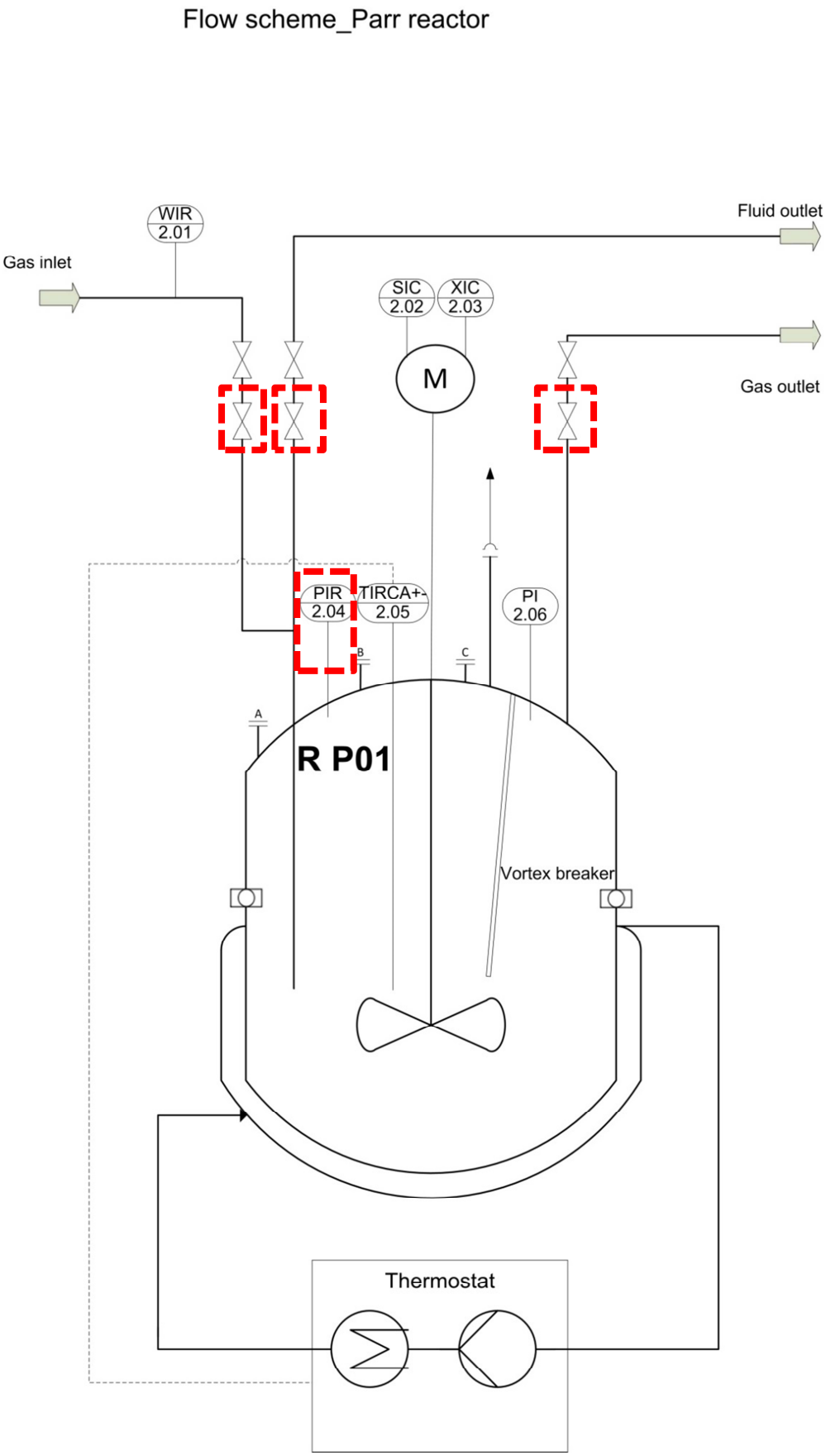

Figure 17: Parr 4568 reaction system, flow scheme; modifications made in the course of this thesis are indicated by red dashed lines. Reproduced with permission from [4]. Copyright [2016] American Chemical Society.

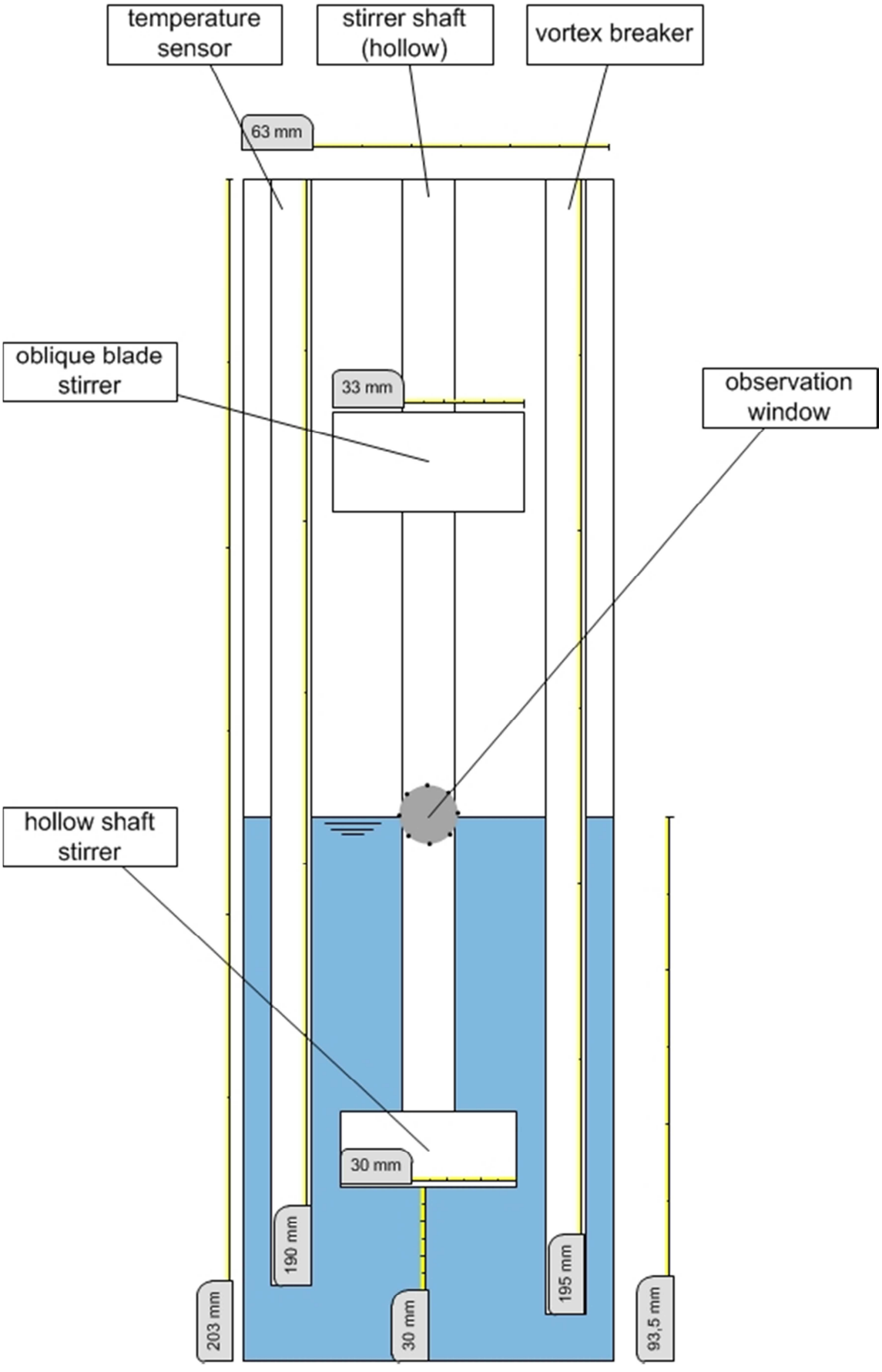

Figure 18: Parr 4568 reaction system, cross section

3.2.3 Büchi ecoclave (glass reactor)

The experiments that were run in the course of this thesis (see also the following chapters) showed that the mechanism of hydrate formation has to be further clarified to gain a deeper understanding of hydrate formation and inhibition. For this purpose, hydrate formation experiments were conducted in a reactor made of glass, which allows for visual observation of the whole hydrate formation process. The goal of these experiments was to determine, whether one of the possible hydrate formation mechanisms is favored under the experimental conditions. The reactor is a "*Büchi Ecoclave 2*" reactor equipped with a propeller-type agitator; temperature is controlled by a "Julabo Presto A40" thermostat. Temperature and pressure were monitored with an "Emerson DeltaV" type process control system. Accuracy of measurements is shown in Table 8.
Figure 19 shows the general view of the reactor, including thermostat and process control system, Figure 20 shows a detailed view of the reaction chamber. The corresponding flow scheme is shown in Figure 21, modifications made in the course of this thesis are indicated by red dashed lines. The cross section of the reaction system is shown in Figure 22.

Figure 19: General view of *Büchi Ecoclave* reactor, including thermostat and process control system

Figure 20: *Büchi Ecoclave* reactor, detailed view

To guarantee the formation of *s II* hydrates and accelerate hydrate formation and the screening procedure, Tetrahydrofuran (THF) was used in all experiments. THF occupies the large cage of *s II*, therefore the formation of *s II* hydrate is guaranteed [2].

Table 8: Accuracy of measurements, Büchi ecoclave

Parameter	Sensor	Accuracy
Pressure *p*	Siemens SITRANS P200	0.25 % characteristic curve deviation (± 0.04 bar)
Temperature *T*	PT100	Class A [83] ± 0.15 + 0.002 * ϑ
Mass *m*	Sartorius LE1003s	±0.001g
Mass flow	Bronkhorst Mättig mini Cori-flow	≤1.12 % of measured value

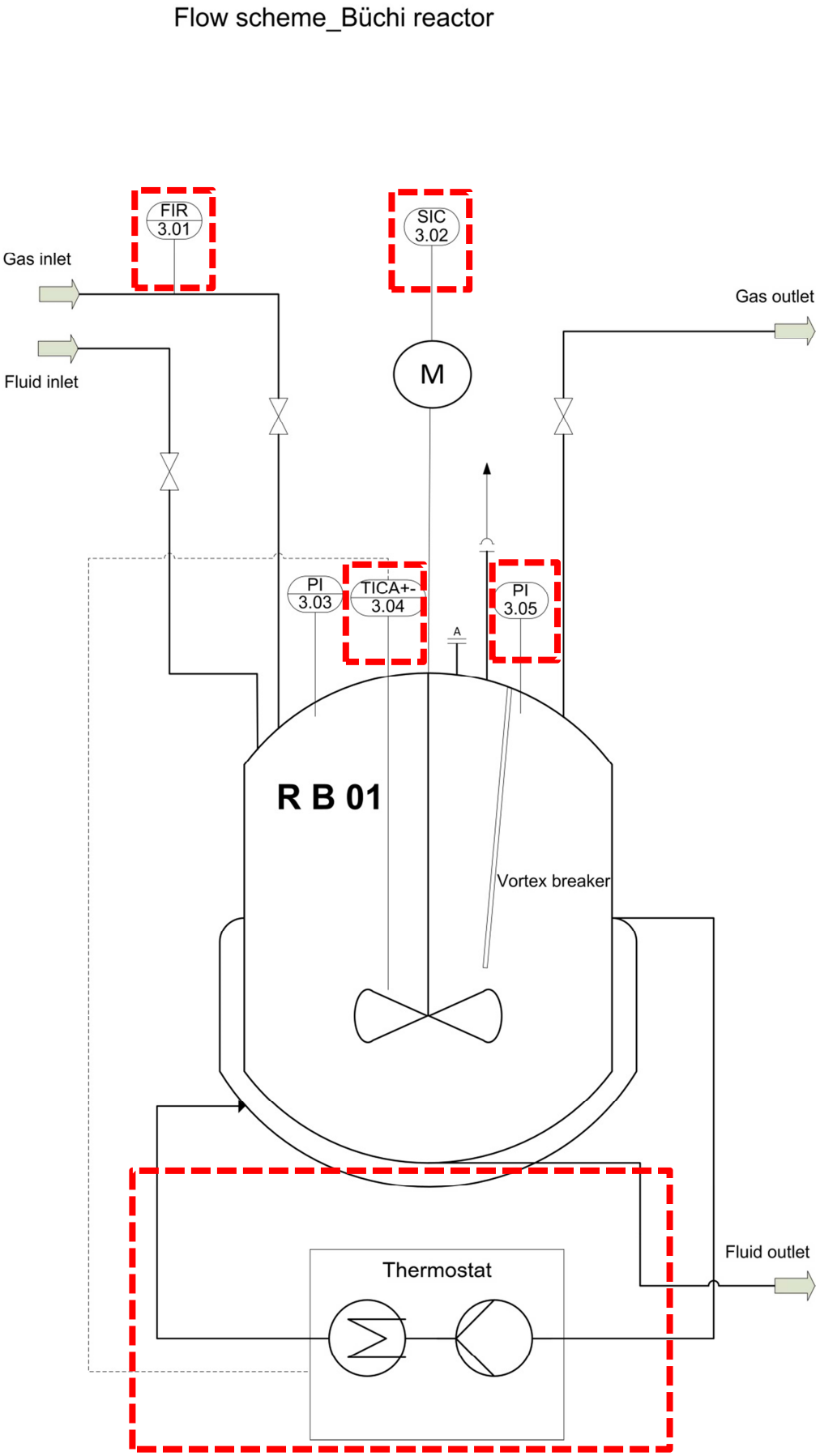

Figure 21: Büchi ecoclave reactor: flow scheme; modifications made in the course of this thesis are indicated by red dashed lines.

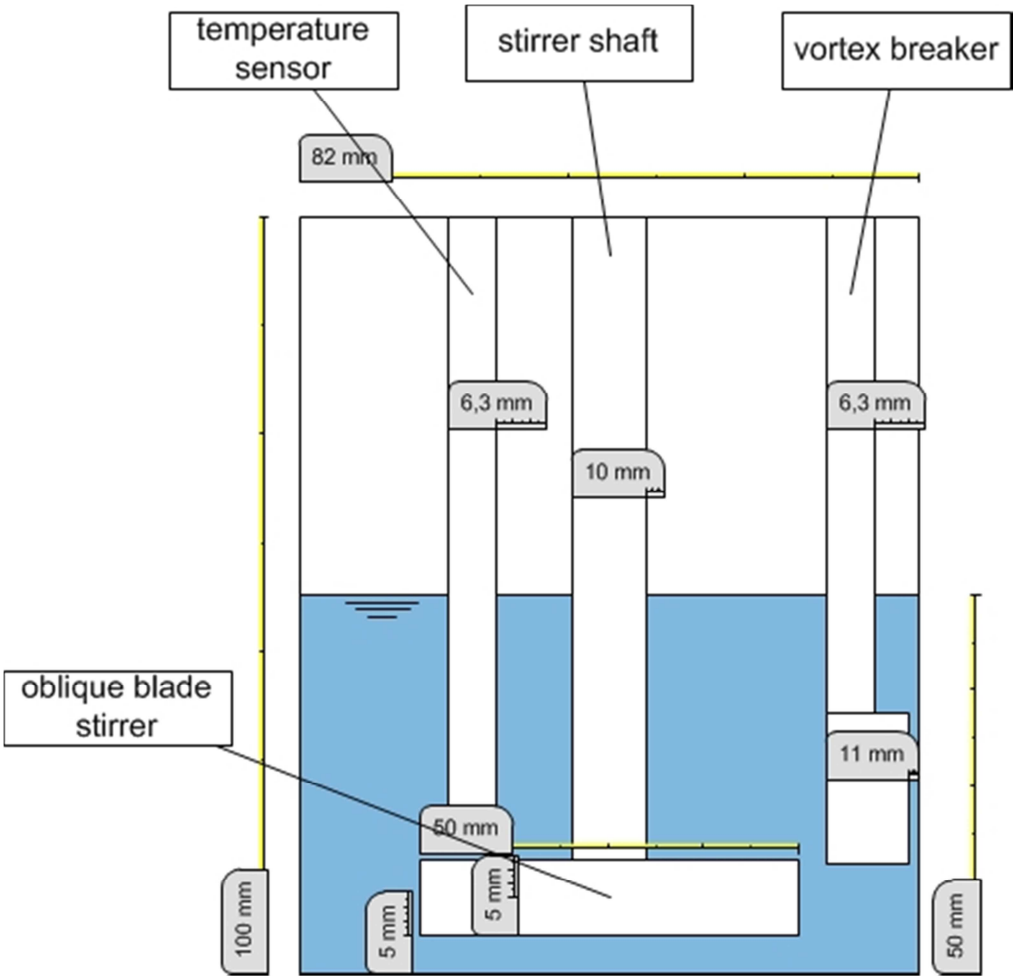

Figure 22: Büchi ecoclave reaction system, cross section

In the following chapters, the experiments conducted in the course of this thesis will be described and discussed in detail.

4 Screening for determining *s II* inhibition suitability

During the course of this thesis, various substances were tested regarding their inhibition potential for *s II* inhibition as well as general interaction with gas hydrate systems. Also, the influence of different agitator types (anchor type stirrer with different arrangement of wiper blades) on gas hydrate formation was investigated.
These experiments were conducted as a first “screening” in a low-pressure reaction system. Screening in this case means that a great number of substances were tested for their inhibition potential as a first estimate to find out promising candidates which were then allowed for the more detailed high-pressure experiments (see chapter 6).
Tetrahydrofuran (THF) was added in all of the experiments for two reasons: it guarantees the formation of *s II* hydrates and it greatly accelerates hydrate formation. The experiments thus were used to speed up the whole process of inhibition research as well as to include *s II* in the research.

4.1 Experimental procedure

The empty reactor was tempered at 20 °C. After that, the reactor was tested for leakage by pressurizing with methane to 5.5 bar(g) and closing off the reactor. If the pressure loss was lower than 0.2 bar within 30 minutes, the experiment was continued by filling the reactor with water and THF (in a molar ratio of 17:1) and inhibitor, where required. In chosen experimental series, the reactor was filled before the leakage test. This is indicated in Table 9.

After filling respectively leakage testing, the reactor was purged 3 times with methane to remove air and retain a pure “methane atmosphere”. For this, the reactor was pressurized with methane to a pressure of about 5.5 bar(g) and then pressure was released to a value of about 0.5 bar(g) to avoid back mixing with the laboratory air. In total, a minimum dilution of 1:90 (3 times purging with at least 4,5 bar difference in pressure each) was reached.
After purging, the reactor was filled with methane to a pressure of 5.5 bar(g), the agitator was set to 50 min^{-1} and the thermostat to 5 °C. The reaching of an agitator speed > 48 min^{-1} marked the beginning of the experiment. If inhibitor was used, concentrations of 1, 3 and 5 % wt. were investigated; each inhibitor was tested in at least 3 experiments per concentration.

Different anchor type stirrers with different “wiper blade layouts” were used in the experiments. The wiper blades scrape at the reactor wall to prevent ice or hydrate layer

formation at the vessel wall. The different wiper blade configurations are described in detail in Figure 23. [85–89]

Stirrer *without* wiper blades

Stirrer with *bottom* wiper blades

Stirrer *bottom+1* wiper blades

Stirrer *with all* wiper blades

Figure 23: Different anchor type stirrers

Stirring conditions had to be turbulent in the course of this thesis due to two reasons: higher turbulence ensures a faster hydrate formation and hence, testing potential inhibitors at "difficult" conditions (thus finding "better" inhibitors); also, turbulence has more resemblance to field conditions in pipelines, where potential inhibitors would be applied.
Hence, to guarantee turbulence inside the reactor, the stirrer operates at high frequency, and a modified Reynolds number of approximately 9472 is reached (see equation [4.1]). The built-in components, like probe tubing, resistance thermometer, etc. that could act as vortex breakers, are not accounted for:

$$\boldsymbol{Re_R = \frac{N * d^2 * \rho}{\eta} = \frac{\frac{50}{60s} * (0.131\ m)^2 * 986.88 \frac{kg}{m^3}}{1.49 * 10^{-3} \frac{kg}{m * s}} \approx 9472} \qquad [4.1]$$

Values for density and viscosity of the water-THF mixture were taken from [90]. The calculation was done for a temperature value of 298 K.
Stirrer frequency *N* was 50 min^{-1}, diameter *d* of the anchor type stirrer (without accounting for the wiper blades) was 131 mm, the density *ρ* of the water-THF mixture at 20 °C is 986,88 kg/m^3 and the dynamic viscosity *η* at 20 °C is $1.49*10^{-3}$ kg/m*s [90].

The Reynolds number is a dimensionless quantity that is defined as the ratio of inertial forces to viscous forces and is used to describe dynamic similitude between different cases of fluid flow. There are three different "areas" or flow regime types characterized by the Reynolds number: the laminar flow ($Re < Re_{cr}$, see below) regime, the transition area of the flow regime ($Re_{cr} < Re < Re_{turb}$) and the turbulent flow regime ($Re > Re_{turb}$).

For stirring processes, the so-called *critical* Reynolds number Re_{cr}, that defines where a flow starts to be turbulent, has a value of $Re_{cr} = 30$ [91].
With a value of 9472, the Reynolds number inside the IKA LR 2000 reaction system is well inside the transition area, which is ranged between Reynolds numbers of *30* and *10000* [91]. Above a Reynolds number of 10000, the flow in a stirred process is seen as fully turbulent.

The different experimental conditions for all of the experimental rows are listed in Table 9 to Table 13, the arrangement was chosen for better clarity.

Table 9: Experimental conditions, *s II* screening (1)

Experiment	Stirrer type / wiper blades				Filling	
	with all	***bottom+1***	***bottom***	***without***	**before leakage testing (LT)**	**after**
Blind1	x					x
Blind 2	x					x
Blind 3	x				x	
Blind 4				x	x	
Blind 5				x	x	
Blind 6		x			x	
Blind 7		x			x	
Blind 8		x			x	
Blind 9			x			x
Blind 10			x			x
Blind 11			x			x
Tylose H20P2 1% V1		x			x	
Tylose H20P2 1% V2		x			x	
Tylose H20P2 1% V3		x			x	
Tylose H20P2 3% V1		x			x	
Tylose H20P2 3% V2		x				x
Tylose H20P2 3% V3			x			x
Tylose H20P2 5% V1			x			x
Tylose H20P2 5% V2			x			x
Tylose H20P2 5% V3			x			x

Table 10: Experimental conditions, *s II* screening (2)

Experiment	Stirrer type / wiper blades				Filling	
	with all	***bottom+1***	***bottom***	***without***	**before LT**	**after LT**
Blind 12			x			x
Blind 13			x			x
Blind 14			x			x
Blind 15			x			x
Blind 16			x			x
Tylose H300P2 1%			x			x
Tylose H300P2 1%			x			x
Tylose H300P2 1%			x			x
Tylose H300P2 3%			x			x
Tylose H300P2 3%			x			x
Tylose H300P2 3%			x			x
Tylose H300P2 5%			x			x
Tylose H300P2 5%			x			x
Tylose H300P2 5%			x			x
Polyvinyl acetate 1%			x			x
Polyvinyl acetate 1%			x			x
Polyvinyl acetate 1%			x			x
Polyvinyl acetate 3%			x			x
Polyvinyl acetate 3%			x			x
Polyvinyl acetate 3%			x			x
Polyvinyl acetate 5%			x			x
Polyvinyl acetate 5%			x			x
Polyvinyl acetate 5%			x			x

Table 11: Experimental conditions, *s II* screening (3)

Experiment	Stirrer type / wiper blades				Filling	
	with all	***bottom+1***	***bottom***	***without***	**before LT**	**after LT**
Polyvinylpyrrolidone K90 1%			x			x
Polyvinylpyrrolidone K90 1%			x			x
Polyvinylpyrrolidone K90 1%			x			x
Polyvinylpyrrolidone K90 3%			x			x
Polyvinylpyrrolidone K90 3%			x			x
Polyvinylpyrrolidone K90 3%			x			x
Polyvinylpyrrolidone K90 5%			x			x
Polyvinylpyrrolidone K90 5%			x			x
Polyvinylpyrrolidone K90 5%			x			x
Glycerol 1%			x			x
Glycerol 1%			x			x
Glycerol 1%			x			x
Glycerol 3%			x			x
Glycerol 3%			x			x
Glycerol 3%			x			x
Glycerol 5%			x			x
Glycerol 5%			x			x
Glycerol 5%			x			x

Table 12: Experimental conditions, *s II* screening (4)

Experiment	Stirrer type / wiper blades				Filling	
	with all	***bottom+1***	***bottom***	***without***	**before LT**	**after LT**
Blind 17	x					x
Blind 18	x					x
Blind 19	x					x
PEG 600 1%	x					x
PEG 600 1%	x					x
PEG 600 1%	x					x
PEG 600 3%	x					x
PEG 600 3%	x					x
PEG 600 3%	x					x
PEG 600 5%	x					x
PEG 600 5%	x					x
PEG 600 5%	x					x
KSCN 1%	x					x
KSCN 1%	x					x
KSCN 1%	x					x
KSCN 3%	x					x
KSCN 3%	x					x
KSCN 3%	x					x
KSCN 5%	x					x
KSCN 5%	x					x
KSCN 5%	x					x
KSCN 5%	x					x
KSCN 5%	x					x
KSCN 5%	x					x
B_2O_3 1%	x					x
B_2O_3 1%	x					x
B_2O_3 1%	x					x
B_2O_3 1%	x					x
B_2O_3 3%	x					x
B_2O_3 3%	x					x
B_2O_3 3%	x					x

Table 13: Experimental conditions, *s II* screening (5)

Experiment	Stirrer type / wiper blades				Filling	
	with all	***bottom+1***	***bottom***	***without***	**before LT**	**after LT**
B_2O_3 3%	x					x
B_2O_3 5%	x					x
B_2O_3 5%	x					x
B_2O_3 5%	x					x
EG 1%	x					x
EG 1%	x					x
EG 1%	x					x
EG 3%	x					x
EG 3%	x					x
EG 3%	x					x
EG 5%	x					x
EG 5%	x					x
EG 5%	x					x
DGluc 1%	x					x
DGluc 1%	x					x
DGluc 1%	x					x
DGluc 3%	x					x
DGluc 3%	x					x
DGluc 3%	x					x
DGluc 5%	x					x
DGluc 5%	x					x
DGluc 5%	x					x
Ino 1%	x					x
Ino 1%	x					x
Ino 1%	x					x
Ino 1%	x					x
Ino 3%	x					x
Ino 3%	x					x
Ino 3%	x					x
Ino 5%	x					x
Ino 5%	x					x
Ino 5%	x					x

4.2 Results and discussion

Various substances were tested regarding their inhibition potential for *s II* inhibition as well as general interaction with gas hydrate systems. Also, the influence of different agitator types (anchor type stirrer with different arrangement of wiper blades) on gas hydrate formation was investigated.
These experiments should be seen as a first “screening” in a low-pressure reaction system, main focus was on finding promising candidates for the high-pressure experimental series. Nonetheless, especially the variation of stirrer configurations yielded interesting results.

In the following tables, induction times of the respective experimental series are compared to determine whether the tested substances cause a significant change in induction time and hence, if the substance has an inhibiting or promoting effect on gas hydrate formation.

To evaluate the screening experiments conducted with the *IKA LR 2000* system, induction times as well as statistics are shown in Table 14 and Table 15. Normality was tested with *Shapiro-Wilk* tests (level of significance: 95 %), testing for outliers was done via *Dixon-Q* tests (level of significance: 95 %).

In Table 14 and Table 15, the letter “a” in the column “Normally distributed” means “not enough values to test for normality”, the “+” means “normal distribution cannot be rejected”, which is interpreted as “normally distributed” for further testing, e. g. for outliers.
A “-“ means “not normally distributed”.

In the column “Outliers?”, an “a” also means “not enough values for testing”, a “-“ means “no outliers on tested level of significance”, a “+” would mean “outliers” and the letter “b” means “testing according to Dixon Q not possible, because data was not normally distributed”.

Table 14: Results of *s II* screening, Part 1

	No. of exp.	Induction time t_{ind} [min]								
		Mean	Std. dev.	Rel. std. dev. [%]	Coeff. of variation	Minimum	Maximum	Range (Maximum – Minimum)	Normally distributed?	Outliers?
BV1+2	**2**	36.38	0.412	1	0.011	36.08	36.67	0.58	a	a
BV4+5	**2**	59.97	19.634	33	0.327	46.08	73.85	27.77	a	a
BV6+7+8	**3**	35.71	4.278	12	0.120	31.12	39.58	8.47	+	-
BV9+10+11	**3**	37.16	3.997	11	0.108	34.60	41.77	7.17	+	-
H20 1%	**3**	30.08	8.610	29	0.286	23.93	39.92	15.99	+	-
H20 3%, E2+3	**3**	64.72	28.072	43	0.434	44.87	84.57	39.70	a	a
H20 5%	**3**	**98.16**	**25.869**	**26**	**0.264**	**79.92**	**127.77**	**47.85**	**+**	**-**
BV 12-16	**5**	34.87	5.404	15	0.155	29.05	43.20	14.15	+	-
H300 1%	**3**	42.33	7.817	18	0.185	34.05	49.58	15.53	+	-
H300 3%	**3**	**63.92**	**7.526**	**12**	**0.118**	**55.67**	**70.40**	**14.73**	**+**	**-**
H300 5%	**3**	**52.75**	**4.701**	**9**	**0.089**	**47.88**	**57.27**	**9.38**	**+**	**-**
PVAc 1%	**3**	36.59	1.556	4	0.043	34.97	38.07	3.10	+	-
PVAc 3%	**3**	**49.02**	**15.808**	**32**	**0.323**	**30.78**	**58.88**	**28.10**	**+**	**-**
PVAc 5%	**3**	**58.67**	**10.928**	**19**	**0.186**	**46.62**	**67.93**	**21.32**	**+**	**-**
PVP 1%	**3**	**76.93**	**8.113**	**11**	**0.105**	**71.23**	**86.22**	**14.98**	**+**	**-**
PVP 3%	**3**	**62.33**	**8.929**	**14**	**0.143**	**52.17**	**68.90**	**16.73**	**+**	**-**
PVP 5%	**3**	**108.84**	**49.096**	**45**	**0.451**	**80.08**	**165.53**	**85.45**	**-**	**b**
Gly 1%	**3**	**64.84**	**14.341**	**22**	**0.221**	**48.42**	**74.87**	**26.45**	**+**	**-**
Gly 3%	**3**	**59.64**	**4.356**	**7**	**0.073**	**55.17**	**63.87**	**8.70**	**+**	**-**
Gly 5%	**4**	**80.18**	**26.805**	**33**	**0.334**	**60.52**	**119.50**	**58.98**	**+**	**-**

Table 15: Results of *s II* screening, Part 2

	No of exp.	Induction time t_{ind} [min]								
		Mean	Std. dev.	Rel. std. dev. [%]	Coeff. of variation	Minimum	Maximum	Range (Maximum – Minimum)	Normally distributed?	Outliers?
Blind 17-19	3	36.83	1.547	4	0.042	35.18	38.25	3.07	+	-
PEG 1%	3	39.75	6.532	16	0.164	33.40	46.45	13.05	+	-
PEG 3%	**3**	**79.34**	**40.944**	**52**	**0.516**	**55.48**	**126.62**	**71.13**	**-**	**b**
PEG 5%	**3**	**55.49**	**10.183**	**18**	**0.184**	**43.95**	**63.20**	**19.25**	**+**	**-**
KSCN 1%	**3**	**95.38**	**16.793**	**18**	**0.176**	**80.85**	**113.77**	**32.92**	**+**	**-**
KSCN 3%	**3**	**96.67**	**16.452**	**17**	**0.170**	**82.30**	**114.62**	**32.32**	**+**	**-**
KSCN 5%	**5**	**177.09**	**88.602**	**50**	**0.500**	**76.17**	**299.75**	**223.58**	**+**	**-**
B2O3 1%	**4**	**66.18**	**17.455**	**26**	**0.264**	**40.58**	**79.87**	**39.28**	**+**	**-**
B2O3 3%	**4**	**80.40**	**17.271**	**21**	**0.215**	**65.05**	**105.18**	**40.13**	**+**	**-**
B2O3 5%	**3**	**57.66**	**12.794**	**22**	**0.222**	**47.73**	**72.10**	**24.37**	**+**	**-**
EG 1%	3	40.44	1.326	3	0.033	39.22	41.85	2.63	+	-
EG 3%	**4**	**75.88**	**43.006**	**57**	**0.567**	**41.32**	**136.28**	**94.97**	**+**	**-**
EG 5%	**3**	**49.32**	**10.948**	**22**	**0.222**	**39.83**	**61.30**	**21.47**	**+**	**-**
DGluc 1%	3	44.24	19.671	44	0.445	28.57	66.32	37.75	+	-
DGluc 3%	3	38.03	3.907	10	0.103	33.93	41.72	7.78	+	-
DGluc 5%	3	37.91	3.736	10	0.099	33.93	41.35	7.42	+	-
Ino 1%	4	43.71	16.603	38	0.380	29.57	64.92	35.35	+	-
Ino 3%	3	36.23	6.617	18	0.183	32.27	43.87	11.60	-	b
Ino5%	3	42.70	3.504	8	0.082	38.80	45.58	6.78	+	-
Blind 17-19	3	36.83	1.547	4	0.042	35.18	38.25	3.07	+	-

Substances that increased the mean induction time by at least 30 % (compared to the respective blind experiments) were deemed as "**promising inhibitors**" and are listed in **bold**. They are recommended to enter high-pressure testing.

Although experiments with PVP K90 had a negative result in the test for normal distribution, a trend to inhibitive behavior is shown. Thus, and because PVP is also widely used in the field as a KHI [7, 8] as well as in lab-scale experiments [92], it is still recommended to test PVP in the high-pressure experiments.

PEG is also recommended for high-pressure testing, even though the test on normal distribution was negative at 3 % wt., since all of the determined induction times were significantly higher than those of the blind experiments.

The substances "H300" and "PVAc" are underlined separately. They both caused shifts in induction times but also procedural problems in the experiments. They formed highly viscous, sticky gels. Therefore they were not recommended for high-pressure testing.

The inhibitor candidates that were recommended to enter high-pressure testing are *Tylose H20P2*, *PVP K90*, *Glycerol*, *PEG 600*, *KSCN* and B_2O_3.

In the course of experiments, the idea to investigate a "homologous series" of OH-groups, meaning substances with an increasing number of OH-groups per volume element, came up. The goal of these experiments was the determination of the influence of OH-groups on hydrate formation, e. g. if there is an "optimal OH concentration" for inhibition.
The substances chosen for the investigations were *ethylene glycol*, *D-Glucose* and *Inositol*.
Although *D-Glucose* and *Inositol* did not cause the 30 % increase in induction times during the low-pressure experiments, they were nonetheless investigated in the high-pressure experiments to conclude the experimental series. Results of these experiments are discussed in detail in chapter 7.

Regarding the influence of THF on induction times, it still has to be clarified if THF only gets built in the cages as a guest molecule and the promoting effect is simply caused by the formation of structure *s II* instead of structure *s I* hydrate; this could be the case since e. g. adding small amounts of propane to methane would result in a "dramatic decrease in hydrate pressure…due to the structure change (*s I* to *s II*)." ([2], p. 299) and resulting from the

decrease in hydrate pressure, the driving force for hydrate formation at a given (system) pressure would be higher. This would then lead to an increase in hydrate formation rate and of course also the induction time would be lowered.
But of course, THF could (additionally?) influence hydrate formation in another way, e. g. by facilitating the formation of hydrate structures by interacting with hydrogen bonds of water molecules.

Hydrates formed in presence of THF seem to be softer and more “paste-like” in their morphology.
The paste-like structure / the change in morphology could be caused by some kind of mixed structure formed between the clathrate “network” and the THF molecules. If this really is the case or if the paste-like hydrate structure is caused by the low pressure in the experiments (and hence of the small “methane to THF ratio”), has to be further investigated, e. g. by RAMAN investigation of the formed hydrate structures.

Reducing the stirrer frequency while hydrate formation is already taking place still has an effect on the hydrate formation rate [85]. This can be seen in Figure 24, where the stirrer was switched off between the two black lines. Effects of the stirrer frequency on gas consumption rate also were found in [92], for propane hydrate formation experiments in a hydrate formation cell.

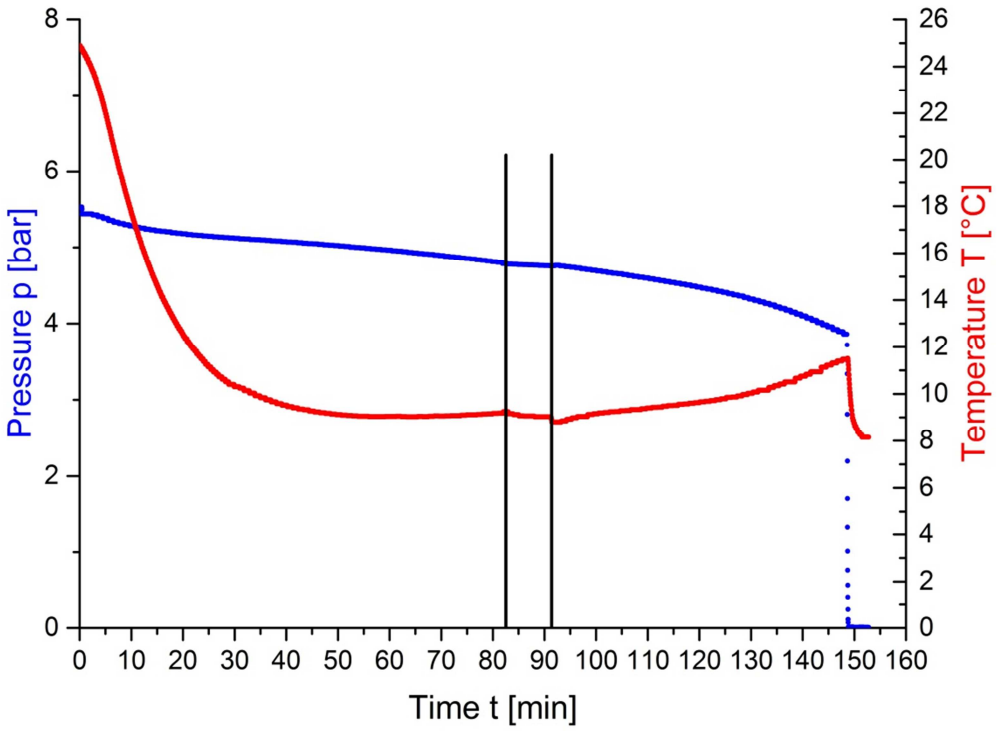

Figure 24: Stirrer switched off during hydrate formation experiment. Pressure (left ordinate) and temperature (right ordinate) are plotted against time (abscissa). It can be seen that pressure reduction (equals hydrate formation) is slower during stirrer standstill.

The effect of liquid phase turbulence on gas hydrate formation has been long-known (e. g. [2]).

A new aspect that was found in the course of this work was the influence of stirrer configurations on hydrate formation. It was found out that the wiper blades *in the gas phase* had significant influence on hydrate formation, although they were not in contact with the liquid phase. This observation led to the mounting of an additional gas phase stirrer inside the high-pressure autoclave (Parr 4568, see chapter 11.1.2), where the phenomenon could be reproduced. In the high-pressure experiments, the additional gas phase stirrer also reduced induction times significantly. Although it was known for a long time that turbulence at the gas-water interface and inside the liquid phase is critical for hydrate formation [2], the effect that solely increasing the gas phase turbulence had on hydrate formation was a surprising finding.

5 Determination of “optimal” parameters for s I screening

This chapter shows the process of finding the optimal parameters for the high pressure / *s I* inhibition experiments. Part of this work has also been published in [84].

5.1 Experimental procedure

To find references for pipeline operating conditions, a literature research was done. System pressures of 120 bar (Alliance pipeline connecting from British Columbia (CA) to Illinois (US) as a reference for permafrost-region pipelines [93]) and 135 bar (Interconnector, connecting Bacton (GB) to Zeebrugge (BE) [94]). Furthermore, a “high-pressure reference” was done at 160 bar(g). Temperatures of 4 °C and 6 °C were investigated.

To simulate pipeline-like conditions, the experimental procedure was as follows:

Water (Milli-Q water with a conductivity of 1–3 µS/cm) was filled in the reactor. Then, the reactor was tempered to 20°C ± 0.5°C.

After this, the reactor was purged 3 times with methane (in a purity of ≥99.5%, provided by Messer Industriegase) to remove air and retain a pure “methane atmosphere”. For this, the reactor was pressurized with methane to a pressure of about 6.5 bar(g) and then pressure was released to a value of about 0.5 bar(g) to avoid back mixing with the laboratory air. In total, a minimum dilution of 1:216 (3 times purging with at least 6 bar difference in pressure each) was reached.

Finally, the reactor was filled with methane to the “target pressure” of the experimental series. Reaching of the highest pressure value marked the beginning of the experiment. Then, the reactor was slowly cooled to experimental temperature to simulate the temperature drop in the pipeline from the drilling point onwards and between compressor stations in the pipeline. The resulting pressure drop from cooling and dissolution of methane in water then corresponds to the pressure drop inside the pipeline.

To guarantee turbulence inside the reactor (in analogy to the turbulent flow inside a pipeline), the stirrer operates at high frequency, and a modified Reynolds number of approximately 1974 is reached (see equation [5.1]). The built-in components, like probe tubing, resistance thermometer, etc. that could act as vortex breakers, are not accounted for:

$$Re_R = \frac{n * d^2 * \rho}{\eta} = \frac{\frac{200}{60s} * (3.0 * 10^{-2} m)^2 * 1000 \frac{kg}{m^3}}{1.52 * 10^{-3} \frac{kg}{m * s}} \approx 1974 \quad [5.1]$$

Stirrer frequency *N* was 200 min^{-1}, diameter *d* of the hollow shaft stirrer (without additional oblique blade stirrer) was 30 mm, the density *ρ* of water at 5 °C is approximately 1000 kg/m³ and the dynamic viscosity *η* of water at 5 °C is 1.52*10^{-3} kg/m*s. The values at 5 °C were chosen as a “good average” between the conditions at 4 °C resp. 6 °C. With a value of 1974, the modified Reynolds number is well in the transition area between laminar and fully turbulent flow.

To ascertain statistically significant results, multiple measurements (at least 5 per experimental series) were conducted. In each of those experiments, fresh water was used to avoid the so-called memory effect (see also chapter 2.4). [84]

For reasons of clarity, the experimental conditions as well as the “reference pipelines” are shown in Table 16.

Table 16: References and experimental parameters, determination of operating conditions

Reference	Denomination of experimental series	Pressure *p* [bar(g)]	Temperature T_1 [°C]
[95] High pressure comparative value	HSS 160 bar 4 °C	160	4
[95] High pressure comparative value	HSS 160 bar 6 °C	160	6
[94] Interconnector	HSS 135 bar 4 °C	135	4
[93] Alliance-Pipeline	HSS 120 bar 4 °C	120	4

Also, simulations to determine the equilibrium pressure of methane hydrate under the given conditions were conducted before the experiments to ascertain that hydrate formation was feasible from a thermodynamic point of view. For this, the software “CSMHyd”, developed by the working group of Prof. Sloan, came to use [2].
Determined equilibrium pressures were:
p (4 °C) = 38.5 bar
p (6 °C) = 46.7 bar
The experimental parameters were all significantly above these values; therefore, a high “theoretical super-saturation” is reached (see also Figure 3 in chapter 2.2). Therefore, the

driving force is high enough so that hydrate formation should in principle take place in every experiment. [95]

5.2 Results and discussion

This chapter shows the results of the determination of “optimal” parameters for the following *s I* screening. Part of this work has also been published in [84].

The evaluation of results is shown exemplarily for one experiment (see Figure 25). The determined induction times are then shown in Table 17.

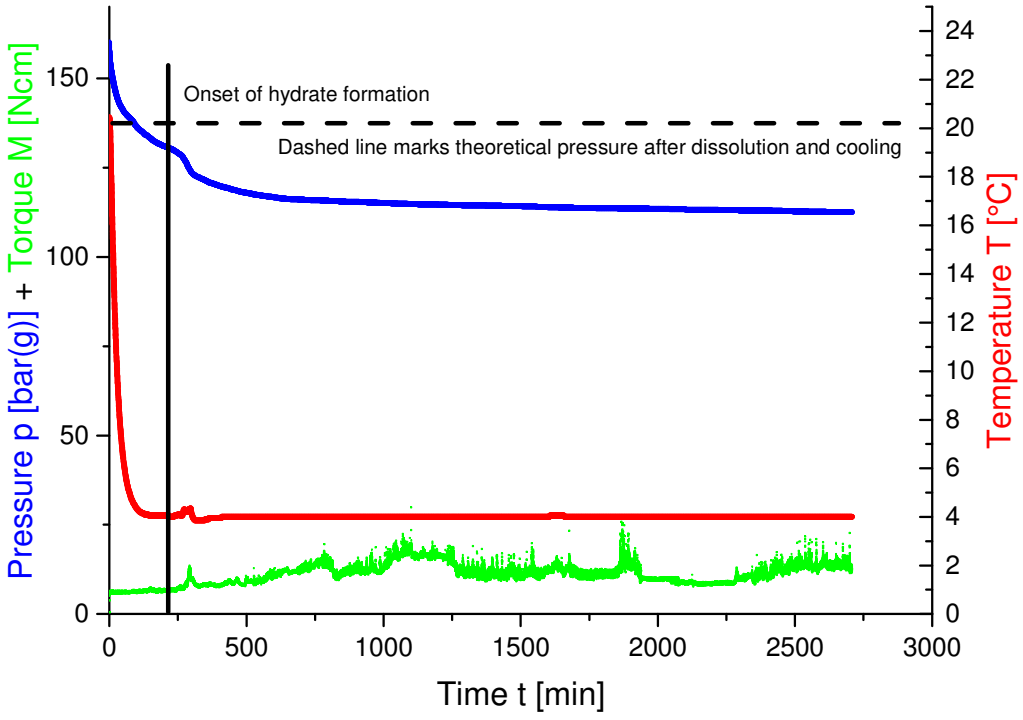

Figure 25: Exemplary hydrate formation experiment. Pressure and stirrer torque (left ordinate) as well as temperature (right ordinate) are plotted against time (abscissa). The dashed line marks the theoretical system pressure after dissolution of methane in the water phase as well as cooling to target temperature. The onset of hydrate formation is characterized by a “faster” decrease in pressure with simultaneous increase in temperature (see also below) and marked by the vertical black line.

Figure 25 shows pressure and stirrer torque (1st ordinate) as well as temperature (2nd ordinate) plotted against time t (abscissa). Starting point of each experiment is the point of highest pressure, before cooling to target temperature. The pressure drop in the beginning is caused by dissolution of methane in water as well as cooling to the “target” temperature of

4 °C, the dashed line in Figure 25 highlights the obtained pressure. Below, the calculation is shown exemplarily for a pressure of 160 bar(g) and a target temperature of 4 °C (as in Figure 25).

At first, the theoretical starting pressure for hydrate formation without consideration of solubility and cooling effects is calculated via the van-der-Waals equation:

$$p = \frac{n\,R\,T}{V - n\,b} - \frac{a\,n^2}{V^2} \qquad [5.2]$$

With a molar amount of methane (measured by Coriolis mass-flow meter) of 3.06 mole, a starting temperature T of 293.15 K and a volume of 0.35 dm^3, the theoretical starting pressure p_{start} results as follows (the van-der-Waals-coefficients were taken from [96]):

$$p_{start} = \frac{3.06\ mole * 0.08314 \frac{bar\ dm^3}{k*mol} * 293.15K}{0.35 dm^3 - 3.06 mole * 0.0431\ dm^3 mole^{-1}} - \frac{2.303 bar\ dm^6 mole^{-2} * 3.06^2 mole^2}{0.35^2 dm^6} = 165.6\ bar \qquad [5.3]$$

In a next step, the pressure is calculated for a temperature of 4 °C and a molar amount of 3.06 mole, by use of the van-der-Waals-equation:

$$p_{4°C} = \frac{3.06\ mole * 0.08314 \frac{bar\ dm^3}{K*mole} * 277.15K}{0.35 dm^3 - 3.06 mole * 0.0431\ dm^3 mole^{-1}} - \frac{2.303 bar\ dm^6 mole^{-2} * 3.06^2 mole^2}{0.35^2 dm^6} = 147.2\ bar \quad [5.4]$$

This corresponds to the pressure change caused by the cooling process.

The dissolution of methane is considered as follows:
according to Lange’s handbook of chemistry [97], the dissolubility coefficient for Methane at 4 °C is $\lambda_1 = 0.003467123 \left[\frac{g}{100g\ water \cdot bar}\right]$.

Based on the conditions of no hydrate formation taking place and water being only existent as liquid phase, the dissolved amount of methane in water (m_{H2O} = 249.5 g) accounts to:

$$c_{w1} = \lambda \cdot p_{K1} \cdot \frac{m_{H2O}}{100} = 0.003467123 * 165.6 \cdot \frac{249.5}{100} \frac{g \cdot bar \cdot g}{g \cdot bar} \approx 1.43g \qquad [5.5]$$

This corresponds to a molar amount of $n_{dissolution}$ = 0.09 mole. The pressure after dissolution of methane is then calculated as follows:

$$p = \frac{(n_{start} - n_{dissolution}) * R * T}{V - (n_{start} - n_{dissolution}) * b} - a \frac{(n_{start} - n_{dissolution})^2}{V^2} \qquad [5.6]$$

$$p_{dissolution,4°C} = \frac{(3.06 - 0.09)\ mole * 0.08314 \frac{bar\ dm^3}{K*mole} * 293.15K}{0.35 dm^3 - (3.06 - 0.09) mole * 0.0431\ dm^3 mole^{-1}} - \frac{2.303 bar\ dm^6 mol^{-2} * (3.06 - 0.09)^2 mole^2}{0.35^2 dm^6}$$

$$p_{dissolution,4°C} = 160.2\ bar \quad [5.7]$$

The effects of dissolubility and cooling add up to a “total” pressure reduction, based on the theoretical starting pressure of 165.6 bar.

The total pressure reduction (based on the theoretical starting pressure of 165.6 bar) then amounts to:

$$\Delta p_{4°C} = p_{start,20°C} - p_{dissolution,4°C} + p_{start,20°C} - p_{cooling,4°C} \quad [5.8]$$

$$\Delta p_{4°C} = (165.6 - 160.2 + 165.6 - 147.2)bar = \mathbf{23.8\ bar} \quad [5.9]$$

Simplifications have been made, since both processes were described separately. In reality, both processes occur in parallel and also influence each other. Nonetheless, the calculated values equal the experimental data in good approximation.

A “successful” hydrate formation is characterized by a pressure drop with simultaneous rise (peak) in temperature (marked by the vertical line in Figure 25). The temperature peak is caused by the exothermic nature of hydrate formation, which, in the beginning of the macroscopic formation phase, is faster and more intense than the temperature controlling thermostat can handle. As mentioned in chapter 11.1.3, only *induction times* were determined in these series of experiments, the *induction time* being marked by an increase in temperature by at least 0.1 °C during one minute.

Table 17 shows exemplarily the induction times of four series of experiments. Experiment 6 at 135 bar(g) was conducted to gain a higher statistical certainty because of the high variance in this series of measurement. “N. f.” in experiments 7 and 8 at 135 bar(g) means “no formation of gas hydrates during experimental time”. Table 18 shows the corresponding statistical parameters of all experiments with successful hydrate formation. All series of experiments were normally distributed and had no outliers according to the Dixon-Q-test (level of significance was 0.95). [84]

Table 17: Induction times, determination of „optimal“ parameters for high-pressure experiments [84]

Experimental conditions / series of measurement	Induction time [min]							
	1	2	3	4	5	6	7	8
160 bar(g) 4 °C	248	138	150	87	107	--	--	--
160 bar(g) 6 °C	158	110	139	108	105	--	--	--
135 bar(g) 4 °C	278	n. f.	2783	n. f.	1590	876	268	301
120 bar(g) 4 °C	2889	1888	641	1123	361	--	--	--

Table 18: Statistical data, determination of „optimal“ parameters for high-pressure experiments [84]

	Number of experiments	Mean [min]	Standard deviation [min]	Rel. standard deviation [%]	Minimum [min]	Median [min]	Maximum [min]	Normally distributed?	Outlier?
160 bar(g) 4 °C	5	146	62	42	87	138	248	yes	no
160 bar(g) 6 °C	5	124	23	19	105	110	158	yes	no
135 bar(g) 4 °C	8	1016	1009	99	268	588	2783	yes	no
120 bar(g) 4 °C	5	1381	1023	74	361	1123	2889	yes	no

Analysis of the results shows that the measurements conducted at 160 bar(g) possess the lowest mean deviation and therefore the “best” predictive accuracy for the induction time of all experiments shown. These experimental parameters seem to be a promising basis for the development of a hydrate prediction model in the system used.

The experiments conducted at 160 bar(g) and 6 °C possess an even lower standard deviation than those conducted at 160 bar(g) and 4 °C. This seems surprising, since the temperature driving force for hydrate formation is higher at 4 °C than at 6 °C, which should also be reflected in a reduced standard deviation. It should be noted, however, that the first experiment conducted at 4 °C has a very high induction time of 248 min, which greatly influences the mean induction time and standard deviation.

Also, 4 °C is a more realistic “field value” for the operation of deep-sea pipelines, since 4 °C is the water temperature in the relevant depth. Therefore, it is recommended to conduct experiments at 4 °C as future reference for inhibitor testing as well as the development of a prediction model.

The increase of the standard deviation in the experimental series at 135 and 120 bar(g) could be explained by the lower driving force of hydrate formation at lower pressures. So, phenomena like the presence of possible nucleation sites could have a stronger effect.

In any case, the experimental conditions at 135 resp. 120 bar(g) are deemed unsuitable for the development of a prediction model because of the high standard deviation.

Measurements showed that higher pressures lead to a decrease in standard deviation of the experiments. One possible explanation could be the higher driving force of hydrate formation at higher pressures so that effects like the distribution of nucleation sites have lower significance. [84]

6 Screening for determining s I inhibition suitability[2]

In this chapter, the high-pressure screening experiments to find suitable candidates for *s I* inhibition are shown and discussed.

6.1 Experimental procedure

After determining the optimal parameters (→chapter 5), numerous substances were investigated regarding their inhibition suitability for *s I* inhibition as well as their influence on *s I* hydrate formation in general. In the course of this thesis, a "new" and more accurate pressure transducer was installed to increase accuracy of measurements. This new pressure transducer was used in the experiments shown in this chapter (and further on). Details on modifications of equipment are shown and discussed in chapter 11.1.
The experimental procedure was analogous to that in chapter 5.1, but in addition, the tested substance was added in the water phase in concentrations of 1, 3 or 5 % wt. of water phase. For each concentration, at least 3 experiments were conducted. Fresh water was used in every experiment to avoid the so-called "memory effect" and also for better resemblance to the pipeline case.

Also, so-called *flammability tests* were carried out after the experiments. For this, a portion of formed hydrate was taken and it was tried to set the hydrate (or rather the included methane) on fire with a conventional lighter. Flammability of hydrates is a sign of high gas saturation as well as the ability to release the included gas and can give valuable information on the consistency of the formed hydrates. The flammability is evaluated together with the other qualitative signs for high gas saturation, meaning that hydrates with high gas saturation usually show strong "hissing" during decomposition as well as hydrate particles that "jump off" the hydrates because of the sudden release of gas.

The effects like hissing and jumping off were investigated in each experiment. However, flammability tests were not conducted when inhibiting substances that were flammable themselves were investigated. This could have caused misinterpretations and therefore, no flammability tests were carried out in these cases. [50, 98, 99]

[2] Reproduced in part with permission from [4]. Copyright [2016] American Chemical Society.

6.2 Results and discussion

In this chapter, the results of the *s I* screening at the conditions determined before (→ chapter 5.2; 160 bar(g) and 4 °C) are shown and discussed. At first, the determined induction times and parameters are shown for the tested substances as an overview. After that, phenomena are discussed.
The possible influence of functional molecular groups is discussed in detail in chapter 7, with a focus on the influence of OH-groups. After that, the "prototype experiments" are discussed in chapter 8.
It is to be mentioned that also more blind experiments have been conducted at the conditions of 160 bar(g) and 4 °C. This was also done after each modification of the reactor, as mentioned in chapter 11.1.

Figure 26 shows a sample experiment to illustrate again the evaluation of induction time and plug formation time. As defined in chapter 11.1.3, the induction time is the first increase in temperature by 0.1 °C within one minute with possible (slight) decrease in pressure, but not necessarily the formation of hard hydrate plugs. The plug formation time, however, is marked by a significant increase in stirrer torque M (15 or 25 Ncm, see also detailed definition in chapter 11.1.3). In some experiments, there were significant differences between induction time and plug formation time, in others they were identical. To account for this, the so-called "delay time" as difference between plug formation time and induction time, was defined and is also shown in the results tables of the following chapters.

The results shown in each chapter contain a table with the individual results of each experiment. Important parameters are shown, namely:

- the induction time t_{ind} [min];
- the plug formation time t_{pl} [min];
- the delay time ($t_{ind} – t_{pl}$) [min];
- the maximum torque during the experiment M_{max} [Ncm] as criterion for "hardness" / morphology of the formed hydrates;
- the stirrer switch-off time t_{St} [min] to account for turbulence changes during the course of the experiment;
- the induction pressure p_{ind} [bar(g)] (pressure at the time t_{ind});
- the plug formation pressure p_{pl} [bar(g)] (pressure at the time t_{pl});
- the delay pressure ($p_{pl} – p_{ind)}$ [bar]; it is defined contrary to the delay time, so that a positive value results);

- and a reference pressure after 1000 minutes experimental time p_{1000} [bar(g)] to gain insight into the overall hydrate formation rate of the experiment.

After that, a table with the statistical data (mean, standard deviation and coefficient of variation) on the above-mentioned parameters is shown for each experimental series (meaning that statistical analysis was conducted on all the experiments at a given concentration of a given inhibitor).

Then, induction times and plug formation times (as the “most important” parameters for evaluating inhibition potential of a given substance) are compared in graphical form.

Again, one important thing to mention is that in experiments with no gas hydrate formation (which also means ***good inhibition potential***), the induction and plug formation times were set as 4000 minutes, although the actual values were possibly much higher than that. So, the set time of 4000 minutes acts as a “worst case estimate for good inhibitors”.

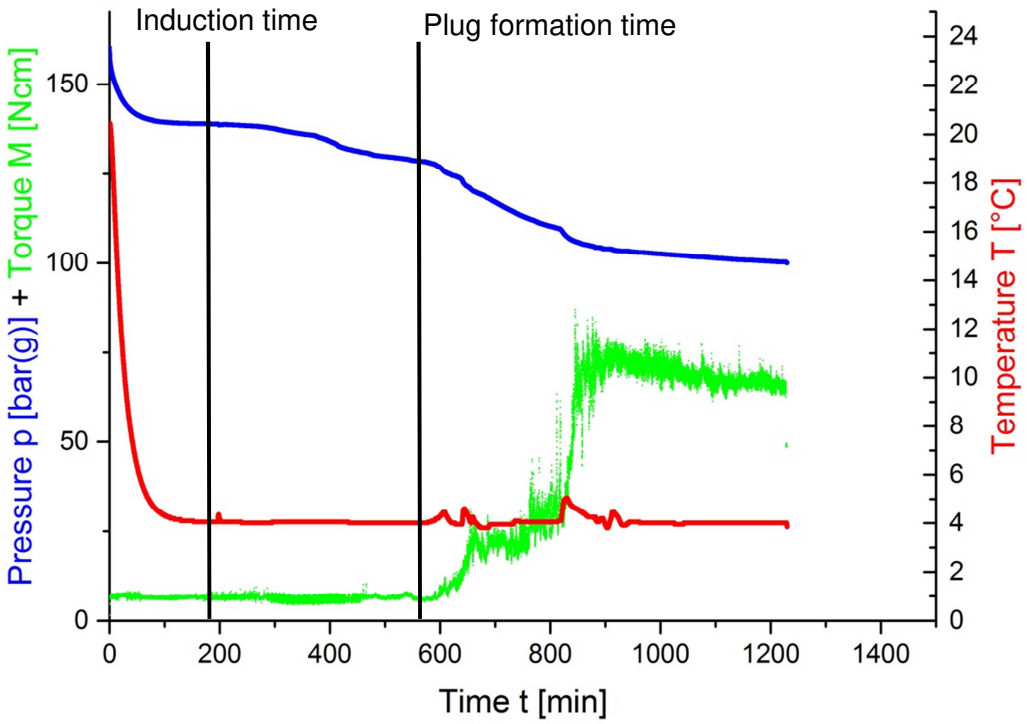

Figure 26: Sample experiment with induction time and plug formation time. Pressure and stirrer torque (left ordinate) as well as temperature (right ordinate) are plotted against time (abscissa). Induction time and plug formation time (as defined in chapter 11.1.3) are marked by vertical black lines.

6.2.1 Blind experiments / stirrer modifications

Table 19 shows the individual results of the “new” blind experiments after modification of the pressure transducer (BlindPT) as well as after installing the additional gas phase stirrer (BlindGPS), Table 20 shows the corresponding statistical data. It has to be mentioned that the BlindGPS experiments do have an additional stirrer in the gas phase but also contain the “normal” hollow shaft stirrer in the liquid phase that came to use in the other experiments.
The statistical data that are shown in all the following tables are explained briefly below:

- $\bar{x}$ is the arithmetic mean of a series of measurements;
- *s* is the standard deviation of a series of measurements;
- *s* [%] is the relative standard deviation of a series of measurements;
- and *v* is the coefficient of variation, which is defined as quotient of standard deviation and arithmetic mean.

Table 19: Individual results of experiments; Blind experiments / stirrer modifications[3]

Experiment	t_{ind}	t_{pl}	(t_{pl} - t_{ind})	M_{max}	t_{St}	p_{ind}	p_{pl}	(p_{ind} - p_{pl})	p_{1000}
	[min]			[Ncm]	[min]	[bar(g)]			
BlindPT-01	686	704	19	22.5	1239	138	137.8	0.2	122.3
BlindPT-02	126	126	0	10.8	214	139	139	0	-
BlindPT-03	671	863	192	143.4	1307	137.7	125	12.7	112.8
BlindPT-04	920	1123	203	21.4	1245	138.2	130.6	7.6	134.7
BlindGPS-01	684	684	0	120	1107	138.8	138.8	0	115
BlindGPS-02(2)	293	293	0	212.3	-	137.7	137.7	0	107
BlindGPS-03	193	193	0	100.4	1019	137.7	137.7	0	107.6
BlindGPSR-04	100	234	135	212.3	3943	139.1	130.5	8.6	98.3

[3] Reproduced in part with permission from [4]. Copyright [2016] American Chemical Society.

Table 20: Statistical data of experimental series; Blind experiments / stirrer modifications[4]

		No. of exp.	t_{ind}	t_{pl}	$(t_{pl} - t_{ind})$	M_{max}	t_{St}	p_{ind}	p_{pl}	$(p_{ind} - p_{pl})$	p_{1000}
			[min]			[Ncm]	[min]	[bar(g)]			
Blind PT	$\bar{x}$	4	601	704	104	49.53	1001	138.23	133.10	5.12	123.27
	s		336	422	109	62.81	526	0.56	6.55	6.17	10.98
	s [%]		56	60	105	127	52	0	5	120	9
	v		0.56	0.60	1.05	1.27	0.52	0.00	0.05	1.20	0.09
Blind GPS	$\bar{x}$	4	317	351	34	161.25	2023	138.33	136.18	2.15	106.98
	s		257	226	67	59.49	1663	0.73	3.82	4.30	6.83
	s [%]		81	64	200	37	82	1	3	200	6
	v		0.81	0.64	2.00	0.37	0.82	0.01	0.03	2.00	0.06

Table 21: Typical appearance of formed hydrates; BlindPT and BlindGPS

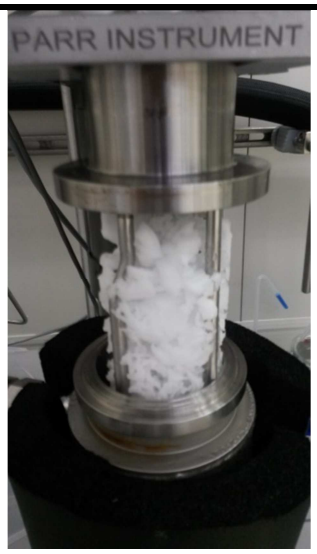	
BlindPT	BlindGPS[5]

The experiments showed that mean induction times and plug formation times are significantly reduced by addition of the gas phase stirrer. Also, in the experiments with additional GPS, there is no delay time in most experiments, meaning that when hydrates are formed, they are almost instantly hard in their morphology and form plugs instead of tiny nuclei that are distributed throughout the reactor.

[4] Reproduced in part with permission from [4]. Copyright [2016] American Chemical Society.

[5] Reproduced with permission from [4]. Copyright [2016] American Chemical Society.

The maximum stirrer torque also is significantly higher in the experiments with GPS, which is a sign for “harder” hydrates, or at least of more hydrates being formed inside the reactor so that the increase in stirrer torque carries more weight (more volume is occupied by hydrates, even if they would have the same “hardness” per volume area).
Experiments with high values for M_{max} also show lower values for p_{1000} than the other experiments. This does not seem surprising, since more methane inside the hydrates should of course lead to the formation of more stable (and hence “harder”) hydrates.

As can be seen in Table 21, differences between hydrates formed with and without GPS are also clearly visible in hydrate morphology. Experiments with GPS have a “flaky” appearance, which also is a sign of more gas saturation; also, the right picture above shows that hydrates already “jumped off” because of the high gas saturation and sudden decomposition when opening the reactor.
It should be mentioned that in the following, pictures of the formed hydrates are only shown when the morphology is “special”, meaning that interesting phenomena that deviate from “normal” hydrates, can be seen. Also, since different camera systems with different aspect ratios were used in the course of this work, pictures do not have the same size in all experiments shown. This was done to keep the “natural” aspect ratio in which pictures were taken and hence give the best quality pf pictures.

Induction and plug formation pressures do not show great differences between experimental series. However, it can be seen that there can be even a difference of 12 bar in delay pressure. Hence, hydrate nuclei could grow for a long time before an actual plug is formed.

The phenomenon of drastically reduced induction times when adding a stirrer to the gas phase also occurred in some of the low-pressure experiments and could be verified in the Parr 4568 reactor. Not only the transport at the gas-liquid interface, but also the turbulence in the gas phase therefore seems to have a great influence on hydrate formation.
This thesis is also supported by the very “hard” hydrates and the drastic increase in stirrer torque in the experiments with additional stirrer compared to the ones without. Also, hydrates in the experiments with added gas phase stirrer showed stronger “hissing” while decomposing at the end of experiments, thus having a higher gas saturation.
The higher gas saturation is also undermined by the lower p_{1000} values in the experiments with GPS, meaning that with GPS, pressure decreases more in the same time due to more methane being stored inside the formed hydrates.

All of this could be an indication for a transport- or diffusion-controlled dependency for saturation of the hydrates and therefore a confirmation of the “nucleation at the interface” theory. Further experiments, with e. g. only stirring the gas phase, could put this theory to evidence.
Also, a method for measuring the gas saturation of the hydrates inside of the reactor has to be developed. First steps to develop this method by introducing the p_{1000}-value as well as doing input and output gas-flow measurements, have been taken. It has to be noted that the theoretical capacity of the formed hydrates cannot be used because the focus of the experiments was on determination of induction times and therefore, experiments were often terminated after hydrate formation, without waiting for equilibrium (and therefore maximum saturation).

The “wavelike” reduction of pressure, which occurred in many experiments, could be caused by a “shredding” effect of the stirrer. Already formed hydrate nuggets are separated into smaller pieces and therefore, new surface area for hydrate formation is generated. This could indicate some kind of diffusion resistance effect (like postulated by [100]) and could also be a confirmation for the “nucleation at the interface” theory. Another possible explanation is the distribution of nucleation sites throughout the reactor. If there is only one critical nucleus for nucleation, curves are expected to look different than with many nucleation sites. This could also influence the temperature curves and lead to the strong temperature fluctuations.

Also, an interesting phenomenon occurred in “stirrer torque behavior”: there were experiments with strong and fast increase in stirrer torque with a “high peak” in stirrer torque. This is presumably caused by the formation of one “big” hydrate crystal, meaning that the growth phase starts at one point of the reactor because “one big critical nucleus” is formed.
However, it could also be possible that a “piece” of hydrate is formed that is of the same size as in other experiments, but somehow gets caught between the stirrer and other installations inside the reactor. This could result in a drastically increased stirrer torque although the formed hydrates would be of the same consistency. Although this seems unlikely compared to the formation of a “big” hydrate crystal, visual observation of the reactor’s inside, e. g. by means of an endoscope-camera-system, could be of great assistance to further clarify the phenomenon.

Figure 27 shows the graphical visualization of the induction and plug formation times to summarize the blind experiments.

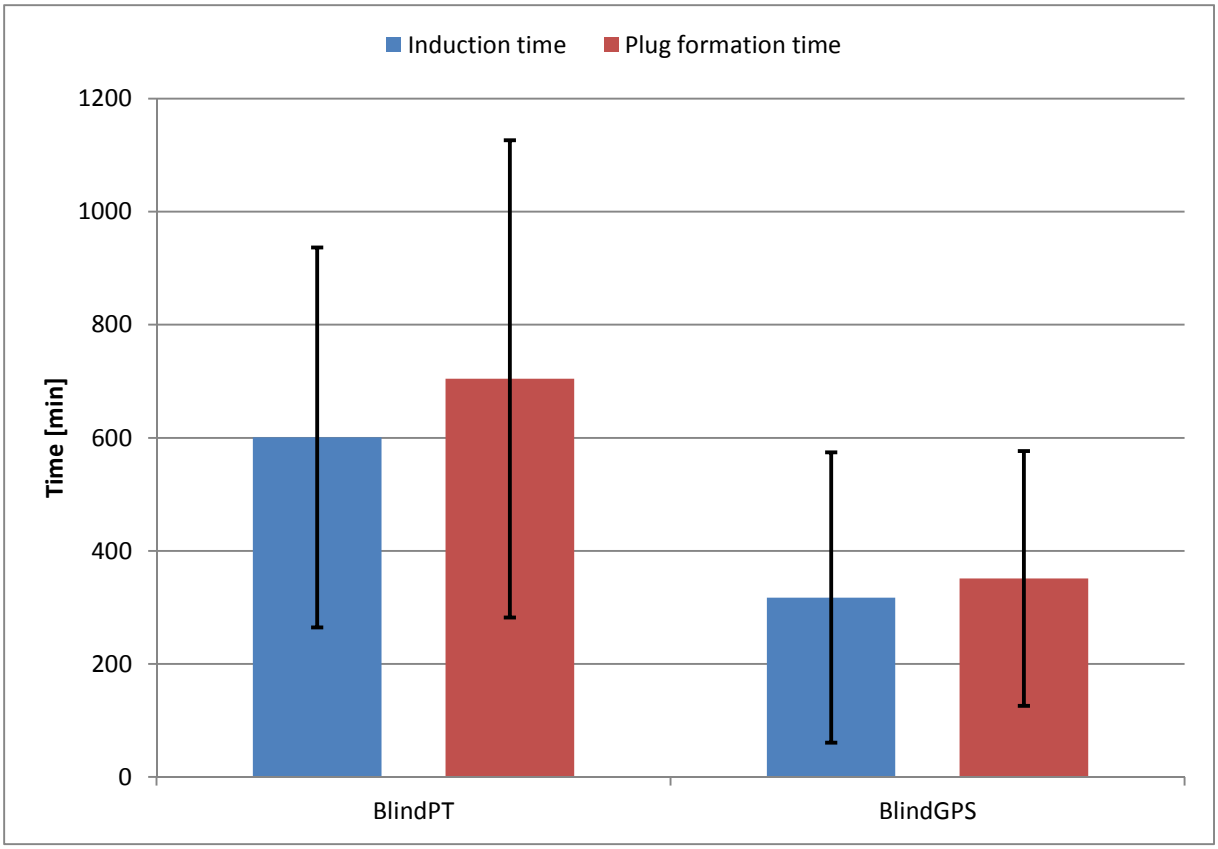

Figure 27: Comparison of t_{ind} and t_{pl}; Parr 4568, Blind experiments

In the course of the experiments with “high torque peak”, the torque peak often decreases with time, which could again indicate a “shredding” effect of the stirrer. Since the torque reduction in these experiments is often accompanied by strong temperature fluctuations, which could also indicate “new nucleation sites” for hydrate formation, this theory appears likely. In any case, high stirrer torques with strong torque fluctuations often correlate with strong fluctuations in temperature.

One important point to understand the temperature fluctuations is also given in the experimental setup: the thermostat has a target temperature of 4 °C that it tries to keep constant under all circumstances. So, the strong fluctuations also with temperature falling, is partly caused by the “countersteering effect” of the thermostat, meaning the cooling that gets stronger with increasing temperature inside the reactor.

In all experiments, temperature fluctuations seem to strongly depend on stirrer frequency, which also supports the “shredding theory” mentioned above. In some experiments, the stirrer was switched off to prevent mechanical damage, which is directly reflected in a reduction of temperature fluctuations. Also, the rate of pressure reduction decreases drastically when the stirrer is switched off, even when hydrate formation is already taking place. The effect of phase boundary transport seems to be lower than the effect of the stirrer.

6.2.2 Tylose H20P2

After the “new” blind experiments, the screening regarding *s I* inhibition suitability began. The first substance which entered high-pressure experiments was “Tylose H20P2”. It has to be mentioned that after the measurements with 1, 3 and 5 % wt. of H20P2, the additional gas phase stirrer was installed (see above). Therefore, the graphical comparison of substances versus blind experiments is split in two parts: Figure 28 shows the experimental series of 1, 3 and 5 % of H20P2 in comparison to the “BlindPT” experiments, Figure 29 shows the other tested substances in comparison to the “BlindGPS” experiments, beginning with “H20P2 0.1 %”.

First, the experimental data are shown in tabular form, then, phenomena are mentioned and discussed, the chapter concludes with a graphical visualization in Figure 28 and Figure 29.
Table 22 shows the individual results for “Tylose H20P2”, Table 23 the corresponding statistical data.

Table 22: Individual results of experiments; H20P2

	t_{ind}	t_{pl}	(t_{pl} - t_{ind})	M_{max}	t_{St}	p_{ind}	p_{pl}	(p_{ind} - p_{pl})	p_{1000}
	[min]			[Ncm]	[min]	[bar(g)]			
H20P2-1%-01	244	701	456	51.4	-	138.7	126.1	12.6	113.1
H20P2-1%-02	910	910	0	48.8	1566	138.1	138.1	0	134
H20P2-1%-03	1148			7.2	-	138.7	138.7	0	138.8
H20P2-3%-01	452	452	0	63.5	1347	138.3	138.3	0	115.5
H20P2-3%-02	598	598	0	51.6	1185	139.3	139.3	0	116.4
H20P2-3%-03	2504	2504	0	53.1	4083	139.5	139.5	0	139.8
H20P2-3%-04	2136	2136	0	55.9	2535	139.2	139.2	0	139.5
H20P2-5%-01	755	755	0	112.3	1745	140.8	140.8	0	123.6
H20P2-5%-02	546	546	0	85.4	5418	141	141	0	123.2
H20P2-5%-03	1934	1934	0	38.7	2725	141.8	141.8	0	141.9
H20P2-0.1-01	352	352	0	212.3	1072	137.4	137.4	0	104.7
H20P2-0.1-02	164	164	0	86.8	4076	139.2	139.2	0	98.5
H20P2-0.1-03	668	668	0	80	1677	137.6	137.6	0	105.2
H20P2-0.1-04	82	82	0	82.5	4060	140.5	140.5	0	101.3

Table 23: Statistical data of experimental series; H20P2

		No. of exp.	t_{ind}	t_{pl}	(t_{pl} - t_{ind})	M_{max}	t_{St}	p_{ind}	p_{pl}	(p_{ind} - p_{pl})	p_{1000}
			[min]			[Ncm]	[min]	[bar(g)]			
H20P2-1%	$\bar{x}$	3	767	920	152	35.80	1566	138.50	134.30	4.20	128.63
	s		468	224	264	24.80	-	0.35	7.11	7.27	13.66
	s [%]		61	24	173	69	-!	0	5	173	11
	v		0.61	0.24	1.73	0.69	-	0.00	0.05	1.73	0.11
H20P2-3%	$\bar{x}$	4	1423	1423	0	56.03	2288	139.08	139.08	0.00	127.80
	s		1049	1049	0	5.29	1340	0.53	0.53	0.00	13.69
	s [%]		74	74	-	9	59	0	0	-	11
	v		0.74	0.74	-	0.09	0.59	0.00	0.00	-	0.11
H20P2-5%	$\bar{x}$	3	1078	1078	0	78.80	3296	141.20	141.20	0.00	129.57
	s		748	748	0	37.24	1902	0.53	0.53	0.00	10.68
	s [%]		69	69	-	47	58	0	0	-	8
	v		0.69	0.69	-	0.47	0.58	0.00	0.00	-	0.08
H20P2-0.1	$\bar{x}$	4	317	317	0	115.40	2721	138.68	138.68	0.00	102.43
	s		260	260	0	64.66	1575	1.46	1.46	0.00	3.14
	s [%]		82	82	-	56	58	1	1	-	3
	v		0.82	0.82	-	0.56	0.58	0.01	0.01	-	0.03

Table 24 shows photos that were taken of the formed hydrates in each series of experiments.

Table 24: Special phenomena in hydrate morphology; Tylose H20P2

 H20P2-1%	 H20P2-3%
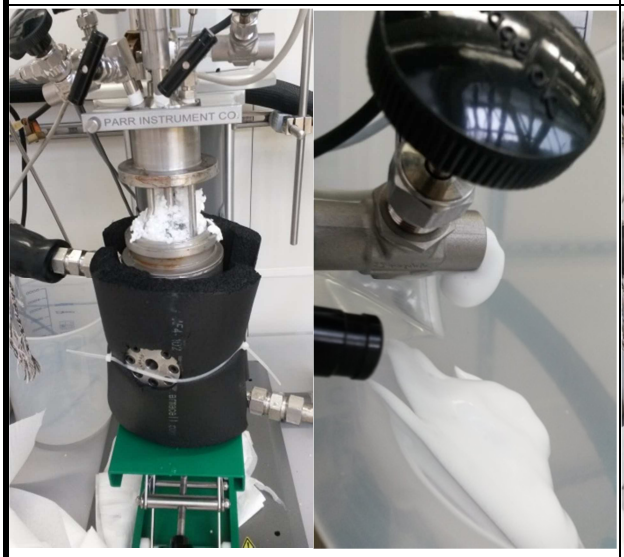 H20P2-5%	 H20P2-0.1%

Induction and plug formation times seem to be slightly higher when 1 % of H20P2 is present. Formed hydrates were very “foamy” in consistence, which is also indicated in the M_{max} values. Pressure did not decrease very much, which could also be caused by formation of foam. In the third experiment with 1 % wt. the induction time could be clearly seen in the temperature curve, but there was no plug formation time detected because the M_{max} value stayed too low.

With 3 % of H20P2 present, almost the same observations can be made, but the torque values are higher, which could indicate differences in the formed morphology of the hydrates.

This can also be seen in Table 24, where there is a clear indication that “hard” hydrates are formed at the bottom (and hence influence stirrer torque).

At 5 % wt. observations are again quite similar but torque values are even higher (in 2 out of 3 experiments).

With 0.1 % of H20P2 present, observations are almost the opposite. Induction and plug formation times are low (in the range of the “BlindGPS” values or even lower), the formed hydrates are hard (though lower than the “BlindGPS” experiments) and the p_{1000} values indicate that the formed hydrates contain a lot of methane. This was also confirmed by the morphology; hydrates were again very “flaky”, “jumped off” the stirrer and even were the first ones that tested positive for flammability (see Table 24).

There also was an increasing occurrence of foam with increasing concentration of Tylose in parallel with the above-mentioned changes in hydrate morphology, which could indicate that Tylose molecules not only act as inhibitor and prevent hydrate cages from forming, but also that the molecules are included in newly formed structures, like “Tylose-hydrate complexes”. The foam also “came out” the reactor during depressurization in the end of experiments; this phenomenon intensified with increasing concentrations of H20P2 (see Table 24).

Also, the strong promoting effect of small amounts of Tylose could indicate the integration of Tylose inside such structures and that Tylose molecules act as nucleation starters for hydrate formation in low concentration. Tylose could act as “normal” guest in hydrates, but form different structures than *s I* or *s II*, too. These structures This could also be the case since crystallization rate in crystallization processes strongly depends on the structure of the formed crystals [2], which could also be an explanation of the strong promoting effects of H20P2 at 0.1 % wt.. However, these structures would have to be “bigger” than conventional hydrate structures regarding their cage sizes, since Tylose is a big molecule that could not simply be included into “normal” hydrate structures.

Experiments showed that Tylose can delay hydrate formation in higher concentrations, but causes the formation of very high-saturated and hard hydrates when only used in small amounts (0.1 % wt.). This could mean that Tylose can be categorized as a THI, which only inhibits in high concentrations, but acts as a promoter at under-inhibited conditions. This “under-inhibition” is also a common problem in industrial applications [2, 7]. Also, in case of KHI, concentration plays a critical role in performance.

The formation of “foam” could be seen as a “small success” for an inhibitor, since foam could still be transportable in a pipeline, even though hydrate formation was not totally suppressed.

In any case, further investigation of the formed structures, e. g. via Raman spectroscopy could help to gain insights. In this context, experiments at additional concentrations of Tylose make sense to further understand the concentration dependencies and / or tendencies of different formed morphologies. Also, the influence of THF on Tylose-high-pressure experiments or mixtures of only Tylose and THF should be investigated further.

The course of hydrate formation experiments should also be observed visually to check if the formation of foam is the “end product of reaction” or if maybe there is some kind of oscillating behavior with foam being formed and converted to “hard” hydrates again and again.

In conclusion, it can be said that Tylose H20P2 is not recommended as pipeline inhibitor because of the promoting effect at low concentrations.

6.2.3 Glycerol

The next inhibitor tested in the high-pressure experiments was Glycerol. Again, individual results and statistical data are shown in form of tables, specific characteristics are shown in photos and a graphical comparison of induction and plug formation times to the corresponding “Blind” experiments is shown in Figure 29.

Table 25 shows the individual results for Glycerol, Table 26 the corresponding statistical data.

Table 25: Individual results of experiments; Glycerol

	t_{ind}	t_{pl}	(t_{pl} - t_{ind})	M_{max}	t_{St}	p_{ind}	p_{pl}	(p_{ind} - p_{pl})	p_{1000}
	[min]			[Ncm]	[min]	[bar(g)]			
Gly-1%-01	221	221	0	31.4	343	131	131	0	110.3
Gly-1%-02	543	674	132	164.5	4107	138.1	127.7	10.4	103.6
Gly-1%-03	154	343	189	79.7	1579	138.4	129.5	8.9	106.2
Gly-1%-04	733	855	122	93.7	1150	138	130.7	7.3	116.1
Gly-3%-01	231	435	204	121.6	4096	139	130.6	8.4	99.6
Gly-3%-02	519	519	0	183.3	1027	128.8	128.8	0	102.4
Gly-3%-03	1666	2003	336	116.4	2683	139.4	126.6	12.8	138.9
Gly-3%-04	147	305	158	75.5	1307	139.4	130.8	8.6	99.9
Gly-5%-01	201	530	328	84.3	-	139.3	128.5	10.8	102.4
Gly-5%-02	107	539	432	92.3	1578	139.9	129.2	10.7	102.6
Gly-5%-03	171	505	334	168.7	1284	139.2	127.1	12.1	106.1

Table 26: Statistical data of experimental series; Glycerol

		No. of exp.	t_{ind}	t_{pl}	(t_{pl} - t_{ind})	M_{max}	t_{St}	p_{ind}	p_{pl}	(p_{ind} - p_{pl})	p_{1000}
			[min]			[Ncm]	[min]	[bar(g)]			
Gly-1%	$\bar{x}$	4	413	523	111	92.33	1795	136.38	129.73	6.65	109.05
	s		273	293	80	55.02	1625	3.59	1.50	4.61	5.45
	s [%]		66	56	72	60	91	3	1	69	5
	v		0.66	0.56	0.72	0.60	0.91	0.03	0.01	0.69	0.05
Gly-3%	$\bar{x}$	4	641	815	175	124.20	2278	136.65	129.20	7.45	110.20
	s		702	796	139	44.47	1411	5.24	1.95	5.37	19.17
	s [%]		110	98	79	36	62	4	2	72	17
	v		1.10	0.98	0.79	0.36	0.62	0.04	0.02	0.72	0.17
Gly-5%	$\bar{x}$	3	160	525	365	115.10	1431	139.47	128.27	11.20	103.70
	s		48	18	58	46.59	208	0.38	1.07	0.78	2.08
	s [%]		30	3	16	40	15	0	1	7	2
	v		0.30	0.03	0.16	0.40	0.15	0.00	0.01	0.07	0.02

Table 27: Special phenomena in hydrate morphology; Glycerol

Gly-1%

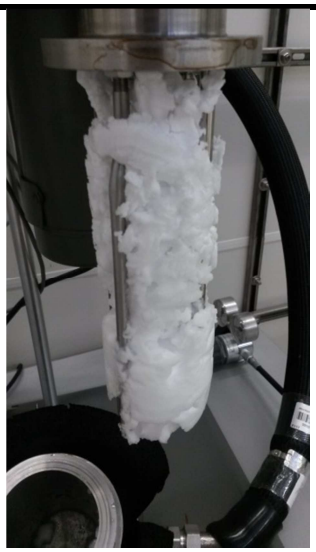

Gly-3%

Gly-5%

With 1 % wt. of Glycerol present, there seems to be a slightly inhibiting effect regarding induction and plug formation times. It is noticeable that there occurs a delay time in 3 out of 4 experiments, meaning that hydrate formation seems to start by slowly forming nuclei with no

significant increase in torque in the beginning of experiments. However, the M_{max} values show that torques are high, at least in long-running experiments, although lower than in the blind experiments. Pressures after 1000 minutes of experimental time are comparable to those in the blind experiments.
The morphology is quite noticeable since there seem to be two different “areas” inside the reactor: the upper part of the formed hydrates (above the reactor’s liquid phase) are “flaky” and seem to have high gas saturation; the lower part, however, seems sticky, almost as if “glued together” and seems more like “wet snow”. This was observed at all concentrations of glycerol and can be seen in Table 27. These different areas are also formed with 3 and 5 % wt. of Glycerol present. In all experiments, the “lower” hydrates were very difficult to remove from the stirrer axis.

At 3 % wt. there seems to be an inhibiting effect, at least in 2 out of 4 experiments. Again, delay times occur in most experiments. M_{max} and p_{1000} values are in the range of the blind experiments, but again, different hydrate morphologies are formed depending on the height inside the reactor.

At 5 % wt. Glycerol could act as a promoter regarding induction times, but regarding plug formation times, they seem to be in the range of blind experiments or even higher. There are delay times in every experiment, all of them even longer than the induction times, which could indicate a really long “phase of slow formation of hydrate nuclei”. M_{max} and p_{1000} values are comparable to those in the blind experiments.

Hydrates in the lower area were non-flammable in all of the experiments; however, some of the “upper” hydrates were tested positive for flammability (at 3 and 5 % wt.).

The “wet snow morphology” that all of the hydrates in the glycerol experiments showed could indicate that glycerol acts as some kind of “glue” and somehow forms new structures of hydrates. This could also be an explanation for the high stirrer torque values in some of the experiments.

To find out why the hydrates have different morphology depending on their height inside the reactor as well as on the “inside” / near the agitator shaft, the amount of glycerol in each “area” has to be measured. Again, Raman measurements of the formed hydrate structures are recommended to find out, if *s I*, *s II* or some other structures are formed and likewise, how hydrates are influenced by glycerol. Also, it could be investigated, if the different formed

morphology types (“upper” and “lower” hydrates in the reactor) have different composition or dissociation times as well as gas saturation. This could also help to clarify if the non-flammability of the “lower” hydrates is caused by lower gas saturation in these hydrates or if the “shell” of the lower hydrates is so hard, that dissociation of trapped gas to the outside is rendered impossible.

In any case, glycerol is not recommended as an inhibitor in pipelines, until the “glue” effect is fully understood, since the formed hydrates are very hard and the risk of pipeline damage therefore would be very high.

6.2.4 Potassium thiocyanate

The next substance that was investigated was KSCN. Because of its ionic character and the resulting “charges”, it was thought possible that KSCN could interact with the hydrogen bonds of gas hydrates

Table 28 shows the individual results for KSCN, Table 29 the corresponding statistical data. Graphical comparison with the corresponding “blind” experiments is again done in Figure 29.

Table 28: Individual results of experiments; KSCN

	t_{ind}	t_{pl}	$(t_{pl} - t_{ind})$	M_{max}	t_{St}	p_{ind}	p_{pl}	$(p_{ind} - p_{pl})$	p_{1000}
	[min]			[Ncm]	[min]	[bar(g)]			
KSCN-1%-01	187	187	0	68.9	1251	139.8	139.8	0	109.5
KSCN-1%-02	69	209	141	54.3	-	141	132.4	8.6	108
KSCN-1%-03	162	323	162	50.2	-	140.9	131.8	9.1	113.7
KSCN-3%-01	238	445	207	194.3	1199	135	123.5	11.5	102.1
KSCN-3%-02	94	434	340	71.3	-	142.3	129.5	12.8	110.9
KSCN-3%-03	459	761	303	73.7	-	136.8	124.9	11.9	105.2
KSCN-5%-01	1015	1535	520	212.3	-	137.7	128.4	9.3	137.7
KSCN-5%-02	3572	4043	471	27.3	-	138.4	127.3	11.1	138.4
KSCN-5%-03	3450	3957	507	38.6	-	139.2	126.4	12.8	139.3

Table 29: Statistical data of experimental series; KSCN

		No. of exp.	t_{ind}	t_{pl}	$(t_{pl} - t_{ind})$	M_{max}	t_{St}	p_{ind}	p_{pl}	$(p_{ind} - p_{pl})$	p_{1000}
			[min]			[Ncm]	[min]	[bar(g)]			
KSCN-1%	$\bar{x}$	3	139	240	101	57.80	1251	140.57	134.67	5.90	110.40
	s		62	73	88	9.83	-	0.67	4.46	5.12	2.95
	s [%]		45	31	87	17	-	0	3	87	3
	v		0.45	0.31	0.87	0.17	-	0.00	0.03	0.87	0.03
KSCN-3%	$\bar{x}$	3	264	547	283	113.10	1199	138.03	125.97	12.07	106.07
	s		184	186	69	70.33	-	3.80	3.14	0.67	4.46
	s [%]		70	34	24	62	-	3	2	6	4
	v		0.70	0.34	0.24	0.62	-	0.03	0.02	0.06	0.04
KSCN-5%	$\bar{x}$	3	2679	3178	499	92.73	-	138.43	127.37	11.07	138.47
	s		1442	1424	26	103.70	-	0.75	1.00	1.75	0.80
	s [%]		54	45	5	112	-	1	1	16	1
	v		0.54	0.45	0.05	1.12	-	0.01	0.01	0.16	0.01

With 1 % wt. of KSCN present, there seems to be a promoting effect regarding induction times as well as plug formation times. Delay times occur in 2 out of 3 experiments. M_{max} are lower than in the BlindGPS experiments, which indicates the formation of slightly softer hydrates (although they would still be too hard for safe pipeline operation). Pressures after 1000 minutes experimental time are in the range of or even slightly higher than in the blind experiments. Induction pressures are slightly higher than in the blind experiments, which could indicate that less methane is incorporated into the formed hydrates. Together with the promoting effect regarding formation times, these phenomena (M_{max} as well as p_{ind} values) could indicate that KSCN is somehow incorporated into the hydrate cages. This has to be clarified using further methods of investigation, e. g. spectroscopic measurements of the formed hydrate structures.

With 3 % wt. of KSCN present, induction times seem slightly reduced compared to the blind experiments, though plug formation times seem slightly higher. Also, there are long delay times in all of the experiments. Maximum torques are lower than in the blind experiments,

with one exception in the first experiment, where the M_{max} value is nearly at 200 Ncm. Pressure values are in the range of the blind experiments.

At 5 % wt. KSCN seems to have a strong inhibiting effect regarding induction times as well as plug formation times. Also, the delay times are even longer than at 3 % wt.. Stirrer torques are significantly lower than in the blind experiments, with the exception of the first experiment, where the torque is in the range of the blind experiments. Pressures after 1000 minutes of experimental time are of course a lot higher than in the BlindGPS experiments, since hydrate formation started after more than 1000 minutes in all experiments.

Experiments with KSCN support the hypothesis that KSCN could inhibit in a thermodynamic way and / or form different hydrate structures, like “KSCN-hydrate-complexes”, as was also mentioned for other substances tested above.
All experiments at 1, 3 and 5 % wt. show the “wavelike” pressure curves that also occurred in other experiments. This could be caused by the formed hydrates being again crushed by the stirrer, which could indicate some kind of “brittleness” of the formed hydrates. This “brittleness” could also be indicated in the reduced torque values in most experiments.

The “multiple starts” of hydrate formation (formation→crushing→formation…) could also be reflected by the strong fluctuations in temperature curves during experiments.
There seems to be a connection between the amplitudes of stirrer torque and the amplitudes of temperature peaks: in the experiments at 5 % wt. the torque amplitude is lower in the mean, which is also reflected in the temperature peaks: the peaks are “smaller” as well. “Softer” hydrates are possibly more difficult to crush than the brittle ones in the “3 % series”. Also, the possibility of a completely changed hydrate structure in presence of (5 %) KSCN is supported again.

All in all, KSCN is not fully recommended as a pipeline inhibitor, because from the current state of knowledge, under-inhibition could again cause a promoting effect and lead to even faster blockage of pipelines.

6.2.5 Iron(II) sulfate heptahydrate

The next substance tested for its inhibition suitability was iron in form of Iron(II) sulfate heptahydrate. As mentioned in chapter 11.1.2, the idea for testing it came up in the course of the “long-induction-times-after-standstill” problem. Due to the ionic character and hence the strong “charges”, interaction with hydrogen bonds should again be possible. It has to be mentioned that only low concentrations of iron (0.1 % wt.) were investigated in the course of this work (due to the idea of iron ions somehow being “washed out” during standstill, see chapter 11.1.2).

Table 30 shows the individual results of experiments, Table 31 the corresponding statistical data; graphical comparison with the BlindGPS experiments is also shown in Figure 29.

Table 30: Individual results of experiments; Iron(II) sulfate heptahydrate

	t_{ind}	t_{pl}	$(t_{pl} - t_{ind})$	M_{max}	t_{St}	p_{ind}	p_{pl}	$(p_{ind} - p_{pl})$	p_{1000}
	[min]			[Ncm]	[min]	[bar(g)]			
Iron-0.1%-01	76	224	148	87.3	-	138.9	128.1	10.8	97.1
Iron-0.1%-02	4000	4000	0	12.6	-	no h.f.	no h.f.	no h.f.	121.7
Iron-0.1%-03	692	834	142	64.3	-	138.1	133.1	5	117.9
Iron-0.1%-04	3000	3000	0	10.5	-	no h.f.	no h.f.	no h.f.	138.9
Iron-0.1%-05	151	298	148	139.7	-	139	132.3	6.7	99.7

Table 31: Statistical data of experimental series; Iron(II) sulfate heptahydrate

		No. of exp.	t_{ind}	t_{pl}	$(t_{pl} - t_{ind})$	M_{max}	t_{St}	p_{ind}	p_{pl}	$(p_{ind} - p_{pl})$	p_{1000}
			[min]			[Ncm]	[min]	[bar(g)]			
Iron 0.1 %	$\bar{x}$	5	1584	1671	88	63	-	139	131	8	115
	s		1801	1723	80	54	-	0	3	3	17
	s [%]		114	103	91	86	-	0	2	40	15
	v		1.14	1.03	0.91	0.86	-	0.00	0.02	0.40	0.15

Table 32: Special phenomena in hydrate morphology; Iron(II) sulfate heptahydrate

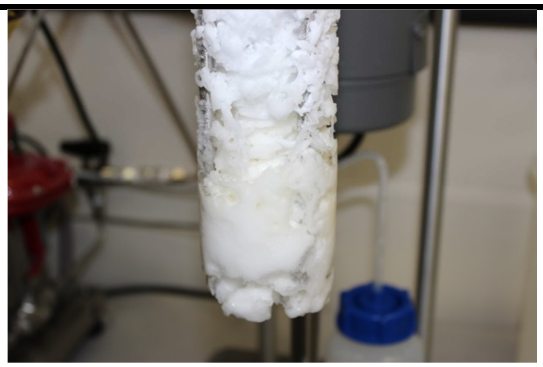	
Iron 0.1%_a	Iron 0.1%_b

Iron(II) sulfate heptahydrate shows strongly mixed behavior when present at 0.1 % wt.. 2 out of 5 experiments show strong inhibiting tendencies regarding induction and plug formation times as well as stirrer torque and pressure. One thing jumping to mind is that experiment 02 has a slightly lower p_{1000} value than expected, although there were no hydrates formed and no temperature increase detectable. It still has to be clarified what caused this behavior.

Experiments 01 and 05 showed very short induction times, plug formation times were in the range of the blind experiments. M_{max} values were slightly lowered compared to the blind experiments, pressure after 1000 minutes as well.
Experiment 03 had a slightly longer induction time (but still comparable to BlindGPS experiment 01), and slightly longer plug formation time.
An interesting aspect is that in experiments with delay times, the delay time was around 140 to 150 minutes each time, which could indicate that the delay is caused by the same phenomenon.

Regarding morphology, an interesting phenomenon occurred. When adding iron to the water, the water changed its color to yellow. After hydrates had been formed, there seemed to be some kind of “iron separation” throughout the reactor: in the lower part of the reactor, hydrates still had yellow areas, in the upper part, they were white; leftover water in the reactor was still yellow (see Table 32). The interesting part to find out in future experiments is if iron (or sulfate) is somehow included into the hydrate structure. Otherwise, this could be interesting to know for further clarifying the formation mechanism as well as for industrial applications, e. g. in deionizing water (which is already done by hydrates for sea water).

All in all, Iron(II) sulfate heptahydrate is recommended for further research with additional methods of investigation as well as in varying concentrations.

Also, additional iron-containing substances should be investigated to clarify if the observed effects are caused by the iron or the sulfate ions (or both).

6.2.6 Conclusion

To conclude this chapter, Figure 28 and Figure 29 show the graphical comparison of the induction and plug formation times of all tested substances as a summary.

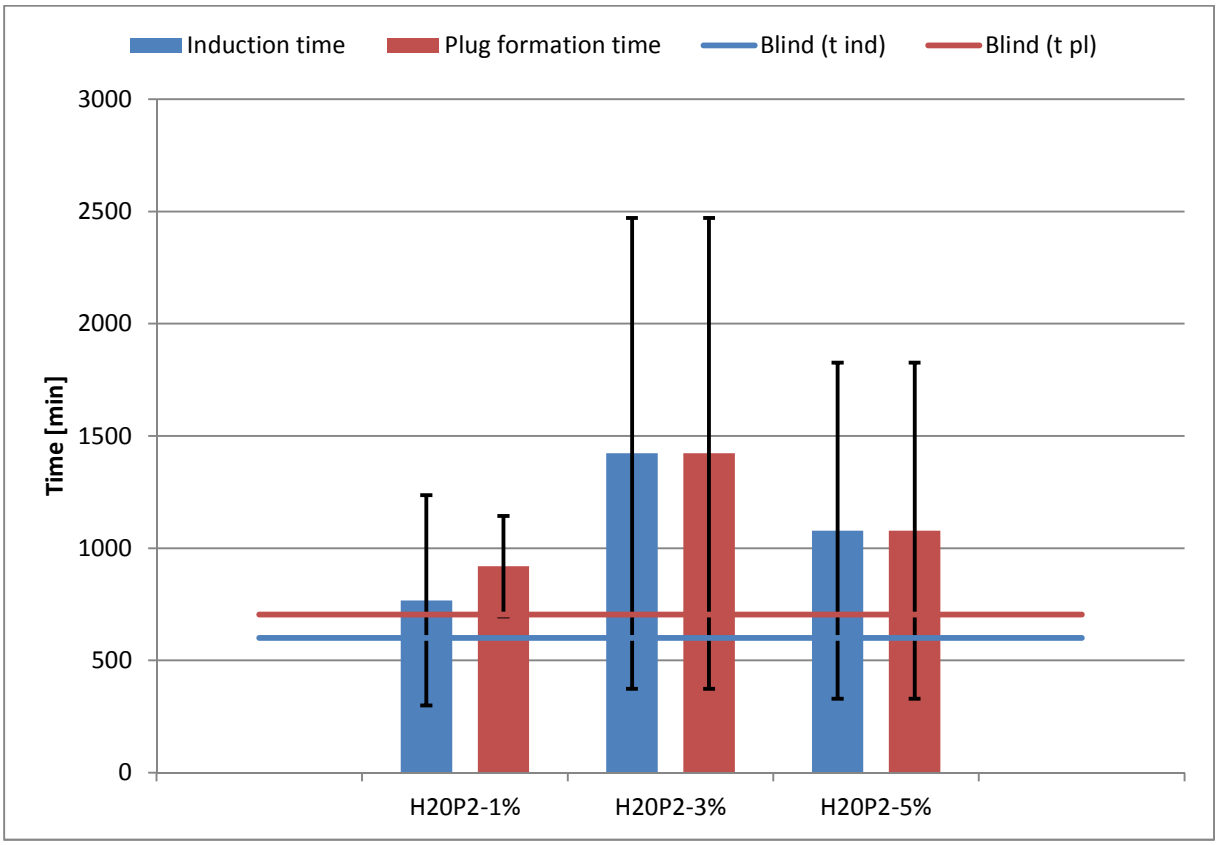

Figure 28: Comparison of t_{ind} and t_{pl}; Parr 4568, Screening, Part 1

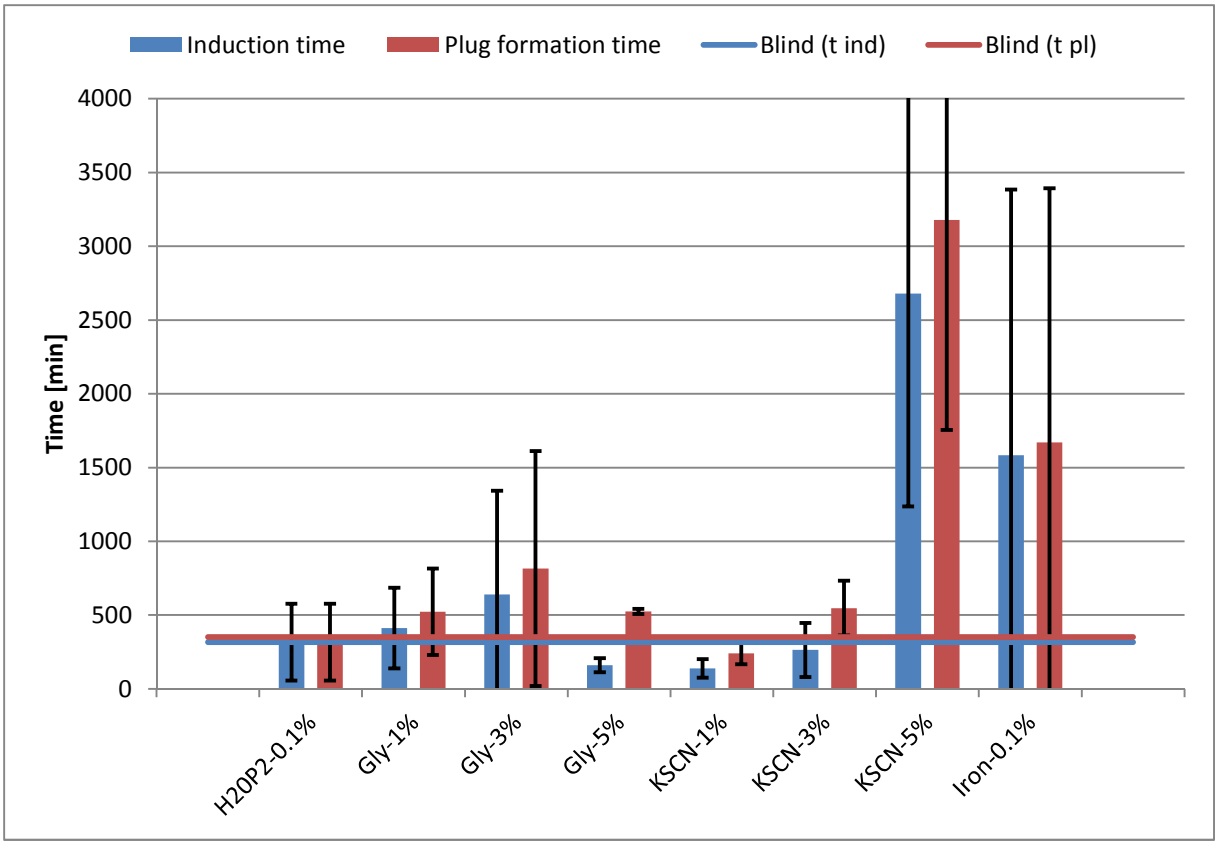

Figure 29: Comparison of t_{ind} and t_{pl}; Parr 4568, Screening, Part 2

The tested substances did not always show the same behavior for *s I* inhibition as for *s II* inhibition. Tetrahydrofuran seems to not only act as promoter and *s II* forming guest molecule, but also to interfere with the hydrate formation mechanism in a still unknown manner. Substances that can act as promoter without THF present (e. g. Gly at higher concentrations, KSCN at lower concentrations), show inhibitive tendencies when THF is present. One possible explanation is that THF interacts with the functional groups in some of the tested molecules or maybe even forms totally different hydrate-THF-functional-group „mixed structures“. This also applies for the substances tested in the following chapters, especially “THF-OH-group-interactions” are probable.

Also, the possibility that different hydrate structures are formed through different mechanisms still cannot be fully excluded. Further experiments, e g. with propane or other *s II* forming guests, without presence of THF, have to be conducted in the Parr 4568 reactor, to clarify this.

7 Influence of functional molecular groups on GH formation [4][6]

Because of the concentration-dependent phenomena in the experiments with glycerol (see chapter 6), the idea came up to investigate substances with an increasing number of OH-groups per volume element, like a "homologous series of OH-groups". Goal of these investigations was to find out if there is a correlation between the number of OH groups per volume element and influences on gas hydrate formation. The substances chosen for these investigations were ethylene glycol (EG), D(+)-glucose (DGluc) and myo-Inositol (Ino).

Molecular structures of these substances are shown in Table 5.

7.1 Experimental procedure

The experimental procedure was identical to chapter 6.1.

7.2 Results and discussion

Again, individual results and corresponding statistical data are shown in tabular form for each substance. A graphical comparison of induction and plug formation times of all substances against blind experiments is shown in Figure 30.

7.2.1 Ethylene glycol

Table 33 shows the individual results of experiments with Ethylene glycol, Table 34 the corresponding statistical data.

[6] Reproduced with permission from [4]. Copyright [2016] American Chemical Society.

Table 33: Individual results of experiments; Ethylene glycol

	t_{ind}	t_{pl}	$(t_{pl} - t_{ind})$	M_{max}	t_{St}	p_{ind}	p_{pl}	$(p_{ind} - p_{pl})$	p_{1000}
	[min]			[Ncm]	[min]	[bar(g)]			
EG-1%-01	270	421	151	143.4	1381	139.1	129	10.1	104
EG-1%-02	211	211	0	113	-	131.7	131.7	0	100.1
EG-1%-03	202	202	0	85	-	133	133	0	97.6
EG-1%-04	206	206	0	122.9	-	132.1	132.1	0	101.6
EG-3%-01	110	385	275	75.7	-	140.8	128.7	12.1	102.9
EG-3%-02	358	358	0	78.6		126.9	126.9	0	105.5
EG-3%-03	82	274	193	211.4	584	141.1	130.5	10.6	111.7
EG-5%-02	406	949	543	54.4	1272	138	116.8	21.2	113.1
EG-5%-03	192	382	190	212.3	1283	137.2	124.5	12.7	102.8
EG-5%-04	925	991	66	11.4	1245	137.7	137.1	0.6	136.8

Table 34: Statistical data of experimental series; Ethylene glycol

		No. of exp.	t_{ind}	t_{pl}	$(t_{pl} - t_{ind})$	M_{max}	t_{St}	p_{ind}	p_{pl}	$(p_{ind} - p_{pl})$	p_{1000}
			[min]			[Ncm]	[min]	[bar(g)]			
EG-1%	$\bar{x}$	4	222	260	38	116.08	1381	133.98	131.45	2.53	100.83
	s		32	107	75	24.28	-	3.46	1.72	5.05	2.68
	s [%]		14	41	200	21	-	3	1	200	3
	v		0.14	0.41	2.00	0.21	-	0.03	0.01	2.00	0.03
EG-3%	$\bar{x}$	3	183	339	156	121.90	584	136.27	128.70	7.57	106.70
	s		152	58	141	77.52	-	8.11	1.80	6.60	4.52
	s [%]		83	17	91	64	-	6	1	87	4
	v		0.83	0.17	0.91	0.64	-	0.06	0.01	0.87	0.04
EG-5%	$\bar{x}$	3	508	774	266	92.70	1267	137.63	126.13	11.50	117.57
	s		377	340	248	105.78	19	0.40	10.25	10.35	17.43
	s [%]		74	44	93	114	2	0	8	90	15
	v		0.74	0.44	0.93	1.14	0.02	0.00	0.08	0.90	0.15

When 1 % of EG is present, induction and plug formation times seem slightly reduced compared to the BlindGPS experiments. Only one experiment showed a delay time. Maximum stirrer torques and pressures after 1000 minutes are in the range of or even slightly lower than those in the blind experiments. All these phenomena could again indicate

that EG is somehow incorporated into the hydrates or forms some kind of “EG-THF-hydrate complex”.
The formed hydrates also seem to be brittle, which is again indicated by the high “fluctuation” in the temperature curves and in the wavelike pressure reduction. The promoting effect seems to be very “dependable”, since there are almost no fluctuations in induction times.

At 3 % wt. induction times seem slightly reduced, but plug formation times slightly longer compared to the blind experiments. 2 out of 3 experiments show a delay time, which is longer than the induction time in both cases. In 2 experiments, stirrer torques are lower than in the blind experiments, but the last experiment at 3 % shows an extremely high stirrer torque. Pressures after 1000 minutes are in the range of those in the blind experiments.
Again, there are “brittleness indicators”, like wavelike pressure reduction and temperature curve fluctuations.

With 5 % wt. of EG present, induction times seem slightly higher than in the blind experiments in 2 out of 3 experiments. Those 2 experiments also show higher plug formation times than the blind experiments. However, one of the experiments shows both values in the range of the blind experiments, which results in a very high standard deviation for this series of experiments. One of the experiments has a very high M_{max} value, one slightly lower than in the blind experiments and one a far lower value of only 11.4 Ncm. p_{1000} values are in the range of the blind experiments, with the exception of the third experiment, where plug formation started just before 1000 minutes had passed, which of course is reflected in the high value for p_{1000}:

In some experiments, the “wet snow”-effect observed for glycerol, occurred. This could be caused by the quite similar structure as well as similarities in the number of OH groups per volume element. OH groups that are not sterically hindered, seem to well interact with the hydrate hydrogen bonds. A possible way of interaction is also shown in [4]. It postulates the formation of “EG-hydrate complexes” by forming new hydrogen bonds between EG and the water molecules and can also be applied to glycerol (above) and other OH-containing molecules (below). Of course, these assumptions are just a first attempt of explanation and still have to be verified, e. g. by spectroscopic measurements (Raman,..).

All in all, EG is not recommended for use as an inhibitor, since it seems to act as a promoter at lower concentrations. This effect also seems to be “dependable”, meaning that an under-inhibition with high certainty would result in hydrates being formed at low induction times.

Also, the formed hydrates are very hard in some cases, which increases risks of pipeline damage.

7.2.2 D(+)-Glucose

Table 35 shows the results of experiments with Glucose, Table 36 again the statistical data.

Table 35: Individual results of experiments; D(+)-Glucose

	t_{ind}	t_{pl}	(t_{pl} - t_{ind})	M_{max}	t_{St}	p_{ind}	p_{pl}	(p_{ind} - p_{pl})	p_{1000}
	[min]			[Ncm]	[min]	[bar(g)]			
DGluc-1%-01	153	153	0	134.1	-	132.1	132.1	0	97.8
DGluc-1%-02	153	298	145	212.4	1230	138.5	131.8	6.7	108.5
DGluc-1%-03	189	189	0	211.7	-	130.2	130.2	0	99.4
DGluc-3%-01	402	537	135	42.6	1119	137.3	130.3	7	113.6
DGluc-3%-02	172	323	151	74.4	1265	138.7	128.8	9.9	108.4
DGluc-3%-03	140	325	185	97.8	-	139.5	125.3	14.2	102.7
DGluc-3%-04	396	574	178	99.3	1150	137.3	130.4	6.9	111.7
DGluc-3%-05	215	225	9	81.2	-	131.2	130.8	0.4	109.1
DGluc-5%-01	199	492	294	96.4	1250	138.5	126.9	11.6	104.4
DGluc-5%-02	249	249	0	145.4	-	130.3	130.3	0	102.8
DGluc-5%-03	236	236	0	212.3	1290	131.4	131.4	0	108.2

Table 36: Statistical data of experimental series; D(+)-Glucose

		No. of exp.	t_{ind}	t_{pl}	$(t_{pl} - t_{ind})$	M_{max}	t_{St}	p_{ind}	p_{pl}	$(p_{ind} - p_{pl})$	p_{1000}
			[min]			[Ncm]	[min]	[bar(g)]			
DGluc-1%	$\bar{x}$	3	165	213	48	186.07	1230	133.60	131.37	2.23	101.90
	s		21	75	83	45.01	-	4.35	1.02	3.87	5.77
	s [%]		13	35	173	24	-	3	1	173	6
	v		0.13	0.35	1.73	0.24	-	0.03	0.01	1.73	0.06
DGluc-3%	$\bar{x}$	5	265	397	132	79.06	1178	136.80	129.12	7.68	109.10
	s		125	151	71	23.00	77	3.27	2.27	5.04	4.14
	s [%]		47	38	54	29	7	2	2	66	4
	v		0.47	0.38	0.54	0.29	0.07	0.02	0.02	0.66	0.04
DGluc-5%	$\bar{x}$	3	228	326	98	151.37	1270	133.40	129.53	3.87	105.13
	s		26	144	169	58.18	28	4.45	2.35	6.70	2.77
	s [%]		11	44	173	38	2	3	2	173	3
	v		0.11	0.44	1.73	0.38	0.02	0.03	0.02	1.73	0.03

With 1 % wt. of DGluc present, induction as well as plug formation times seem slightly lower than in the blind experiments. Stirrer torques are very high, which indicates the formation of very hard hydrates. Induction pressures seem lower than in the blind experiments which could indicate that somehow DGluc interacts directly with methane (e. g. by forming hydrogen bonds with the hydrogen atoms of methane) or that DGluc forms some kind of “pre-cages” with water or in some other way increases the solubility of methane in water. This could also cause the slight promoting effect. Pressures after 1000 minutes seem also slightly lower than in the blind experiments, but the effect is not as strong as with the induction pressures.

The formed hydrates seem to be brittle and the stirrer is able to crush already formed hydrates, which again results in wavelike pressure curves as well as in temperature fluctuations. In one of the experiments, the formed hydrates were flammable, which indicates a high gas saturation of the hydrates as well as the possibility for trapped gas molecules to diffuse to the “outside” of the formed hydrates.

With 3 % wt. of DGluc present, induction and plug formation times show mixed behavior: 3 out of 5 experiments show slightly lowered induction times with plug formation times in the range of blind experiments. The other 2 experiments show induction times in the range of

blind experiments, but with slightly higher plug formation times. Stirrer torques also show mixed behavior but are lower than those of the blind experiments.
There are delay times in every experiment. Induction pressures are in the range of blind experiments with the exception of experiment 05, which shows a similar behavior like the experiments at 1 % wt.. Pressures after 1000 minutes are in the range of blind experiments.

At 3 % wt. the promoting effect seems slightly lower than at 1 % wt.. The formed hydrates again seem hard and brittle.

At 5 % wt. induction times are generally low, being in the rage of or slightly lower than in blind experiments. Plug formation times also are low with one exception in experiment 01. Also, experiment 01 is the only one that shows a delay time. Stirrer torques again show mixed behavior with experiment 03 having a very high M_{max} value. 2 out of 3 experiments again show the phenomenon of a reduced induction pressure that already occurred at lower concentrations of DGluc. This could again indicate an influence that DGluc has on the solubility of methane, or even the formation of complexes of DGluc, methane and / or water.
Pressures after 1000 minutes are in the range of blind experiments.
Again, there are fluctuations in the temperature curves and pressure is reduced wavelike. Also, stirrer torque shows strong fluctuations. All these phenomena again indicate the formation of brittle hydrates that are crushed by the stirrer.

Experiments at all tested concentrations of DGluc resulted in the formation of brittle hydrates. The phenomenon of wavelike pressure reduction combined with temperature fluctuations, which indicates the formation of brittle hydrates, which are formed and then crushed again by the stirrer, also occurred at all concentrations.
Morphology of the hydrates was comparable to the experiments with glycerol; hydrates in the upper part of the reactor were again “flaky”, hydrates in the lower part of the reactor looked like “wet snow”.
Again, this could indicate some kind of “glue effect” that leads to the formation of “water-DGluc-complexes”. DGluc and glycerol are very similar in this matter.

All in all, DGluc is not recommended for use as an inhibitor in pipelines, due to the promoting effect as well as the possible “glue effect”.

7.2.3 myo-Inositol

The last substance tested in the “homologous series of OH-groups” was *myo-Inositol (Ino)*. The molecular structure can be found in Table 5 in chapter 3.1.

Again, results of experiments are at first shown in tables, the graphical comparison for all substances investigated in this chapter is shown in Figure 30.

Table 37 shows the individual results of the tests on myo-Inositol, Table 38 shows the statistical data on those experimental series.

Table 37: Individual results of experiments; myo-Inositol

	t_{ind}	t_{pl}	$(t_{pl} - t_{ind})$	M_{max}	t_{St}	p_{ind}	p_{pl}	$(p_{ind} - p_{pl})$	p_{1000}
	[min]			[Ncm]	[min]	[bar(g)]			
Ino-1%-01	108	108	0	185	2621	140	140	0	105.8
Ino-1%-02	364	501	138	138.3	-	140	134	6	103.5
Ino-1%-03	204	204	0	94.9	-	131.9	131.9	0	102.1
Ino-1%-04	368	368	0	212.3	3994	138	138	0	105.5
Ino-3%-01	258	258	0	41.3	-	131	131	0	115.7
Ino-3%-02	128	251	123	212.3	849	141.3	133.8	7.5	98.8
Ino-3%-03	145	145	0	81.3	1558	123.3	123.3	0	88.9
Ino-3%-04	582	708	126	163.7	-	137.5	131.5	6	108
Ino-3%-05	504	659	156	129.6	-	137.7	131	6.7	109.3
Ino-3%-06	314	314	0	32.3	475	129.6	129.6	0	115.6
Ino-5%-01	127	611	484	54	-	116.1	100.4	15.7	83.7
Ino-5%-02	245	245	0	116.3	-	128.9	128.9	0	105
Ino-5%-03	254	254	0	118.6	-	140.1	140.1	0	102.7
Ino-5%-04	424	700	276	55.2	-	137.6	130.2	7.4	110.7
Ino-5%-05	350	350	0	212.3	3070	138.1	138.1	0	103.6

Table 38: Statistical data of experimental series; myo-Inositol

		No. of exp.	t_{ind}	t_{pl}	$(t_{pl} - t_{ind})$	M_{max}	t_{St}	p_{ind}	p_{pl}	$(p_{ind} - p_{pl})$	p_{1000}
			[min]			[Ncm]	[min]	[bar(g)]			
Ino-1%	$\bar{x}$	4	261	295	34	157.63	3308	137.48	135.98	1.50	104.23
	s		128	175	69	51.79	971	3.83	3.69	3.00	1.75
	s [%]		49	59	200	33	29	3	3	200	2
	v		0.49	0.59	2.00	0.33	0.29	0.03	0.03	2.00	0.02
Ino-3%	$\bar{x}$	6	322	389	67	110.08	961	133.40	130.03	3.37	106.05
	s		187	235	75	71.15	550	6.63	3.57	3.72	10.44
	s [%]		58	60	111	65	57	5	3	110	10
	v		0.58	0.60	1.11	0.65	0.57	0.05	0.03	1.10	0.10
Ino-5%	$\bar{x}$	5	280	432	152	111.28	3070	132.16	127.54	4.62	101.14
	s		113	211	221	64.63	#DIV/0!	9.96	15.93	6.97	10.23
	s [%]		40	49	145	58	#DIV/0!	8	12	151	10
	v		0.40	0.49	1.45	0.58	#DIV/0!	0.08	0.12	1.51	0.10

With 1 % wt. of Ino present, induction times are in the range of or even slightly lower than in blind experiments. Plug formation times vary from lower than in blind experiments to one experiment being in the “higher range” of blind experiments (experiment 02). There is a delay time in only one experiment, the delay time with 138 min being high in comparison to the typical induction times at this concentration. Stirrer torques show mixed behavior with 2 out of 4 experiments having really high values (but at long times to stirrer switch-off, which could relativize the effect, since usually the formed hydrates grow “harder” over time and thus a long time to stirrer switch-off usually results in higher torque values). Induction pressures are in the range of blind experiments with one exception in experiment 03, where the induction pressure is slightly lowered. Together with the lower M_{max} value in this experiment, this could again indicate an influence on solubility of methane in water or an interaction between Ino and methane and / or water. Pressures after 1000 minutes are in the range of blind experiments.

At 3 % wt. induction as well as plug formation times show mixed behavior. There are delay times in 3 out of 6 experiments, but no correlation with induction or plug formation times is visible. There seems to be a connection between occurrence of a delay time and stirrer torque: when there is a delay time, M_{max} values seem to be higher than in experiments

without delay time. Nonetheless, stirrer torques show strongly mixed behavior, ranging from very low values (32.3 Ncm) to very high values (212.3 Ncm). Induction pressures also show mixed behavior, with values being lower and in one case even higher than in blind experiments. Lower induction pressures seem to correlate with “softer” hydrates (lower torque values), which again indicates an influence of OH-groups on solubility and / or formation of complexes of some kind. Pressures after 1000 minutes again show mixed behavior, no correlation between p_{1000} and other values (like M_{max}) is visible.

When Ino is present in concentrations of 5 % wt., induction as well as plug formation times show mixed behavior. 2 out of 5 experiments show delay times. In experiments with delay times, stirrer torques are quite low, in the other experiments, torques vary from moderate to very high. Induction pressures show mixed behavior with no obvious correlation to other criteria. Pressures after 1000 minutes also show mixed behavior. Again, there is an experiment (experiment 01) with very low stirrer torque as well as induction pressure and p_{1000} value. This could indicate the formation of “Ino-methane and / or water” complexes again.

Hydrates formed in experiments with Ino showed similar morphology to the experiments with Glycerol.
Again, wave-like pressure reductions with temperature fluctuations occurred at all tested concentrations, which could give evidence to the formation of brittle hydrates that are formed and then crushed by the stirrer again. Also, the temperature curve fluctuations seem to increase in the experiments, where there is a high stirrer torque.

In all experimental series, additional experiments were necessary because induction and plug formation times showed strong mixed behavior.

All in all, myo-Inositol seems to act more as a promoter and is not recommended for further inhibitor testing.

7.2.4 Conclusion

Figure 30 shows the comparison of induction and plug formation times for the “homologous series” of substances with increasing number of OH-groups per volume element.

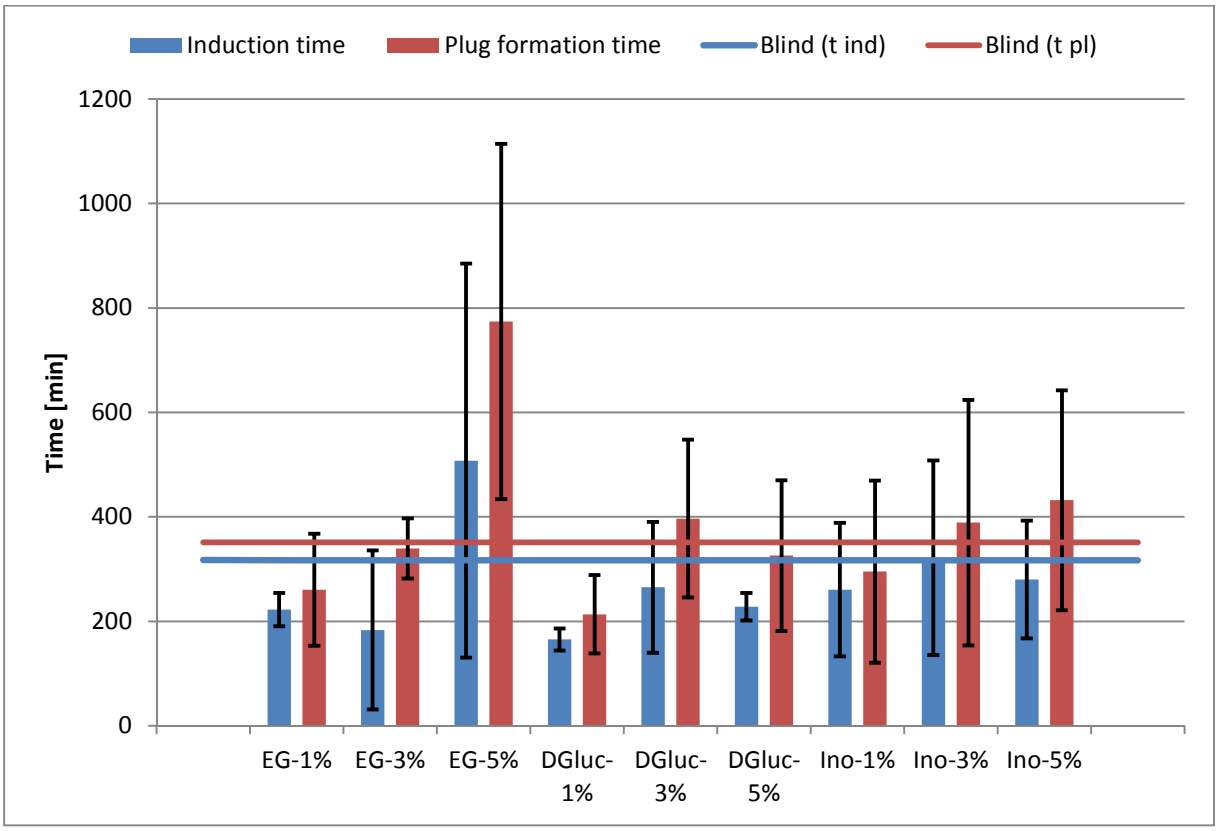

Figure 30: : Comparison of t_{ind} and t_{pl}; Parr 4568; influence of functional molecular groups on GH formation

The substances all seem to act as promoters at certain concentrations. Also, it is again shown how important concentration phenomena generally are in gas hydrate experiments (see also [70]), since the same substance can act in different ways depending on concentration.

EG shows a strong effect of higher concentration leading to higher plug formation times. This could indicate a “thermodynamic inhibiting behavior”, which would not be surprising, since EG has already been used as a thermodynamic hydrate inhibitor in pipelines [2].

It seems that in the “homologous series of OH-groups”, there is a point where a certain number of OH groups per volume element leads to a promoting effect. This could cause the

concentration of OH-groups to be “optimal” for inhibiting at high concentrations of EG, but then decreasing again with DGluc.

To further clarify the effect of OH-groups on gas hydrate formation, investigations of all three substances at very low concentrations (around 0.1 % wt.) could be conducted to check if the very strong promoting effect of Tylose H20P2 (see chapter 6) is also shown by the other substances. Also, experiments at higher concentrations could be conducted to investigate the theory of an “optimal concentration of OH-groups”.

The experiments showed similarities to the low-pressure experiments (see chapter 4). THF seems to not cause the effect observed for e. g. glycerol, where low-pressure experiments showed great inhibiting potential at high concentrations, whereas high-pressure experiments showed a promoting effect.
The dependencies of THF to OH groups have to be further investigated in additional series of experiments, also at high pressures. In addition, experiments with *s II* forming guest molecules (like ethane, without OH-group disturbing functional groups) have to be conducted at high pressures to see if an effect is caused alone by forming different hydrate structures or if THF acts via functional chemical groups.

It is recommended to investigate or calculate the “active OH concentration” of the “homologous series” to clarify how many of the OH-groups can actually interact with water or hydrates and to account for phenomena like steric hindrance. This could be achieved by volumetric titration of a defined amount of substance (either a defined area of a finalized inhibitive coating or a defined mass of inhibiting substance) to determine the OH-number of a given volume. After this, a calculation based on the molar volume of a substance could yield the “active OH concentration”.

Also, further experiments are needed at all concentrations to verify the found effects and to give recommendations for an “optimal inhibiting concentration of OH-groups”.

8 Coating development

This chapter describes the further steps that were taken to develop an inhibitive coating on a model substrate.

8.1 Tests of further promising substances

As an extension of the experiments above, two more substances were investigated regarding their inhibition potential. At first, focus was again on OH-groups, since they should be capable of disturbing hydrogen bonds that are critical for hydrate cage formation.
Even though the three substances tested above rather showed promoting instead of inhibiting tendencies, they showed a strong influence on hydrate formation itself.
Therefore, it was decided to “take the concept further” and polyvinyl alcohol (PVA) was chosen as the next tested substance.

8.1.1 Polyvinyl alcohol

In the PVA molecule, there are also many OH-groups, but the molecules / molecular chains are a lot larger than those of EG, DGluc and Ino.
Since it was assumed that EG, DGluc and Ino did interact with water / hydrates by means of the OH-groups, but their small molecule size somehow lead to the promoting effect (in addition to concentration effects that presumably play a critical role), the idea was to find out the effect that a longer chain / bigger molecule with the same functional groups had on hydrate formation.

Table 39 shows the individual results for experiments with PVA, statistical data is shown in Table 40. Graphical comparison of both tested substances against blind experiments is shown in Figure 31.

Table 39: Individual results of experiments; PVA

	t_{ind}	t_{pl}	(t_{pl} - t_{ind})	M_{max}	t_{St}	p_{ind}	p_{pl}	(p_{ind} - p_{pl})	p_{1000}
	[min]			[Ncm]	[min]	[bar(g)]			
PVA-out-1%-01	311	311	0	115.8	-	127.7	127.7	0	103.1
PVA-out-1%-02	284	558	275	92.8	-	135.6	128.6	7	106.1
PVA-out-1%-03	281	571	290	43	-	135.5	126.2	9.3	104.6
PVA-in-1%-01	116	388	272	73.9	-	136.3	129.2	7.1	109
PVA-in-1%-02	190	428	238	82.4	-	135.9	127.3	8.6	96.7
PVA-in-1%-03	108	324	216	212.4	4146	135.9	129.1	6.8	100.3
PVA-in-3%-01	879	1639	760	65.6	-	139	107.4	31.6	134.6
PVA-in-3%-02	109	380	272	130.8	-	139.9	129.3	10.6	102.8
PVA-in-3%-03	4000	4000	0	11.6	-	no h. f.	no h. f.	no h. f.	135.3
PVA-in-3%-04	4000	4000	0	11.5	-	no h. f.	no h. f.	no h. f.	137.1
PVA-in-3%-05	566	927	362	83.5	-	135.7	123.9	11.8	112.3
PVA-in-3%-06	4000	4000	0	14.8	-	no h. f.	no h. f.	no h. f.	136
PVA-in-5%-01	4000	4000	0	13.6	-	no h. f.	no h. f.	no h. f.	137.4
PVA-in-5%-02	111	715	604	62.7	-	139.1	125.2	13.9	104.4
PVA-in-5%-03	791	1149	358	94.6	-	138.7	130.1	8.6	133.8
PVA-in-5%-04	4000	4000	0	14.6	-	no h. f.	no h. f.	no h. f.	138.3
PVA-in-5%-05	794	1129	334	84.9	-	137.7	125.6	12.1	133.6
PVA-in-5%-06-dis	4000	4000	0	16.8	-	no h. f.	no h. f.	no h. f.	139.7

In Table 39 and Table 40, PVA “out” means that the PVA was dissolved in water outside the reactor before the reactor was filled, PVA “in” means that PVA and water were mixed inside the reactor.

Table 40: Statistical data of experimental series; PVA

		No. of exp.	t_{ind}	t_{pl}	$(t_{pl} - t_{ind})$	M_{max}	t_{St}	p_{ind}	p_{pl}	$(p_{ind} - p_{pl})$	p_{1000}
			[min]			[Ncm]	[min]	[bar(g)]			
PVA-out-1%	$\bar{x}$	3	292	480	188	83.87	-	132.93	127.50	5.43	104.60
	s		17	146	163	37.21	-	4.53	1.21	4.84	1.50
	s [%]		6	30	87	44	-	3	1	89	1
	v		0.06	0.30	0.87	0.44	-	0.03	0.01	0.89	0.01
PVA-in-1%	$\bar{x}$	3	138	380	242	122.90	4146	136.03	128.53	7.50	102.00
	s		45	53	28	77.63	-	0.23	1.07	0.96	6.32
	s [%]		33	14	12	63	-	0	1	13	6
	v		0.33	0.14	0.12	0.63	-	0.00	0.01	0.13	0.06
PVA-in-3%	$\bar{x}$	6	2259	2491	232	52.97	-	138.20	120.20	no h. f.	126.35
	s		1923	1700	303	49.07	-	2.21	11.41	no h. f.	14.89
	s [%]		85	68	130	93	-	2	9	no h. f.	12
	v		0.85	0.68	1.30	0.93	-	0.02	0.09	no h. f.	0.12
PVA-in-5%	$\bar{x}$	6	2283	2499	216	47.87	-	138.50	126.97	no h. f.	131.20
	s		1898	1652	255	37.47	-	0.72	2.72	no h. f.	13.36
	s [%]		83	66	118	78	-	1	2	no h. f.	10
	v		0.83	0.66	1.18	0.78	-	0.01	0.02	no h. f.	0.10

Polyvinyl alcohol at 1 % wt. shows differences when dissolved in water before filling into the reactor (from now on referred to as “external PVA”), compared to mixing inside the reactor (“internal PVA”).

With external mixing, induction as well as plug formation times are in the range of blind experiments. Delay times occur in 2 out of 3 experiments. Standard deviation between the experiments of this series is very low regarding induction and plug formation times. There are differences in M_{max} values, the third experiment has a significantly lower value, although pressure after 1000 minutes and hence gas consumption correspond well between the experiments. Induction pressures are in the range of blind experiments, with the exception of experiment 01, where p_{ind} is slightly lower. An interesting deviation to the experiments in the previous chapter is that in this series, the lower induction pressure corresponds to the highest stirrer torque, which is exactly the opposite as with Ino. Pressures after 1000 minutes are in the range of blind experiments.

Also, stirrer torque shows strongly oscillating behavior in all experiments.

Internal PVA at 1 % wt. shows reduced induction times, but plug formation times in the range of blind experiments. Delay times occurred in all experiments and are higher than the actual induction times. Stirrer torque shows mixed behavior and ranges from lower than blind experiments to very high (but still in the range of blind experiments). Induction pressures are in the lower range of blind experiments, pressures after 1000 minutes as well.
Also, there are “spikes” / a highly oscillating behavior in the torque curve. This, combined with the occurrence of “foam” in all experiments could mean that there are hydrates formed, that then “react” to foam and back. Also it could mean that PVA acts as some kind of anti-agglomerate which allows for hydrates to be formed (high torque) and then “emulsifies” those hydrate particles in the water phase (torque low, foamy behavior).

External mixing was only done at 1 % wt., hence, the following experiments were all conducted with internal mixing (with the exception of “PVA-in-5%-06-dis”, where PVA was completely dissolved in water before filling the mixture into the reactor).

At 3 % wt. experiments showed strongly mixed behavior, which is why more experiments had to be conducted. There is an inhibiting tendency, 2 experiments showed higher induction and plug formation times, 3 experiments showed no hydrate formation at all. Only one experiment showed a slightly lowered induction time (compared to blind experiments) and a plug formation time in the range of blind experiments. In all experiments with hydrate formation (h. f.), delay times occurred, which varied strongly. Also, stirrer torques varied strongly in experiments with hydrate formation. Induction pressures were in the range of blind experiments (experiment 05 even slightly lower), pressures after 1000 minutes as well (experiments 01 and 05 are slightly higher, which is presumably caused by the late plug formation time).
During experiments, again, temperature curve fluctuations and wavelike pressure reduction occurred.

At 5 % wt. experiments again show strong deviations in induction times. One experiment has an induction time that is slightly lower than in blind experiments, the other induction times are higher, 3 out of 6 experiments showed no hydrate formation at all. All plug formation times are significantly higher than in blind experiments, which indicates a strong inhibiting behavior of PVA at this concentration. In all experiments with hydrate formation, delay times occur,

which again vary in length. Stirrer torques are all in the lower range of blind experiments or even below.
Torque is oscillating in the experiments with hydrate formation, temperature fluctuations are moderate. Compared to the experiments at 3 % wt., the wavelike behavior of the pressure curve is damped and the pressure curve falls steeper.
Induction pressures are in the range of blind experiments, pressure after 1000 minutes (in experiment 02, where plug formation occurred before 1000 minutes of experimental time) also is in the range of blind experiments.

PVA could act as a THI in the experiments without hydrate formation, with under-inhibition leading to hydrate formation in the other experiments. This phenomenon could be caused by the effect of “internal” mixing of PVA and water. In some experiments, a “residuum” of PVA was observed at the bottom of the reactor after experiments ended. This could have an effect of under-inhibition in the “upper” reactor areas compared to fully dissolved PVA.

If PVA acts as a THI or KHI, or even as an AA, still has to be clarified, e. g. by investigation of the formed hydrate structures (via RAMAN spectroscopy or other methods).
Also, it is recommended to test PVA at lower concentrations, e. g. at 0.1 % wt., to observe, if the “Tylose effect” of strong promoting at lower concentrations is also observed.

8.1.2 Polyethylene glycol

In parallel, it was decided to test another polymer, PEG, for its inhibiting potential. This was done because the ether groups contained in the molecule also promise a strong interaction potential with water molecules.

Table 41 shows the individual results for PEG, Table 42 the corresponding statistical data. Graphical comparison of PVA and PEG to blind experiments is done in Figure 31.

Table 41: Individual results of experiments; PEG

	t_{ind}	t_{pl}	$(t_{pl} - t_{ind})$	M_{max}	t_{St}	p_{ind}	p_{pl}	$(p_{ind} - p_{pl})$	p_{1000}
	[min]			[Ncm]	[min]	[bar(g)]			
PEG-0.1%-StS-01	3862	4003	142	148.7	-	139.7	134	5.7	139.6
PEG-0.1%-StS-02	4000	4000	0	11.4	-	no h. f.	no h. f.	no h. f.	139.6
PEG-0.1%-StS-03_no stirring	4000	4000	0	-	-	no h. f.	no h. f.	no h. f.	141.4
PEG-0.1%-StS-04	1869	2071	202	90.1	-	132.2	124.4	7.8	132.4
PEG-0.5%-01	983	1159	176	85.1	1568	137.7	130.3	7.4	137.5
PEG-0.5%-02	85	548	464	94.9	-	139.1	123.1	16	98.3
PEG-0.5%-03	305	305	0	104.3	1478	130.3	130.3	0	99.8
PEG-0.5%-StS-01	347	711	364	105.2	1473	137.5	126.3	11.2	104.6
PEG-0.5%-StS-02	495	862	367	156.2	-	137.7	125.1	12.6	107.5
PEG-0.5%-StS-03	457	890	432	145.3	-	138.1	122.4	15.7	111.3
PEG-0.5%-StS-04	369	541	172	97.8	-	127.4	110.7	16.7	97
PEG-0.5%-StS-05	4927	5441	514	32.9	-	138.5	123.3	15.2	138.4
PEG-1%-01	2010	2287	277	212.3	-	137.7	127.6	10.1	137.9
PEG-1%-02	405	687	282	96.7	-	137.4	126.6	10.8	104.7
PEG-1%-03	4338	4720	382	46.6	-	137	122.3	14.7	137.3
PEG-1%-04	140	600	460	212.3	-	138.9	117.3	21.6	100
PEG-1%-05	89	270	181	47.3	-	139.5	130.5	9	109.4
PEG-3%-01	137	474	337	93.8	-	138.5	130.3	8.2	96.9
PEG-3%-02	422	833	411	62.5	1037	138.2	127.6	10.6	111.1
PEG-3%-03	277	277	0	178	-	129.7	129.7	0	100.2
PEG-5%-01	323	323	0	212.3	1355	130.9	130.9	0	102.9
PEG-5%-02	197	578	381	212.4	-	138.9	128.1	10.8	102.6
PEG-5%-03	333	333	0	212.3	640	128.7	128.7	0	102.7

Table 42: Statistical data of experimental series; PEG

		No. of exp.	t_{ind}	t_{pl}	(t_{pl} - t_{ind})	M_{max}	t_{St}	p_{ind}	p_{pl}	(p_{ind} - p_{pl})	p_{1000}
			[min]			[Ncm]	[min]	[bar(g)]			
PEG-0.1%-StS	$\bar{x}$	4	3433	3519	86	83.40	-	135.95	129.20	no h. f.	138.25
	s		1044	965	102	68.89	-	5.30	6.79	no h. f.	3.99
	s [%]		30	27	119	83	-	4	5	no h. f.	3
	v		0.30	0.27	1.19	0.83	-	0.04	0.05	no h. f.	0.03
PEG-0.5%	$\bar{x}$	3	457	671	213	94.77	1523	135.70	127.90	7.80	111.87
	s		468	440	234	9.60	64	4.73	4.16	8.01	22.21
	s [%]		102	66	110	10	4	3	3	103	20
	v		1.02	0.66	1.10	0.10	0.04	0.03	0.03	1.03	0.20
PEG-0.5%-StS	$\bar{x}$	5	1319	1689	370	107.48	1473	135.84	121.56	14.28	111.76
	s		2018	2102	126	48.64	-	4.73	6.26	2.29	15.79
	s [%]		153	124	34	45	-	3	5	16	14
	v		1.53	1.24	0.34	0.45	-	0.03	0.05	0.16	0.14
PEG-1%	$\bar{x}$	5	1396	1713	317	123.04	-	138.10	124.86	13.24	117.86
	s		1824	1854	107	83.98	-	1.06	5.15	5.14	18.33
	s [%]		131	108	34	68	-	1	4	39	16
	v		1.31	1.08	0.34	0.68	-	0.01	0.04	0.39	0.16
PEG-3%	$\bar{x}$	3	279	528	249	111.43	1037	135.47	129.20	6.27	102.73
	s		142	282	219	59.73	-	5.00	1.42	5.56	7.43
	s [%]		51	53	88	54	-	4	1	89	7
	v		0.51	0.53	0.88	0.54	-	0.04	0.01	0.89	0.07
PEG-5%	$\bar{x}$	3	284	411	127	212.33	998	132.83	129.23	3.60	102.73
	s		76	144	220	0.06	505	5.37	1.47	6.24	0.15
	s [%]		27	35	173	0	51	4	1	173	0
	v		0.27	0.35	1.73	0.00	0.51	0.04	0.01	1.73	0.00

With 1 % wt. of PEG present, induction times as well as plug formation times show strong mixed behavior. 2 experiments seem to show a promoting effect, one experiment (experiment 02) is well within the range of blind experiments and 2 experiments show strong inhibitive behavior. There are delay times of almost the same length in all experiments. Maximum stirrer torques range from clearly below blind experiments to very high values, but no correlation can be made out between the length of induction times and the “hardness” of

formed hydrates. Induction pressures are within the range of blind experiments and correlate well within the 1 %-measurement series. Where hydrate formation occurs before 1000 minutes, the p_{1000} values are within the range of blind experiments. Fluctuations in temperature curves as well as wavelike pressure reduction occur within the experiments.

At 3 % wt. induction times vary from the lower range of blind experiments as far as to the upper range. Plug formation times even seem slightly higher than in blind experiments. There are delay times in 2 out of 3 experiments. Stirrer torques vary from clearly below blind experiments up to the upper range of blind experiments' values. One experiment (experiment 03) shows a reduced induction pressure, which in this case correlates with a high M_{max} value and could indicate an influence PEG has on solubility of methane in water or even the formation of "PEG-methane and / or water" complexes. Pressures after 1000 minutes are in the lower range of blind experiments in experiments 01 and 03 and in the "normal" range of blind experiments in experiment 02.
Again, there are fluctuations in temperature curves as well as wavelike pressure reduction.

At 5 % wt. induction times show almost no difference to the blind experiments. Plug formation times also are well within the range of blind experiments. Only one experiment shows a delay time, which is quite high. Stirrer torques rise very high, temperature fluctuations are also strong, but the pressure "waves" are not as distinct as in experiments at lower concentrations. This could indicate that "one big agglomeration" of hydrates is formed instead of brittle hydrates which are then shredded by the stirrer again.
Induction pressures are lower than in blind experiments in 2 out of 3 cases, which, combined with the high stirrer torques as well as the low p_{1000} values, could again indicate the formation of "PEG-hydrate complexes".

Because of the high induction times in some of the experiments at 1 % wt. it was decided to test PEG at even lower concentrations.
At first, PEG in a concentration of 0.5 % wt. was used directly. The "direct" experiments at 0.5 % wt. showed mixed behavior.
Induction times vary strongly, ranging from promoting up to clearly inhibiting effect. Plug formation times are within the range of blind experiments, with experiment 01 having a clearly higher plug formation time. 2 out of 3 experiments showed delay times that varied in their length. Stirrer torques correlate well within the measurement series and are in the lower range of blind experiments or slightly lower. Induction pressures are within the range of blind experiments in 2 out of 3 cases, only experiment 03 having a clearly lower value. Pressures

after 1000 minutes are in the lower range of blind experiments (where hydrate formation occurred before 1000 minutes of experimental time had passed).
The wavelike behavior of the pressure curves was quite pronounced in all of the experiments. Temperature fluctuations are strong as long as the stirrer operates; where it was switched off to prevent mechanical damage, fluctuations stop almost instantly.

Because of the low dosage of PEG in the experiments at 0.5 % wt. and the possibly resulting significance of small differences in weighing in combination with occurring weighing difficulties (PEG is near its melting point at room temperature and therefore more of a viscous fluid than a solid), additional experiments were done with stock solutions of water and PEG.

At first, experiments with stock solution were done at a concentration of 0.5 % wt. Then, a stock solution with a mass fraction of 0.1 % PEG was made to test even lower concentrations of PEG.

At 0.5 % wt. 4 out of 5 experiments show induction times well within the range of blind experiments. Experiment 05, however, has a considerably higher induction time of 4927 minutes. This is clear evidence that the value of 4000 minutes, that was set as induction time when no hydrate formation occurred, has to be regarded a “worst-case” estimation and can even be exceeded by some inhibitors.
Plug formation times are in the upper range of blind experiments or slightly lower in 4 out of 5 experiments and again significantly higher in experiment 05. Delay times occurred in all experiments and were not significantly higher in experiment 05 compared to the other experiments of this series. Stirrer torques were in the range of blind experiments, with experiment 05 being drastically lower.
Only experiment 04 showed a reduced induction pressure, all other experiments were in the range of blind experiments.
Pressures after 1000 minutes were within the range of blind experiments. Interestingly, experiment 04 had the lowest p_{1000} value in this series combined with the lowest induction pressure, although there seemed to be no “big” influence on stirrer torque.
Again, temperature fluctuations occurred as long as the stirrer operated.

At 0.1 % wt. induction times as well as plug formation times are either significantly higher than in blind experiments or no hydrate formation occurs at all. There seems to be a clearly

inhibiting effect. All experiments with hydrate formation have delay times that are very low compared to the induction and plug formation times.
It has to be mentioned that during experiment 03 at 0.1 % wt. of PEG, the stirrer was switched off after tempering to the starting temperature.
For the other experiments, stirrer torques vary from very low (where no hydrate formation occurred) to well in the range of blind experiments.
Induction pressure in experiment 01 is within the range of blind experiments, experiment 04 shows a lowered value. Together with the lower stirrer torque, this could again indicate some influence on the solubility of methane or the formation of complexes of some kind. Pressures after 1000 minutes are in the range of blind experiments (with the exception of experiment 04), with p_{10000} having the highest value in experiment 03, where the stirrer is switched off. This seems not surprising, since other experiments in the course of this work also showed the importance of turbulence in hydrate formation experiments.
The appearance of the experimental courses is quite similar to the experiments with other concentrations of PEG.

All in all, PEG seems to be a promising inhibitor at lower concentrations.

8.1.3 Conclusion

Figure 31 shows the comparison of induction and plug formation times of PVA and PEG versus blind experiments.

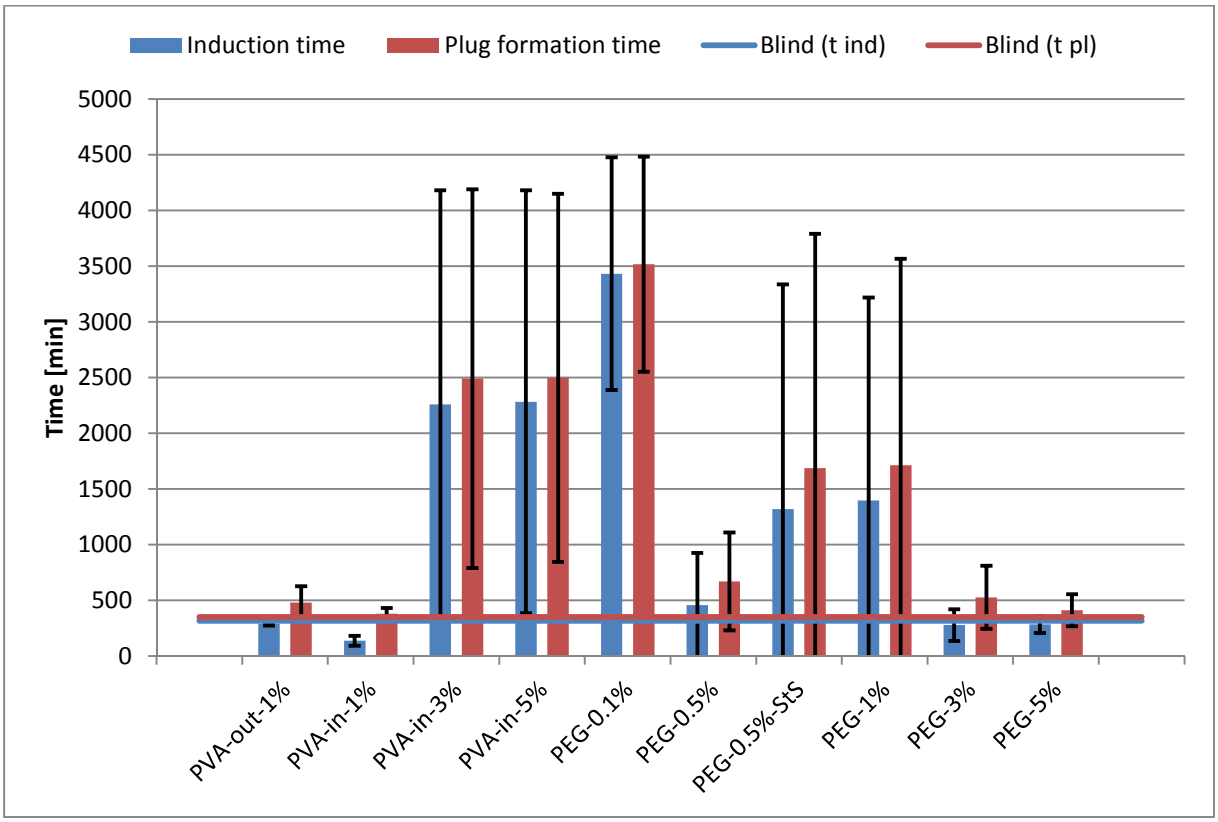

Figure 31: : Comparison of t_{ind} and t_{pl}; Parr 4568; Coating development

PVA seems to act as a promoter at lower concentrations, but has inhibitive potential at higher concentrations. This could indicate that PVA acts as thermodynamic hydrate inhibitor which acts as a promoter when under-inhibiting conditions (low concentrations) are met. Either way, tests at different concentrations should be conducted to fully clarify this phenomenon.

PEG, on the other hand, shows the opposite behavior: at higher concentrations, PEG seems to have a “small” promoting effect or has only small influence on hydrate formation; at lower concentrations, however, there seems to be a stronger effect with clearly inhibiting tendencies at 0.1 % wt..

Because of the great inhibitive potential of PEG at concentrations of 0.1 % wt. and since the concentration at the surface of a developed coating would also be very low, it was decided to

use PEG over PVA in the coating. This also seemed promising because there are applications with PEG as an anti-ice coating [77, 78].
Nevertheless, PVA should be tested at lower concentrations and also be applied as a coating depending on the results of this testing.

8.2 Coating procedure

To reach the goal of a functional inhibitive coating, the following steps were taken:

At first, “prototype vessels” were built out of poly methyl methacrylate (PMMA). This substrate material was chosen because it can be easily shaped to fit inside the reactor. Also, parts of PMMA can be glued together with its own monomer, so that no third-party components (as in other glues) have to be used. Also, PMMA is transparent, so that visual observation through the reactor’s windows still is possible. The prototype was built to fit exactly into the “Parr 4568” reactor (see Figure 32 for the picture and Figure 33 for the reactor’s cross section after inserting the prototype). After completion of the prototype, “new” blind experiments were conducted within the prototype (that was fit inside the reactor) under otherwise exact same conditions as in chapter 5 and 6 (without adding inhibitor).

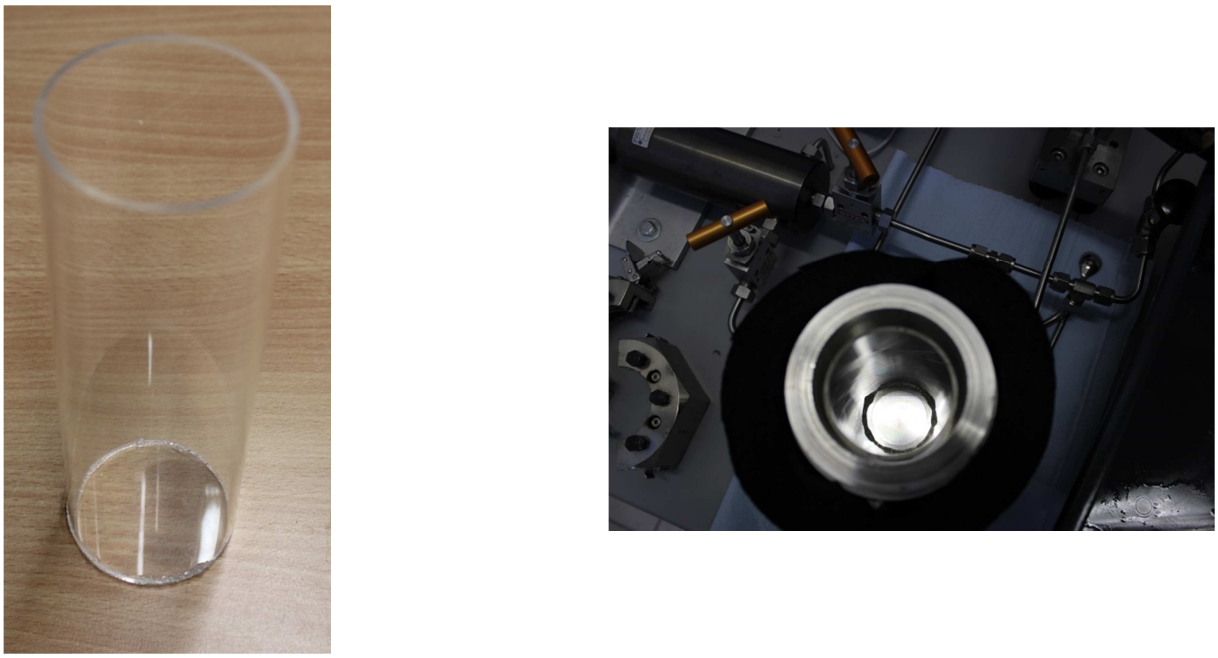

Figure 32: Prototype vessel for testing inhibitive coatings (left); prototype vessel inside of reactor (right)

After completion of the blind experiments, the prototype vessels were coated with promising inhibitors using different linking methods. After this, the prototype vessels were tested inside the Parr 4568 reactor. The performance of the inhibitive coating was then compared to the induction times of the prototype’s blind experiments.

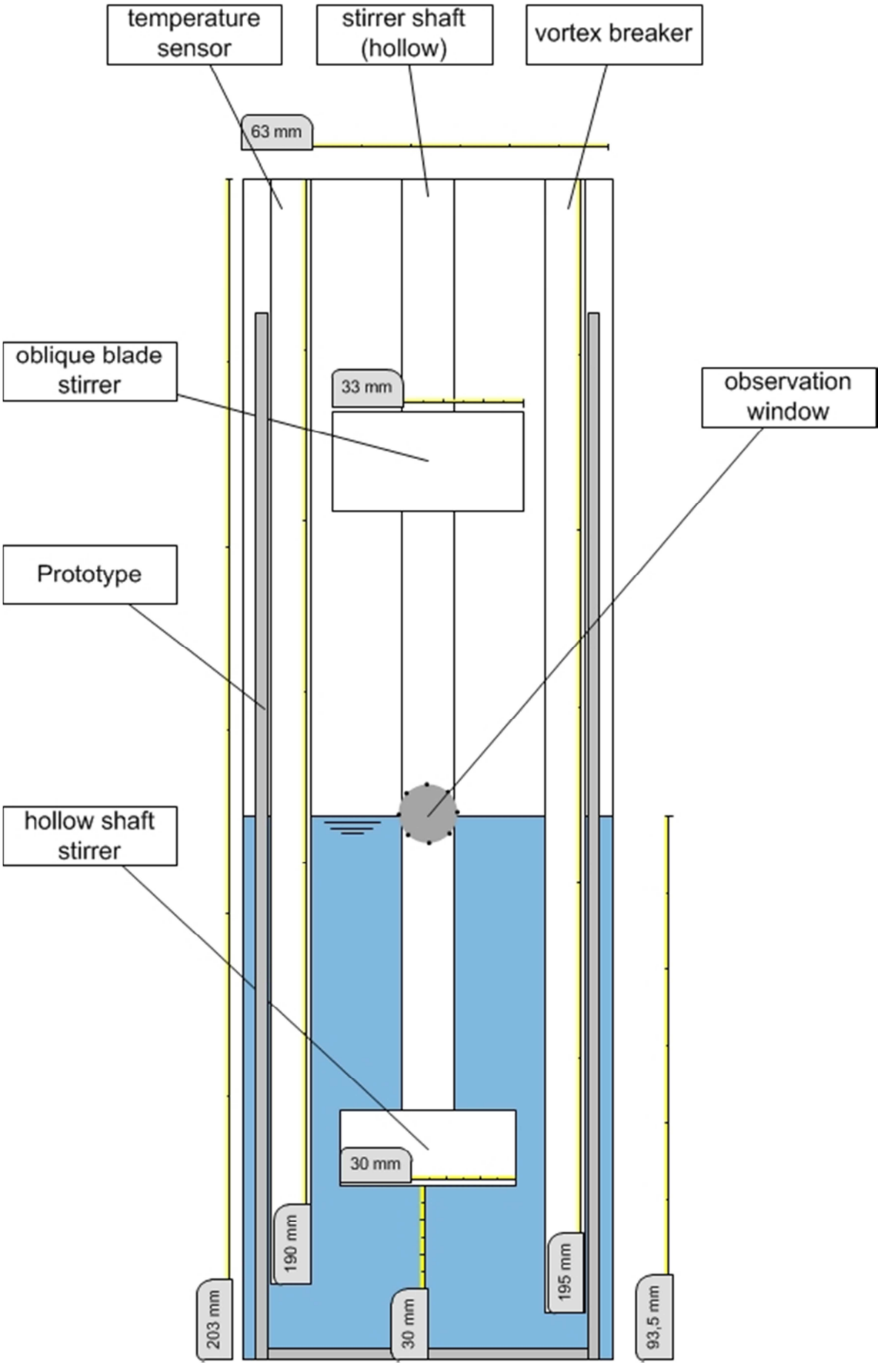

Figure 33: Prototype inside Parr 4568 reaction system, cross section

The most promising coating, or rather the most promising method of fixating inhibitors on the PMMA surface, will be described further.
The method can e. g. be used to link inhibitors that contain OH-groups to the PMMA surface.

Although this linking method differs from the conditions in “real” pipelines, it is comparable and shall act as a proof of concept for permanent inhibitive pipeline coatings.

At first, the inhibitor is treated with sodium to deprotonate OH-groups to the corresponding alkoxide:

[8.1]

Then, the alkoxide is added directly to the inside of the prototype vessel where it reacts with PMMA:

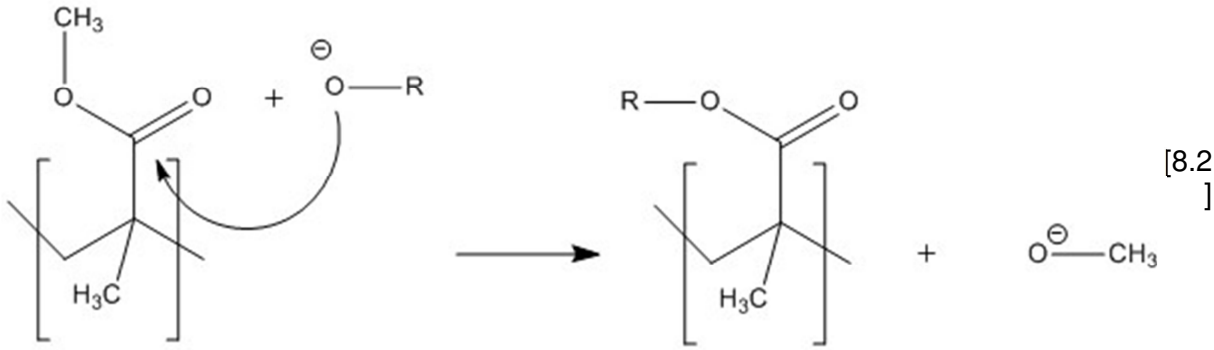

[8.2]

With this, the inhibitor is linked to the PMMA surface.

After the linking reaction has run for sufficient time, residues of the reaction mass are removed and the PMMA surface (with inhibitor) is cleaned with water. Water reacts with the CH_3-alkoxide by forming methanol:

[8.3]

Qualitative proof for the existence of methanol was given by gas chromatography (GC), the data can be found in the annexes. Thus, the proof of concept for coating a model substrate with inhibitor has been given. The results can only be seen as a qualitative statement as yet.
To further investigate the coated surface and draw conclusions to e. g. loading / saturation with inhibitor functional groups or arrangement of the inhibitor molecules on the surface,

additional methods of investigation have to be used, e. g. atomic force microscopy (AFM) or scanning electron microscopy (SEM).

8.3 Coating application

Next step in the development of the inhibitive coating was the conduction of blind experiments in the "prototype" vessel (see above). After that, the prototype was modified and PEG applied as a coating. Then, experiments with the coated prototype were conducted.

8.3.1 Prototype "blind" experiments

Table 43 shows the individual "new blind" experiments done with the prototype vessel inside the Parr 4568 reaction system and Table 44 the corresponding statistical data.

Graphical comparison of the "prototype blind" and "prototype coated with PEG" experiments is done in Figure 34.

Table 43: Individual results of experiments; Prototype blind experiments

	t_{ind}	t_{pl}	$(t_{pl} - t_{ind})$	M_{max}	t_{St}	p_{ind}	p_{pl}	$(p_{ind} - p_{pl})$	p_{1000}
	[min]			[Ncm]	[min]	[bar(g)]			
Prot-Blind-01	1979	1979	0	123.7	2412	135.5	135.5	0	136
Prot-Blind-02	144	144	0	134	658	136.9	136.9	0	103.4
Prot-Blind-03	82	82	0	108.5	501	137.7	137.7	0	102
Prot-Blind-04	269	269	0	125.6	761	137.2	137.2	0	101.1
Prot-Blind-05	134	134	0	106	-	137.3	137.3	0	103.9

Table 44: Statistical data of experimental series; Prototype blind experiments

		No. of exp.	t_{ind}	t_{pl}	$(t_{pl} - t_{ind})$	M_{max}	t_{St}	p_{ind}	p_{pl}	$(p_{ind} - p_{pl})$	p_{1000}
			[min]			[Ncm]	[min]	[bar(g)]			
Prot-Blind	$\bar{x}$	5	522	522	0	119.56	1083	136.92	136.92	0.00	109.28
	s		818	818	0	11.92	892	0.84	0.84	0.00	14.98
	s [%]		157	157	-	10	82	1	1	-	14
	v		1.57	1.57	-	0.10	0.82	0.01	0.01	-	0.14

Induction times in the prototype blind experiments are in most cases lower than in "normal" blind experiments, with one exception: in the first prototype experiment, the induction time was at around 2000 min. It seems surprising that after this the experiments only took a short

time, because all of the experiments were “fresh runs” with intermediate cleaning of the prototype / reactor.
This was maybe caused by the “thermal pretreatment” of the reactor, meaning that an experiment starting after a “pause” caused by inspection of the reactor or similar causes could have a longer induction time compared to an experiment starting right after another experiment was finished (in this case, the pause was at approx. 1 h for cleaning of the reactor etc..). Maybe the residual cold inside the reactor walls had some kind of effect on induction times, although all of the experiments were brought to the same starting temperature of 20 °C after filling and closing off the reactor. This problem is discussed in detail in chapter 11.1.2.
In general it can be said, that the induction times are a little shorter inside the prototype. This could result from a changed “diameter” of the cylindrical reaction vessel which could again result in a changed ratio of surface to volume.
Plug formation times are identical with induction times in all of the experiments, there were no delay times. This could indicate that hydrate formation starts “directly” at a scale that influences pressure as well as stirrer torque.
Stirrer torques are well in the “middle range” of “normal” blind experiments and have moderate values. Induction pressures and pressures after 1000 minutes experimental time are also in the range of those in “normal” blind experiments.

Again, temperature fluctuations as well as wavelike pressure reduction occurred during the experiments. The slopes of pressure curves are slightly different compared to the “normal” blind experiments, pressure does not fall as quickly. This could again be caused by the smaller diameter of the vessel, which results in a slightly reduced surface area. But it is also important to mention that a mechanism was installed to prevent mechanical damage to the prototype vessel. This mechanism switched off the stirrer if the force on the mechanical parts was too high. The mechanism should not have any influence of hydrate formation before the torque was too high. This was considered in the evaluation of experiments, therefore the time at which the stirrer was turned off is indicated in the results.
In any case, differences between the “normal” and the “prototype” blind experiments are only small, regarding the course of pressure, temperature and torque as well as the morphology of the formed hydrates.
It was noted that the formed hydrates showed a strong hissing in the prototype experiments, regarding the “upper area” of the reactor. Presumably, this is caused by the difference in diameter of the prototype compared to the “normal” reactor. This results in the fact that the same amount of hydrates grows higher in the reactor, meaning that the “gas phase stirrer”

could come in contact with the water / hydrate phase and cause a higher turbulence and / or shredding in the hydrate phase.

8.3.2 “Coated” prototype experiments

After running blind experiments with the prototype, experiments with the same prototype, but with applied coating, were conducted. Coating procedure was done with PEG according to the mechanism described above. Verification of the successful coating operation was done by proving the existence of methanol in the residue water after the coating process (also described in above). Measurement of methanol was done via gas chromatography, the chromatogram can be found in the electronic annex. The detection of methanol is a prove for the chemical bond that has formed between the inhibitor PEG and the model substrate PMMA.

Table 45 shows the individual results for the “Coated prototype” experiments; Table 46 shows the corresponding statistical data. Graphical comparison of the “prototype” and “Coated prototype” experiments is done in Figure 34.

Table 45: Individual results of experiments; Coated prototype experiments

	t_{ind}	t_{pl}	$(t_{pl} - t_{ind})$	M_{max}	t_{St}	p_{ind}	p_{pl}	$(p_{ind} - p_{pl})$	p_{1000}
	[min]			[Ncm]	[min]	[bar(g)]			
Prot-Coated-01	793	899	106	137.3	1450	137.4	133.4	4	126.9
Prot-Coated-02	195	195	0	90.4	462	137.7	137.7	0	110.9
Prot-Coated-03	102	203	102	102.2	-	138.6	133.7	4.9	106

Table 46: Statistical data of experimental series; Coated prototype experiments

		No. of exp.	t_{ind}	t_{pl}	$(t_{pl} - t_{ind})$	M_{max}	t_{St}	p_{ind}	p_{pl}	$(p_{ind} - p_{pl})$	p_{1000}
			[min]			[Ncm]	[min]	[bar(g)]			
Prot-Coated	$\bar{x}$	3	363	432	69	109.97	956	137.90	134.93	2.97	114.60
	s		375	404	60	24.40	698	0.62	2.40	2.61	10.93
	s [%]		103	93	87	22	73	0	2	88	10
	v		1.03	0.93	0.87	0.22	0.73	0.00	0.02	0.88	0.10

The first experiment had an induction time of about 800 min, which seems promising compared to the majority of blind experiments. The other experiments show only small differences compared to the blind experiments. Plug formation times show the same trend. 2 out of 3 experiments show delay times of about 100 minutes. Stirrer torques are well in the range of “prototype blind” experiments. Induction pressures are also in the range of blind experiments.
Pressures after 1000 minutes seem slightly higher, even in the experiments, where hydrate formation occurred well before 1000 minutes experimental time. This could indicate a slightly inhibiting effect.

All in all, the inhibitive coating does not seem to cause a big difference in hydrate formation experiments, at least not nearly as big as in the experiments with 0.1 % wt. PEG in solution. Nonetheless, a first coating was applied to the surface and tested successfully.

8.3.3 Conclusion

Figure 34 shows the graphical comparison of the prototype experiments with and without applied coating. “Prot_Blind_b” shows the resulting mean values for induction and plug formation time when the first experiment (that deviated very strongly from the following experiments, perhaps caused by thermal pretreatment of the reactor) is left out.

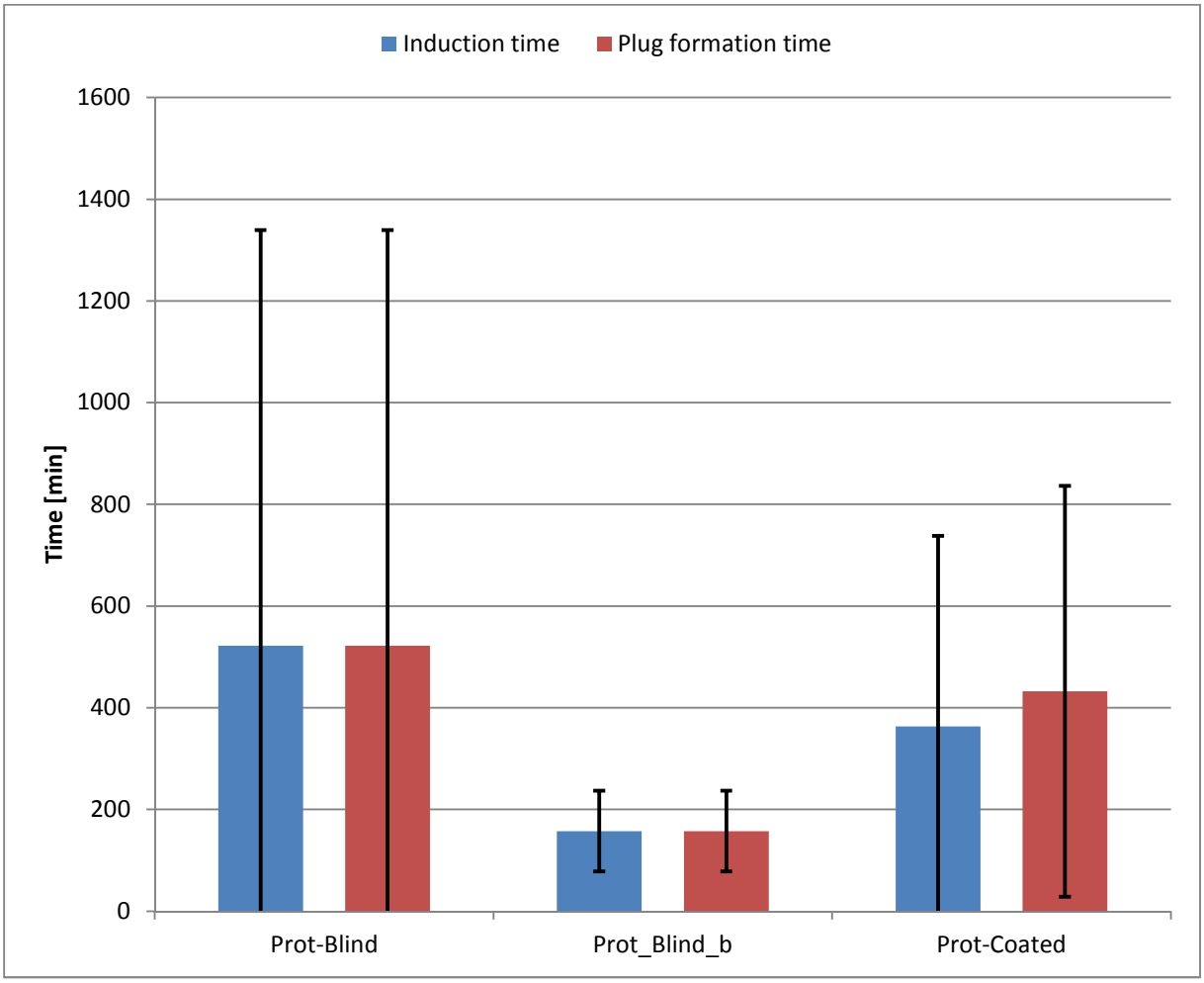

Figure 34: : Comparison of t_{ind} and t_{pl}; Parr 4568; Prototype experiments

Again, it can be seen that there is no significant difference in induction and plug formation times between the “uncoated” and coated prototype. It is to be mentioned that the first “blind” experiment had a very long induction time of about 2000 minutes, which caused the really high standard deviation in the blind experiments. This phenomenon has to be clarified further, as already mentioned in chapter 11.1.2.

Nevertheless, there still seems no strong influence of the coated prototype so far. Further experiments have to be conducted to gain better insight in how the coating “works” and / or could be modified to gain more influence on hydrate formation.

The next steps that have to be taken are the optimization of the effective surface area of the coating that is available for inhibiting hydrate formation.
A higher “surface density” of the functional groups could be reached by roughening the surface of the prototype. This was not done in the course of this work because roughening

the surface would have caused a need for new blind experiments with the roughened prototype. This could not be done in the course of this project due to temporal limitation.

Also, optimizing of the polymer chain length could be done, but since the used PEG was already quite a good inhibitor at very low concentrations of 0.1 % wt., it is recommended to optimize the coating process in a next step and later try focusing on other possible coating candidates.

All in all, the effect of the inhibitive coating is not very significant up to this point.
Nonetheless, this is the first time that a potential inhibitor has been applied as a coating to a substrate surface.

9 Kinetic analyses of s I hydrate formation

This chapter shows the kinetic analyses that were conducted on sorted *s I* experiments in the course of this thesis. At first, the theoretical background is explained, after that, the procedure for analyzing is described in detail. Finally, results are shown and discussed.

9.1 Theoretical background

Kinetic modeling of hydrate formation processes is difficult, since the mechanism of formation still is not fully explored. Also it was found that the described kinetic models in literature are specific for the respective reaction vessels. Also, since crystal structure has a significant influence on the growth rate of crystals in all crystallization processes [2], kinetics for formation of different hydrate structures cannot be easily realized with the same model. The derivation of a model to describe hydrate formation kinetically and predict the so-called *induction times* is therefore very difficult to realize. Approaches with different concepts for modeling the driving force for hydrate nucleation and growth phases have been taken. Most of those approaches are based on the assumption of a constant driving force for hydrate formation, e. g. constant pressure or chemical potential. In this project, experiments were conducted at transient driving-force conditions; therefore those approaches were not applicable.

9.1.1 Englezos-Bishnoi

One of the first attempts to describe hydrate formation mathematically was derived from Englezos et al. in 1987 [101, 102]. The so-called *Englezos-Bishnoi* model describes hydrate formation in a limited timeframe and is seen as the foundation for later derived models.
The model describes the micro kinetics of hydrate formation (mostly structure *s I*) and is based on methane, ethane and their mixtures. Also, the model is limited to a high-pressure stirred tank reactor with constant pressure and can only be applied for reaction times of up to 200 minutes, respectively 100 minutes after the beginning of the nucleation phase. Driving force for hydrate formation is a difference in fugacities, as can be seen in equation [9.1].

According to Englezos, gas hydrate formation takes place in 3 steps:

1. Transport of gas molecules (in)to liquid phase
2. Diffusion of gas trough phase boundary layer around hydrate particles
3. Adsorption and incorporation into hydrate structure [2].

For mathematical modeling, Englezos described steps 2 and 3 and assumed that in equilibrium, gas diffusion into the boundary layer has to be equal to the adsorption rate and resulting to inclusion into hydrate ring structures [2].

The resulting growth rate is expressed by equation [9.1]:

$$\frac{dn_i}{dt} = K^* A_p (f_i^b - f_i^{eq}) \quad [9.1]$$

with:

K^* hydrate formation growth rate constant $[mol \cdot s^{-1}]$
A_p surface area of one hydrate cage at constant pressure and stirrer velocity $[cm^2]$
f_i^b fugacity of component *i* in „bulk“ phase $[bar]$
f_i^{eq} equilibrium fugacity of component *i* in the liquid at the hydrate interface $[bar]$

with

$$\frac{1}{K^*} = \frac{1}{k_r} + \frac{1}{k_d} \quad [9.2]$$

k_r rate constant $[mol \cdot s^{-1}]$
k_d mass transfer coefficient through phase boundary $[mol \cdot s^{-1}]$

The product $K^* A_p$ can be fitted to the experimental data by numeric methods as a combined estimated parameter a, but the above-mentioned restrictions of the model have to be considered.

However, calculation of k_r based on a is really challenging because the specific surface area A_P is pressure-dependent and also depending on stirrer frequency. It can be calculated via the following equation. [103]

$$A_P = \pi * (d_D)^2 \quad [9.3]$$

d_D Particle diameter $[mm]$

k_r: can then be calculated as follows:

$$a = K^* * A_P = (k_r + k_d) * A_P = (k_r + k_d) * \pi * (d_D)^2 \quad [9.4]$$

The determination of the particle diameter d_D is also quite difficult, which can cause further errors in the determination of A_P. The model is well-suited to describe high-pressure hydrate experiments in the early phase of hydrate formation.

9.1.2 Skovborg-Rasmussen

Skovborg and Rasmussen [104] studied the Englezos-Bishnoi model and found restrictions which should be tackled to minimize the possibility of errors, especially in the calculation of k_L. They noted that k_L was obtained at solubility conditions without hydrate formation, which would lead to a significant error, since a small error in the determination of k_L would result in a significantly higher error in K^*

They also suggested that the model could be simplified (with almost negligible errors) by leaving out the crystallization population balance. That is why they derived an equation where the entire hydrate formation is described as mass transfer restriction of the gas through the liquid film at the gas-liquid interface [2]. With this, the number of differential equations was reduced to one equation:

$$\frac{dn}{dt} = k_L A_{(g-l)} c_{wo} (x_{int} - x_b) \qquad [9.5]$$

$A_{(g-l)}$	gas-liquid interface area $[cm^2]$
k_L	mass transfer coefficient through liquid film $[mol \cdot s^{-1}]$
c_{wo}	initial concentration of water $[mol \cdot L^{-1}]$
x_{int}	initial bulk liquid mole fraction of the component $[1]$
x_b	bulk liquid mole fraction of the component $[1]$

9.1.3 Methods of kinetic analysis [105]

There are two principle ways of determining the changes in amount of substance and hence the specific rate law of a given reaction.
The so-called *differential methods* give information on partial order of the participating reactants respectively the rate constant. The so-called *integration methods*, however, use an already known rate law and try to confirm it by integrating the differential rate law. This integrated rate law describes the exact course of changes in the amount of substance if the law fits the process.

Since gas hydrate formation presumably follows a complex mechanism, meaning a mechanism composed of different steps, numerical differential methods of integration are used instead of analytical ones.

In this work, the so-called *fractional life method*, the *differential method* and *estimated value methods* came to use. For the estimated value methods it is important to know, that *a priori* information, like an already existing model, is needed to carry out the estimation. [106]

9.1.3.1 Differential method

Determination of the order of a reaction respectively the partial order for participating components can be done via the *differential method*. For this, the infinitesimal change of reaction rate depending on concentration is considered. With a graphical plot, order of reaction as well as reaction rate constants can be determined. [107–109]

The kinetic equation is as follows:

$$RG := r = \frac{dc}{dt} = k_r * c^l \qquad [9.6]$$

Change of molar amount can be regarded in the same way as change of concentration:

$$RG := r = \frac{dn}{dt} = k_r * n^m \qquad [9.7]$$

To linearize the exponential term, the natural logarithm is taken:

$$\ln(r) = ln\left(\frac{dn}{dt}\right) = \ln(k_r) + m * \ln(n) \qquad [9.8]$$

Plotting $\ln(\frac{dn}{dt})$ against $\ln(n)$ results in a straight line with gradient m and axis intercept $\ln(k_r)$ (see also Figure 35).

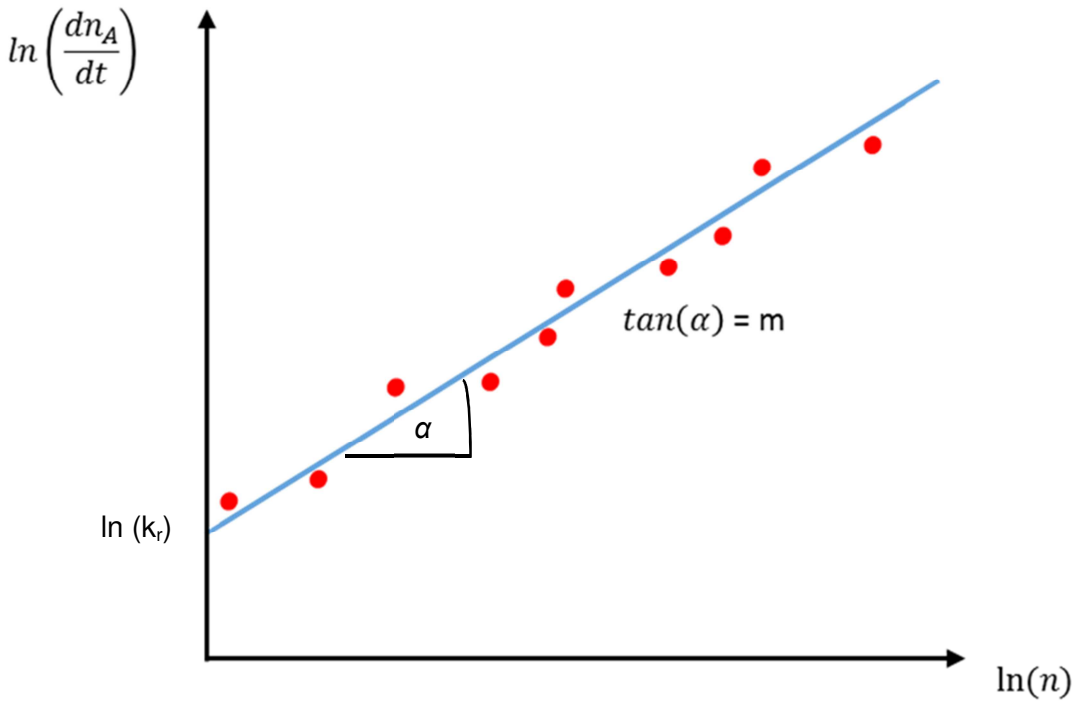

Figure 35: Linearized plot; *differential method*

9.1.3.2 Fractional life method [107, 109–111]

The fractional life method is based on the assumption that the concentration of a reactant decreases by a (previously defined) fraction *f* of the preceding concentration.

For example, the assumption could be that the concentration falls to times 0.8 of the initial concentration in a defined time interval. The following reduction to again times 0.8 of the current concentration will also take place in a time interval that is specific for the reaction.

Plotting the interval times, at which the concentration is reduced by factor *f* against the starting concentrations of the respective intervals results in a straight line whose gradient yields the order of reaction and whose axis intercept describes the reaction rate constant.

The mathematical derivation of the *fractional life method* is shown below:

$$RG = -\frac{dc_A}{dt} = k_r * {c_A}^l \quad [9.9]$$

$$-\int_{c_{A,0}}^{c_A} \frac{dc_A}{{c_A}^l} = k_r * \int_{t_0}^{t} dt \quad [9.10]$$

$$-\frac{1}{1-l} * c_A^{1-l} \,|_{c_{A,0}}^{c_A} = k_r * (t - t_0) \quad [9.11]$$

$$\frac{1}{l-1} * \left[c_A^{1-l} - c_{A,0}^{1-l}\right] = k_r * \Delta t_f \quad [9.12]$$

$$\frac{c_{A,0}^{1-l}}{k_r * (l-1)} * \left[\frac{c_A^{1-l}}{c_{A,0}^{1-l}} - 1\right] = \Delta t_f \quad [9.13]$$

With

$$f^{1-l} = \frac{c_A^{1-l}}{c_{A,0}^{1-l}} \quad [9.14]$$

The final equation results:

$$\frac{c_{A,0}^{1-l}}{k_r * (l-1)} * [f^{1-l} - 1] = \Delta t_f \quad [9.15]$$

Linearizing is done by taking the natural logarithm:

$$\ln(t_f) = ln\left[\frac{f^{1-l} - 1}{k_r * (l-1)}\right] + (1-l) * ln(c_A) \quad [9.16]$$

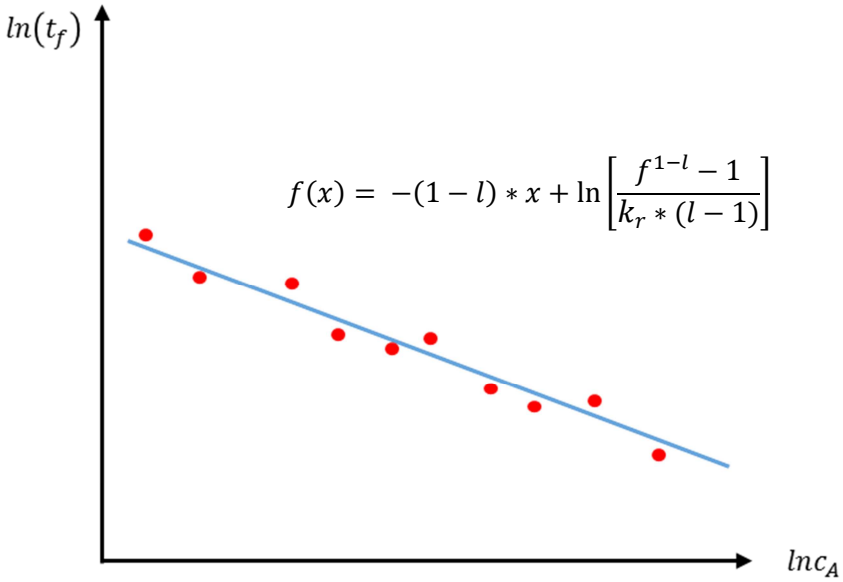

Figure 36: Plot of *fractional life method*; gradient „-(l-1)“ yields reaction order *l*

9.1.3.3 Estimated value methods

Apart from the above-mentioned methods of kinetic analysis, the experimental parameters can also be evaluated statistically.

Goal of a kinetic evaluation is finding a functional correlation between the concentration gradient of a component during reaction and the time. For this, it is necessary to find a mathematical equation that describes the course of reaction with the lowest possible and unsystematic residuals. This equation can be found by fitting an assumed function to the experimental data. For this, optimization algorithms that estimate values based on reasonable starting conditions are used.

A common problem in parameter studies is the determination of a functional correlation between experimental data and the proposed equation. Arbitrarily combining terms to gain a good residual plot in no way reflects the natural law which the reaction follows. Also, polynomial functions are not suited in these methods because they cause an oscillating behavior (around the course of experimental data) and therefore cause a systematic deviation.

Therefore, methods of fitting, which integrate *a priori* information, should be used to reflect the underlying natural law of a reaction. In the case of gas hydrate formation, existing kinetic models could be used and their parameters could be estimated.
The estimation requires choosing of suitable initial values. Otherwise it could be that a local instead of the global minimum is found in the estimation process, which would result in deviations from the desired parameter value [107, 112–114].

9.1.4 Calculation of state variables

In all kinetic analyses, variables of state are needed to determine the kinetic data. In this chapter, the variables of state needed to perform the calculations for this work are briefly explained.

9.1.4.1 Molar volume V_m

The molar volume V_m describes the volume element that is occupied by one mole of a substance, e. g. a gas molecule:

$$V_m = \frac{V}{n} \qquad [9.17]$$

It is used to calculate the molar amount of methane via the *van-der-Waals* equation. which is shown in equation [9.18] in its intense form:

$$\frac{RT}{V_m - b} - \frac{a}{V_m^2} - p = 0 \qquad [9.18]$$

To find an expression for the molar volume, equation [9.18] is multiplied by its common denominator and divided by pressure *p*:

$$V_m^3 - \left(b + \frac{RT}{p}\right) V_m^2 + \left(\frac{a}{p}\right) V_m - \frac{ab}{p} = 0 \qquad [9.19]$$

The solution of this equation is calculated numerically and yields the molar volume V_m. The calculated value must be checked for plausibility, since values could result mathematically that are not consistent with physical considerations. [105, 115]
Numerical solving takes a lot of computing time but is essential for later calculations, since the molar volume V_m is critical for determining the amount of substance *n*.

9.1.4.2 Compressibility factor Z [105, 115]

The compressibility factor *Z* describes the deviation of gas behavior of a gas from "ideal" behavior. An ideal gas has a *Z* value of 1. A value larger than 1 means that the repelling forces of molecules are larger than the attractive forces, which often occurs at high pressures. A value smaller than 1 describes a state where the attractive forces are larger and therefore molecules attract each other. This often occurs at low to moderate pressures.

The compressibility factor describes the ratio of a gas' molar volume V_m to that of an ideal gas that has the same pressure and temperature:

$$Z = \frac{V_m}{V_m^0} \qquad [9.20]$$

With

$$V_m^0 = \frac{RT}{p} \qquad [9.21]$$

the following expression is obtained:

$$Z = \frac{V_m * p}{RT} = \frac{V * p}{n * RT} \qquad [9.22]$$

9.1.4.3 Calculation of molar amount n [105, 115]

The molar amount *n* can be calculated in two ways, both of which are solved numerically.
The first method is the calculation based on the molar volume V_m:

$$n = \frac{V}{V_m} \qquad [9.23]$$

The second method is the calculation based on the compressibility factor *Z*:

$$n = \frac{V * p}{Z * RT} \qquad [9.24]$$

9.1.4.4 Calculation of reaction rate RG [105, 107, 111]

The reaction rate describes the change of molar amount of a substance over time. Reactants are consumed at the same velocity with which reaction products are formed. This is valid for an elementary reaction without intermediates. The infinitesimal change of molar amount *n* is expressed as follows:

$$RG = \frac{dn}{dt} = \frac{dm}{dt} = \frac{dc}{dt} \qquad [9.25]$$

For the hydrate experiments that have been investigated regarding their kinetics, pressure, temperature, stirrer frequency and stirrer torque have been recorded. The change of pressure over time can be seen as “reaction” rate for hydrate formation. Likewise, the change of molar amount of methane can be regarded as reaction rate.

For computation of the changes in molar amount over time, the numerical derivation $\left(\frac{dn}{dt}\right)$ was calculated. The method used to derive was the center-based numerical derivation:

$$f' = \frac{y_{i+1} - y_{i-1}}{x_{i+1} - x_{i-1}} \qquad [9.26]$$

In equation [9.26], *y* means the values of molar amount *n*, *x* means the values of time *t*.

9.1.4.5 Calculation of fugacity coefficients [105, 115]

The derivation for determination of the fugacity coefficient Φ is given below:

$$ln\frac{f}{p} = \frac{1}{RT}\int_0^p \left(V_m - V_{m,ideal}\right)dp \qquad [9.27]$$

with

f	fugacity [bar]
V_m	molar volume [L * mole^{-1}]
$V_{m,ideal}$	molar volume of an ideal gas [L * mole^{-1}]

with

$$\Phi = \frac{f}{p} \qquad [9.28]$$

Φ	fugacity coefficient [1]

the following equation results:

$$\ln \Phi = \frac{1}{RT} \int_0^p \left(V_m - V_{m,ideal}\right) dp \quad [9.29]$$

For an ideal gas, V_m is calculated as follows:

$$V_{m,ideal} = \frac{RT}{p} \quad [9.30]$$

For describing a real gas, the compressibility factor Z is added:

$$V_{m,real} = \frac{RT * Z}{p} \quad [9.31]$$

Combination of the equations results in:

$$\ln \Phi = \frac{1}{RT} \int_0^p \left(\frac{Z-1}{p}\right) dp \quad [9.32]$$

Equation [9.32] is then integrated by the Simpson method, which yields low errors:

$$I_{ab} = \frac{1}{6} \sum_{i=1}^{N} (x_i - x_{i-1}) * \left[f(x_i) + 4 * f(x_{i,middle}) + f(x_{i-1})\right] \quad [9.33]$$

9.1.4.6 Calculating the fugacity [105, 115]

The fugacity is an auxiliary quantity used to describe deviations of a gas from ideal behavior and is defined as follows:

$$f = \Phi * p \quad [9.34]$$

The fugacity describes the effective partial pressure of a component and can deviate strongly from the measured total pressure in the system.

9.1.4.7 Calculating the equilibrium fugacity [2, 95, 105, 115]

According to the *Englezos-Bishnoi* model (see chapter 9.1.1), driving force for hydrate formation is the difference of fugacities *f – f(eq.).*

For calculating it is therefore critical to know the equilibrium fugacity *f(eq.)*. For this, the equilibrium pressure for hydrate formation has to be known.

However, in the course of this work, equilibrium pressure was not reached in the experiments, since the focus was on determination of induction times and measuring equilibrium pressures in the system used would have taken up too much time.
Therefore, to calculate equilibrium pressures, the software *CSMGem* developed by the Sloan group [2] was used. For the temperatures of 4 °C (277.15 K) and 6 °C (279.15 K), the software yielded equilibrium pressures of 38.5 bar(g) and 46.7 bar(g), respectively.

The product of equilibrium pressure and fugacity coefficient then yields the equilibrium fugacity *f(eq.)*:

$$f(eq) = \Phi * p(eq) \quad [9.35]$$

With these state variables, all the calculations described above could be performed. Results are shown in chapter 9.3.

9.2 Procedure [105]

The kinetic investigation was done on sorted experiments out of the “determination of optimal parameters” series. Focus was on trying different methods to find a correlation with the methods described in chapter 9.1. Effects of possible inhibitors were not accounted for to keep the complexity of the model in a reasonable frame.

Analyses required a reasonable limitation of the range of data, since the regarded “reaction” does not take place in the beginning of the experiment. In the system used, the exact starting point of hydrate formation cannot be determined since the visual control of the reactor’s inside is not possible at all times (e. g., when experiments take several days and hydrate formation starts at night).
Hence, a theoretical starting time of hydrate formation had to be determined. Following the formation models of Radhakrishnan, Trout and Moon [40, 41] (*local structuring nucleation hypothesis*), saturated conditions can be seen as optimal starting situation for the formation of heterogeneous crystal nuclei. This starting situation is not identical to the macroscopic induction times that are evaluated in the later inhibitor screenings.

The experimental data contained the variables pressure, temperature, stirrer frequency and stirrer torque. The following state variables had to be calculated based on these values for the kinetic analysis. Some of these calculations took a long time due to the great number of measured data. Therefore, a macro program was written inside the working group to calculate these values. [105]

The calculated state variables to estimate the theoretical starting point (resp. the theoretical starting pressure) of nucleation were molar volume, compressibility factor *Z,* amount of substance *n*, rate of reaction, fugacity coefficient, fugacity and equilibrium fugacity.
The calculated values for the theoretical starting point are found in Table 47. The values of the experiments at 120 bar(g) are not included, since the driving force was quite low in these experiments. This was seen as obstruction to a detailed modeling, since the deviation of values within the experimental series was quite strong.

Table 47: Theoretical starting point of hydrate formation; kinetic analyses

Experiment	Amount of substance Methane n_0 / mol	Theoretical initial pressure p_0 / bar	Total pressure drop $\Delta p_{total} / bar$	Theoretical starting pressure $p_{Nucleation} / bar$
HSS 160 bar 4 °C / Experiment 1	3.04	164.6	24.0	140.6
HSS 160 bar 4 °C / Experiment 2	3.05	165.3	24.1	141.1
HSS 160 bar 4 °C / Experiment 3	3.04	164.6	24.0	140.6
HSS 160 bar 6 °C / Experiment 2	3.03	164.0	21.5	142.4
HSS 160 bar 6 °C / Experiment 4	3.06	165.9	22.0	143.9
HSS 160 bar 6 °C / Experiment 5	3.06	165.9	22.0	143.9
HSS 135 bar 4 °C / Experiment 1	2.55	136.6	17.9	118.7
HSS 135 bar 4 °C / Experiment 7	2.59	138.7	18.4	120.3
HSS 135 bar 4 °C / Experiment 8	2.58	138.2	18.2	119.9

Rate equations were determined via the *fractional life method* (see also chapter 9.1.3.2). *Englezos-Bishnoi* kinetics (see also chapter 9.1.1) were investigated via the software *Matlab*, including the additional *curve fitting toolbox*. Also, *Matlab* was used for investigation via the *differential method* (see also chapter 9.1.3.1).

9.3 Results and discussion [105]

In this chapter, the kinetic analyses of sorted experiments out of the “determination of optimal parameters” are shown and discussed.

Kinetic analyses were conducted on sorted experiments of chapter 5.: the experiments are highlighted in color in Table 48. It is to be mentioned that for the calculations, the induction times were not rounded to whole minutes, but instead used with two decimal places to increase accuracy of the performed calculations.

Table 48: Experiments for kinetic analyses

Measurement series	Induction time [min]					
	1	2	3	4	5	6
HSS 160 bar 4°C	235.97	133.72	148.95	86.93	107.00	--
HSS 160 bar 6°C	158.00	109.73	134.18	108.00	105.00	--
HSS 135 bar 4°C	277.88	2783.00	1589.97	875.78	267.97	300.48
HSS 120 bar 4°C	2889.02	1887.83	641.32	1123.25	361.12	--

Table 49 shows the calculated starting conditions for the kinetic evaluation that are used as basis for the following calculations.

Table 49: Calculated „starting conditions“ for kinetic analyses

Experiment	Molar amount Methane n_0 [mole]	Theoretical starting pressure p_0 [bar]	Total pressure drop Δp_{total} [bar]	Theoretical initial pressure $p_{nucleation}$ [bar]
HSS 160 bar 4 °C / Experiment 1	3.04	164.6	24.0	140.6
HSS 160 bar 4 °C / Experiment 2	3.05	165.3	24.1	141.1
HSS 160 bar 4 °C / Experiment 3	3.04	164.6	24.0	140.6
HSS 160 bar 6 °C / Experiment 2	3.03	164.0	21.5	142.4
HSS 160 bar 6 °C / Experiment 4	3.06	165.9	22.0	143.9
HSS 160 bar 6 °C / Experiment 5	3.06	165.9	22.0	143.9
HSS 135 bar 4 °C / Experiment 1	2.55	136.6	17.9	118.7
HSS 135 bar 4 °C / Experiment 7	2.59	138.7	18.4	120.3
HSS 135 bar 4 °C / Experiment 8	2.58	138.2	18.2	119.9

The results of kinetic analyses are discussed below. One sample evaluation is shown for each method; the remaining results are shown in tables for reasons of transparency. Discussion of the results is done primarily by comparison of the determined rate constants. It has to be mentioned that the values for the “residual sum of squares” (*SSE*) that are calculated and shown in the sample evaluations are not shown in the tables, since the regression coefficient R^2 is shown. *SSE* and R^2 are inversely correlated, meaning that a low *SSE* yields a high R^2. Since regression coefficients are easier to interpret (because their maximal value is “1”; the nearer a value is at 1, the better the regression), they are shown in the tables and values for *SSE* are left out.

9.3.1.1 Englezos-Bishnoi model

In contrast to the other methods, the *Englezos-Bishnoi* model is limited to a defined time interval of hydrate formation. Calculation begins at the theoretical initial pressure $p_{nucleation}$ and ends 100 minutes later. Analysis was done via *Matlab©R2014a* with the additional *Curve fitting toolbox*.

For calculation of K^* (see equation [9.1]) the model function $f(x) = a \cdot x + b$ was used for parameter estimation. $f(x)$ equals the reaction rate $\left(\frac{dn}{dt}\right)$, x characterizes the difference of fugacity $(f - f_{eq})$.

The estimated parameter a equals the product $K^* \cdot A_p$, with K^* following: $\frac{1}{K^*} = \frac{1}{k_r} + \frac{1}{k_d}$.

Table 50 shows the summary of all investigated experiments, Figure 37 shows a sample analysis with all determined parameters below it.

Table 50: *Englezos-Bishnoi* model, summarized parameters [105]

		Estimated parameter a / $\langle K^* \cdot A_p \rangle$	R^2
HSS 160 bar 4 °C	**Experiment 1**	$6.205 \cdot 10^{-6}$	0.9992
	Experiment 2	$9.434 \cdot 10^{-6}$	0.9991
	Experiment 3	$9.466 \cdot 10^{-6}$	0.9991
HSS 160 bar 6 °C	**Experiment 2**	$1.003 \cdot 10^{-5}$	0.9980
	Experiment 4	$9.134 \cdot 10^{-6}$	0.9984
	Experiment 5	$5.138 \cdot 10^{-6}$	0.9525
HSS 135 bar 4 °C	**Experiment 1**	$2.646 \cdot 10^{-5}$	0.9970
	Experiment 7	$1.299 \cdot 10^{-5}$	0.9968
	Experiment 8	$1.110 \cdot 10^{-5}$	0.9862

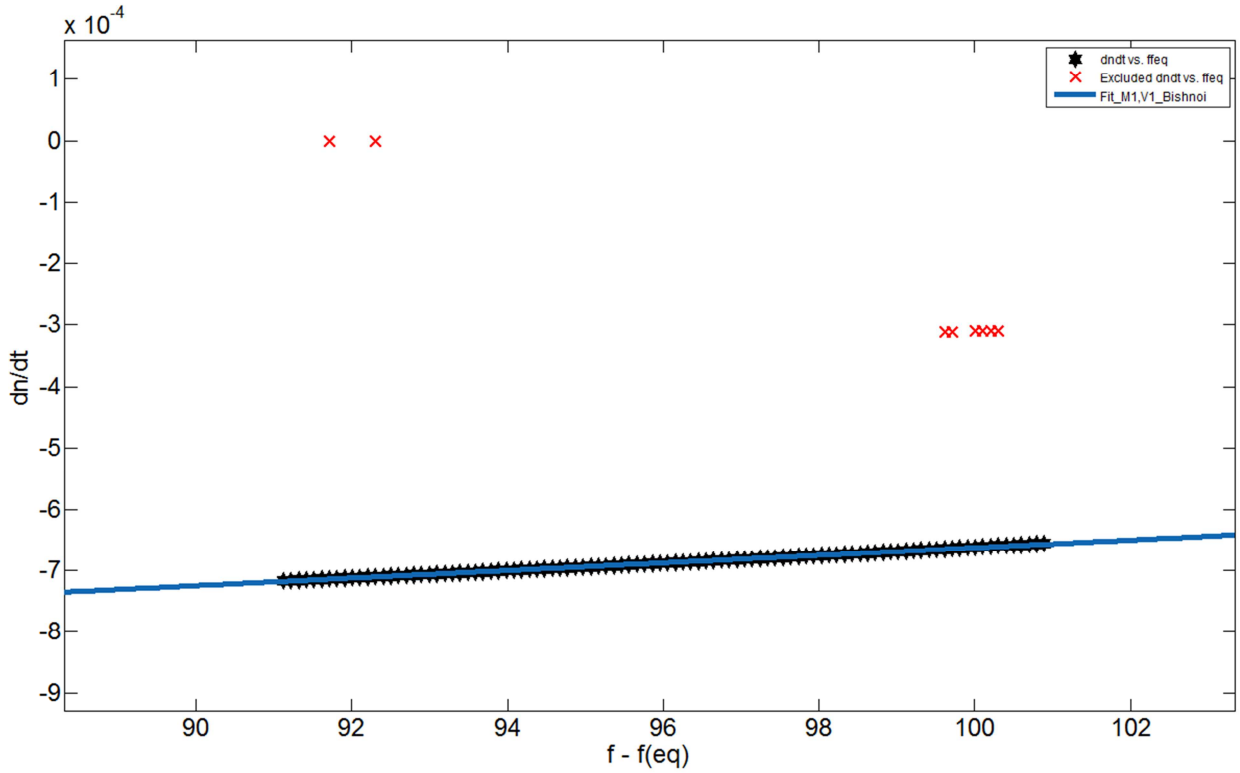

Figure 37: *Englezos-Bishnoi* model, sample experiment, HSS 160 bar(g) 4 °C, experiment 1 [105]

General model:

$$f(x) = a \cdot x + b$$

Coefficients (with 95 % confidence bounds)

a = 6.205e-06 (6.185e-06, 6.225e-06)
b = -0.001283 (-0.001285, -0.001281)

Goodness of fit:

SSE: 6.964e-11
R^2: 0.9992

9.3.1.2 *Differential method*

To validate the parameters gained in chapter 9.3.1.1, the experiments were analyzed via *differential method* in the same time interval as with the *Englezos-Bishnoi* model.
Hence, the process is analyzed from the theoretical initial pressure to 100 minutes later.
The order of reaction (*l*) is determined from the gradient of the regression line and the rate constant k_r is determined from the axis intercept. The estimation parameter *a* describes the order of reaction and estimation parameter *b* the natural logarithm of k_r.

Table 51 shows the summary of all investigated experiments; Figure 38 shows a sample analysis with all determined parameters below it.

Table 51: *Differential method*, summarized parameters [105]

		Parameter a	Parameter b	l	k_r $[mol \cdot s^{-1}]$	R^2
HSS 160 bar 4 °C	**Experiment 1**	-1.431	-5.796	-1.431	$3.04 \cdot 10^{-3}$	0.9708
	Experiment 2	-1.537	-5.29	-1.537	$5.04 \cdot 10^{-3}$	0.9658
	Experiment 3	-1.565	-5.262	-1.565	$5.18 \cdot 10^{-3}$	0.9640
HSS 160 bar 6 °C	**Experiment 2**	-3.628	-3.128	-3.628	$4.38 \cdot 10^{-2}$	0.6280
	Experiment 4	-1.636	-5.199	-1.636	$5.52 \cdot 10^{-3}$	0.9526
	Experiment 5	1.728	-8.732	1.728	$1.61 \cdot 10^{-4}$	0.2373
HSS 135 bar 4 °C	**Experiment 1**	-4.05	-2.465	-4.05	$8.50 \cdot 10^{-2}$	0.8917
	Experiment 7	-8.766	0.9573	-8.766	2.60	0.1026
	Experiment 8	-2.022	-4.942	-2.022	$7.14 \cdot 10^{-3}$	0.9197

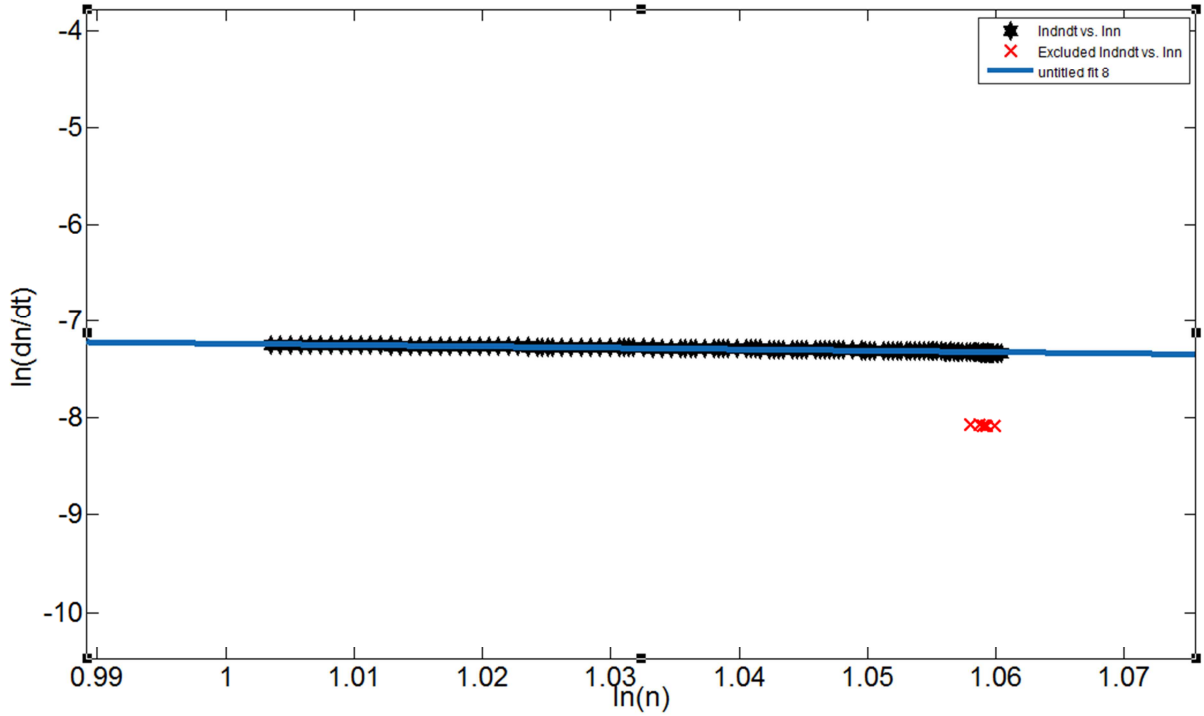

Figure 38: ***Differential method, sample experiment,*** **HSS 160 bar(g) 4 °C, experiment 1 [105]**

General model:

$$f(x) = a * x + b$$

Coefficients (with 95 % confidence bounds):

a =	-1.434	(-1.463, -1.405)
b =	-5.796	(-5.826, -5.766)

Goodness of fit:

SSE: 0.005366

R^2: 0.9708

9.3.1.3 Fractional life method

To calculate rate constants according to the *fractional life* method, the theoretical initial pressure (see Table 49) was used. The corresponding molar amount (*initial molar amount* n_0) was then calculated via the *van-der-Waals* equation. The *fraction f* was chosen in a way that the *end molar amount* n_e equals the referring value of the ending pressure of the experiment. So, the whole course of the respective experiment was investigated, Δt marks the time range for that the calculation was done.

Table 52 shows the summarized parameters of all investigated experiments, Figure 39 and Table 53 show one sample experiment.

Table 52: Overview of all investigated experiments, fractional life method [105]

		f	Δt [min]	I	k_r [mol·s^{-1}]	R^2
HSS 160 bar 4 °C	Experiment 1	0.98000	2560	15.217	$5.35 \cdot 10^{-12}$	0.5193
	Experiment 2	0.98000	1332	11.202	$3.30 \cdot 10^{-10}$	0.6837
	Experiment 3	0.98060	3963	17.895	$4.74 \cdot 10^{-13}$	0.4839
HSS 160 bar 6 °C	Experiment 2	0.97965	6670	11.563	$1.97.10^{-10}$	0.4639
	Experiment 4	0.98125	1334	12.068	$9.00 \cdot 10^{-11}$	0.4751
	Experiment 5	0.98279	5652	15.067	$6.92 \cdot 10^{-12}$	0.5619
HSS 135 bar 4 °C	Experiment 1	0.98000	1222	1.9867	$2.81 \cdot 10^{-6}$	0.0112
	Experiment 7	0.98027	1223	3.1152	$1.03 \cdot 10^{-6}$	0.0657
	Experiment 8	0.981003	1092	1.6886	$3.09.10^{-6}$	0.0043

To extract the parameters shown in Table 52 and Table 53, the following steps were taken.

Equation [9.36] shows the linearization formula, a sample plot of $\ln(t_f)$ against $\ln(c_a)$ is shown in Figure 39.

$$\ln(t_f) = ln\left[\frac{f^{1-l}-1}{k_r \cdot (l-1)}\right] + (1-l) \cdot ln(c_A) \quad [9.36]$$

As mentioned in chapter 9.1.3.2, the *order of reaction* (*l*) and rate constant k_r are then determined from the linear equation. The procedure is demonstrated based on the linear equation seen in Figure 39.

In Figure 39, the following equation results from plotting $ln(c_A)$ against $ln(t_f)$:

$$f\ (c_A) = -14.217 * \ln c_A + 22.199 \quad [9.37]$$

Reaction order l is then determined as follows:

$$1 - l = -14.217 \quad [9.38]$$

The equation yields the following for *l*:

$$l = 15.217 \quad [9.39]$$

With this, the order of reaction is determined.

Determining the rate constant k_r is done after determination of the order *l*.
The axis intercept contains k_r; the operation to calculate k_r is shown below.

$$ln\left[\frac{f^{1-l}-1}{k_r \cdot (l-1)}\right] = 22.199 \quad [9.40]$$

The known values are inserted:

$$22.199 = ln\left[\frac{0.98^{1-15.217}-1}{k_r * (15.217-1)}\right] \quad [9.41]$$

Solving numerically yields the reaction rate constant k_r:

$$k_r = 5.35 * 10^{-12}\ mol * s^{-1} \quad [9.42]$$

The coefficient of determination R^2 provides information on the quality of the regression and hence on the veracity of the obtained rate equation.

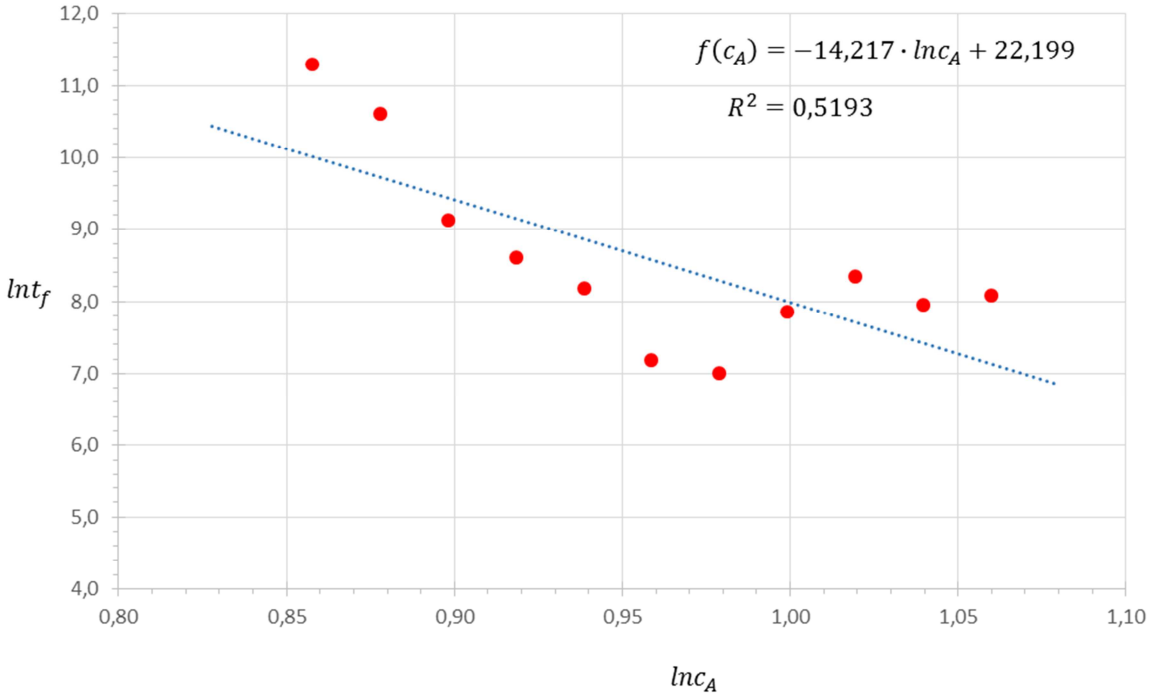

Figure 39: fractional life method, HSS 160 bar(g) 4 °C, experiment 1 [105]

Table 53: fractional life method, HSS 160 bar(g) 4 °C, experiment 1 [105]

Fraction *f*	0.98
Order of reaction *l*	15.217
Rate constant k_r	$5.35 \cdot 10^{-12}$ mol·s^{-1}
Initial pressure p_0	140.7 bar(g)
Initial molar amount n_0	2.8856 mole
Ending pressure p_e	112.5 bar(g)
Ending molar amount n_e	2.3106 mole
Time range Δt	2560 min
Coefficient of determination R^2	0.5193

9.3.1.4 Summary of kinetic analyses

The analyses via the *Englezos-Bishnoi* model yield good correlations for the first 100 minutes after initial nucleation. The found combined rate constants are of the same magnitude. A problem of the model is the specific surface area A_p, which is dependent on pressure and stirrer frequency and therefore cannot be determined under transient conditions. The formation of gas hydrates with constant driving force / constant pressure could lead to better results, but for the reasons already mentioned in chapter 11.1.5, this was not done in the scope of this work.

Analyses via *differential method*, which were also conducted for the first 100 minutes after initial nucleation, also point to the existence of a “combined mechanism” consisting of different steps and with different aspects playing critical roles. There are great differences in the respecting experimental series (with the exception of HSS 160 bar(g) 4 °C) as well as between them.

The analyses via the *fractional-life* method, that describe the whole hydrate formation experiment, show that gas hydrate formation is not a trivial process and is also not comparable to a chemical elementary reaction. Formation rate strongly “fluctuates” over time, which is shown in “bad” regression coefficients. This is probably caused in reaction order shifts or similar processes. Also, diffusion controlled phenomena as well as influence of the stirrer (crushing of hydrates, generation of “new” nucleation sites) could play a role in this.
The “small” rate constants are probably owed to the fact that gas hydrate formation was analyzed in total, with the very slow formation of gas in the end of each experiment.
Still, some sections of gas hydrate formation can be described well with the *fractional-life* method. Nevertheless, the hydrate formation mechanism has to be further clarified to match the “well fitted” areas to actual physical “events”.

It is to be mentioned that for the analyses only reaction rates with negative values were taken into consideration. This was done because the consumption of methane (pressure reduction) was used as criterion for measuring the progress of hydrate formation.
To fit functions to the experimental data, no tests for outliers were conducted. Instead, outliers were identified graphically by means of expert knowledge.

The performed analyses have to be considered as a first approach to model the very complex phenomenon of hydrate formation in the transient system used. They can act as a guide for further modeling as soon as the mechanism of hydrate formation is better

understood, e. g. with help of the Büchi Ecoclave reactor, or at least until the recommended modifications in instrumentation of the reactor (see chapter 11.2) have been made.

10 Custom-tailored inhibitor candidates

This chapter describes the synthesis of custom-tailored inhibitor candidates as well as their investigation, which was conducted in the glass-made reactor. In the first part of this chapter, the synthesis of the custom-tailored candidates is described in detail. In the second part, the procedure of investigation is described. The third part shows results and discussion of the investigations.

10.1 Synthesis

Some of the inhibitor candidates were custom-tailored. Those tailored inhibitors were investigated inside the Büchi Ecoclave reactor, to gain a deeper insight in inhibition ability and mechanisms.

The inhibitors were dendrimers based on glycerol and were produced according to [116] with slight procedure modifications. *[Gn]-ene* and *[Gn]-OH* dendrimers up to the second generation were synthesized, in detail the obtained substances were *[G1.0]-OH*, *[G2.0]-ene* and *[G2.0]-OH*. The substances are shown in Table 54, all the reactants for the different reaction steps are shown in Table 55.

Table 54: Synthesized custom-tailored inhibitor candidates

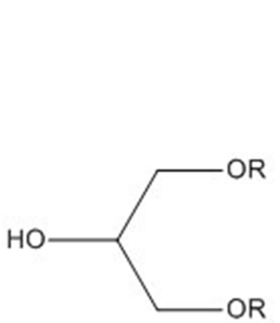	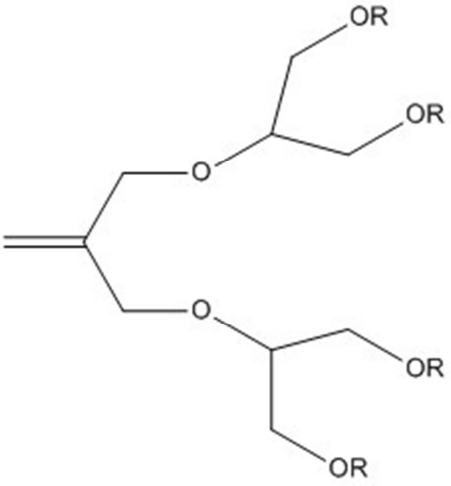	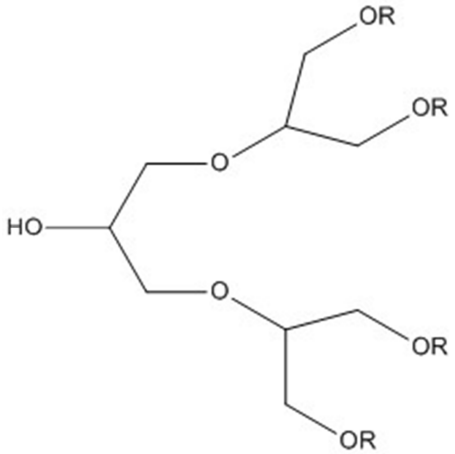
[G1.0]-OH	[G2.0]-ene	[G2.0]-OH

As can be seen in Table 54, the dendrimers “branch out” from generation to generation, which results in an increase of oxygen-containing groups in the molecule, hence in possible interruption of hydrogen bonds. Therefore it was assumed that dendrimers could influence hydrate formation and that the influence increases with higher dendrimer generations. Also,

the difference between “-ene” and “-OH” as head groups and their influence on hydrate formation was investigated.
Experiments were conducted in the Büchi ecoclave reaction system (reactor made of glass) so that a parallel visual observation was possible.

To produce the first generation of OH dendrimers (named *[G1.0]-OH*), acetal protection of triglycerol was performed [117]. For this, triglycerol was brought to reaction with 2,2-dimethoxypropane. Then, para toluenesulfonic acid was added and the reaction was carried out overnight at 30-40 °C:

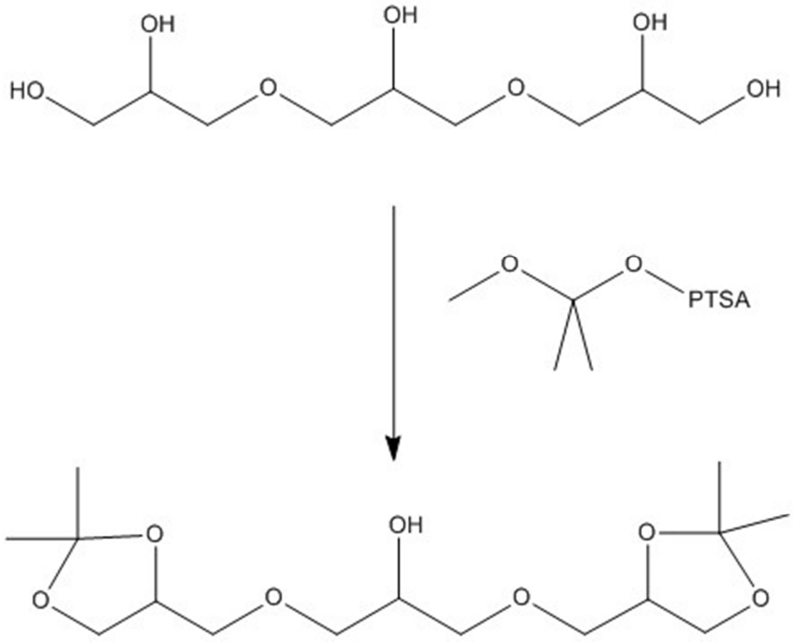

[10.1]

After that, the solution was neutralized by adding triethylamine, followed by evaporating the solvent and purification by filtration over silica gel (ethyl acetate / n-hexane 1:2):

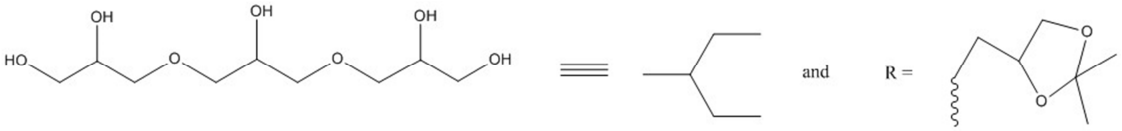

[10.2]

After that, the product was separated in 2 portions. One was tested for inhibition suitability; the other one was used to synthesize further dendrimers.

The next step was the synthesis of *[G2.0]-ene* out of *[G1.0]-OH*. For this, *[G1.0]-OH* was brought to reaction with sodium hydride and MDC in dry THF in the presence of catalytic amounts of KI, [15]crown-5 and [18]crown-6 (both are crown ethers) (This is marked as “a” in

the reaction equation in [10.3]). Purification of the residue was done by distillation, in contrast to [116], where purification was done by HPLC.

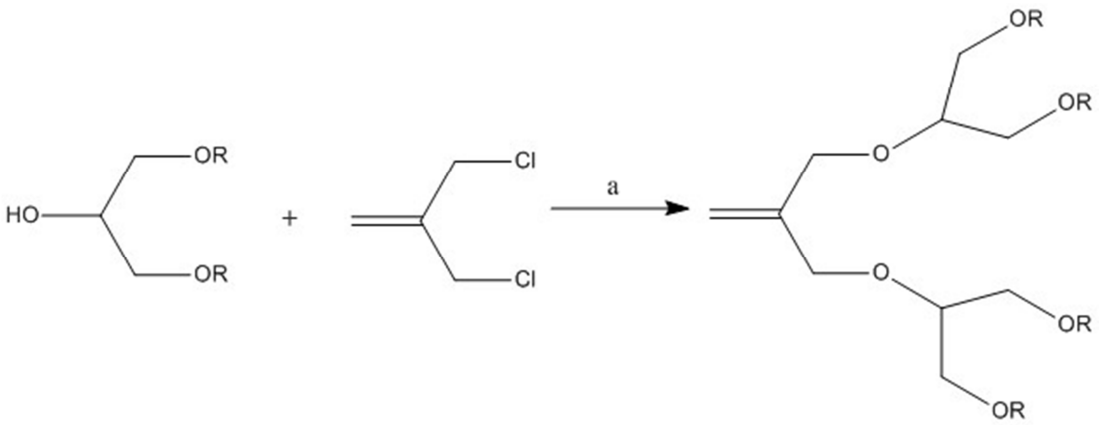

[10.3]

The product was again separated in 2 parts, one was tested for inhibition suitability, the other one was used to synthesize *[G2.0]-OH* as follows:

[G2.0]-ene was ozonolyzed in a mixture of MeOH/CH_2Cl_2 (1:1) and then reduced to the secondary alcohol by treatment with $NaBH_4$. This is described as “b” in [10.4]. Purification was again done by distillation, as opposed to [116], where it was done by extraction with CH_2Cl_2.

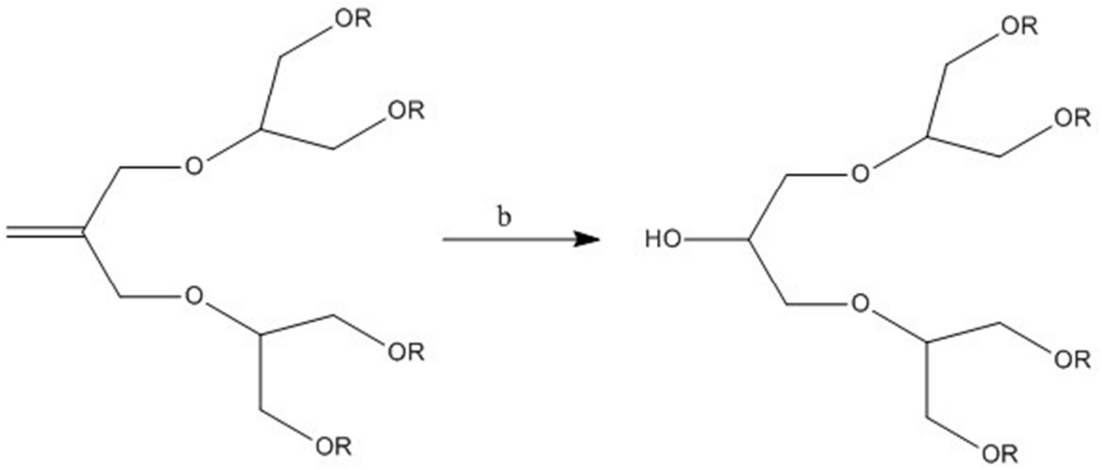

[10.4]

Table 55: Reactants for synthesizing custom-tailored inhibitor candidates

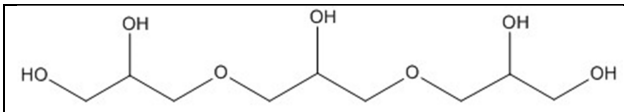	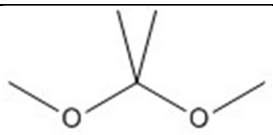
triglycerol	2,2-dimethoxypropane
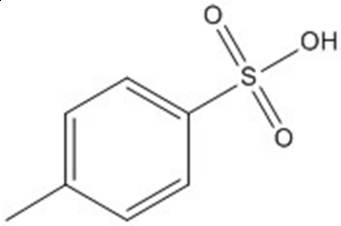	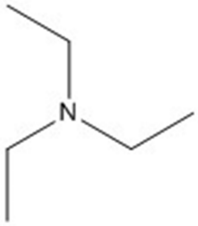
p-toluenesulfonic acid	triethylamine
NaH	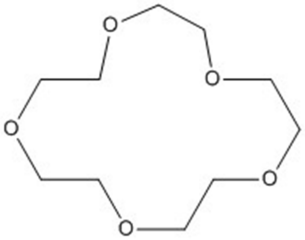
Sodium hydride	[15]crown-5
	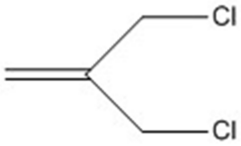
tetrahydrofuran	methallyl dichloride
KI	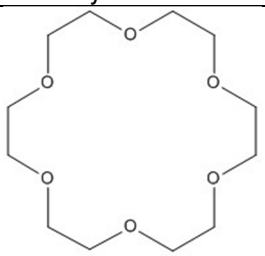
potassium iodide	[18]crown-6
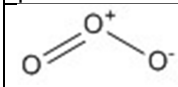	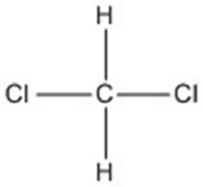
ozone	dichloromethane
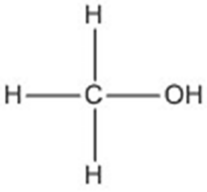	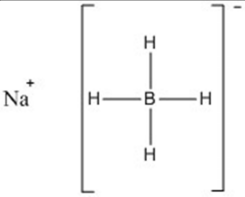
methanol	sodium borohydride

Results of the inhibition suitability tests are shown and discussed below.

10.2 Investigation procedure

Experiments were conducted as follows:

The empty reactor was filled with water and THF (in a molar ratio of 17:1) and inhibitor, where required.
After filling, the reactor was purged 3 times with methane to remove air and retain a pure "methane atmosphere". For this, the reactor was pressurized with methane to a pressure of about 5.5 bar(g) and then pressure was released to a value of about 0.5 bar(g) to avoid back mixing with the laboratory air. In total, a minimum dilution of 1:90 (3 times purging with at least 4,5 bar difference in pressure each) was reached.
After purging, the reactor was filled with methane to a pressure of 8 bar(g), the agitator was set to 250 min^{-1} and the thermostat to 4 °C. The reaching of the "highest" pressure marked the beginning of the experiment.
The only type of inhibitor investigated in this reactor were the custom-tailored inhibitor candidates (see above).

To guarantee turbulence inside the reactor, the stirrer operates at high frequency, and a modified Reynolds number of approximately 6920 is reached (see equation [10.5]). The built-in components, like probe tubing, resistance thermometer, etc. that could act as vortex breakers, are not accounted for:

$$\boldsymbol{Re_R = \frac{N * d^2 * \rho}{\eta} = \frac{\frac{250}{60s} * (0.05\,m)^2 * 986.88 \frac{kg}{m^3}}{1.49 * 10^{-3} \frac{kg}{m * s}} \approx 6920} \qquad [10.5]$$

Values for density and viscosity of the water-THF mixture were taken from [90]. The calculation was done for a temperature value of 298 K.
Stirrer frequency *N* was 50 min^{-1}, diameter *d* of the propeller type stirrer was 50 mm, the density ρ of the water-THF mixture at 20 °C is 986,88 kg/m^3 and the dynamic viscosity η at 20 °C is $1.49*10^{-3}$ kg/m*s [90].

With a value of 6920, the Reynolds number inside the Büchi ecoclave reaction system again is well in the transition area between laminar and fully turbulent flow.

10.3 Results and discussion

In this chapter, first results of the experiments conducted with the “new” glass reactor (Büchi ecoclave) are shown. The experiments include blind experiments (with water, THF and methane; experimental procedure is shown above) as well as experiments with the custom-tailored inhibitor candidates.
Due to the high experimental efforts and difficulties to gain higher generations of the investigated dendrimers in high yields, experiments were only conducted at concentrations of 0.1 % wt. of the respective inhibitor candidate. This was done as a first test to see which of the inhibitor candidates should be investigated further and also enter high-pressure tests.
Tests were also conducted inside the glass reactor to see, if the custom-tailored inhibitor candidates would cause a difference in formation mechanism or formed hydrate structures.

Since the experiments were again conducted with THF and in the low-pressure range, only induction times are compared and discussed.

Individual induction times determined in all of the experiments conducted in the ecoclave system are listed in Table 56, the corresponding statistical data is shown in Table 57.
In Table 57, the “+” in the column “Normally distributed” means “normal distribution cannot be rejected”, which is interpreted as “normally distributed” for further testing, e. g. for outliers.
A “-“ means “not normally distributed”.

In the column “Outliers?”, a “-“ means “no outliers on tested level of significance”, a “+” would mean “outliers” and the letter “b” means “testing according to Dixon Q not possible, because data was not normally distributed”.

Figure 42 shows the graphical comparison of the induction times of all custom-tailored substances versus blind experiments.

Table 56: Individual results of experiments; Custom-tailored inhibitor candidates

Experimental conditions / series of measurement	**Induction time [min]**				
	1	**2**	**3**	**4**	**5**
Blind	165	58	65	165	85
[G1.0]-OH	187	103	540	75	
[G2.0]-ene	165	139	132		
[G2.0]-OH	304	1339	1328	--	--

Table 57: Statistical data of experimental series; Custom-tailored inhibitor candidates

	No. of exp.	Induction time								
		Mean	Std. dev.	Rel. std. dev. [%]	Coeff. of var.	Minimum	Maximum	Range (Maximum – Minimum)	Normally distributed?	Outliers?
Blind	5	108	53	49	0.49	58	165	107	+	-
[G1.0] -OH	4	226	215	95	0.95	75	540	465	+	-
[G2.0] -ene	3	146	17	12	0.12	132	165	33	+	-
[G2.0] -OH	3	991	595	60	0.60	304	1339	1035	-	b

Blind experiments in the Büchi ecoclave system showed induction times ranging from 58 to 165 minutes. Experiment 1 and 4 showed great correlation, experiments 2, 3 and 5 were also in good agreement with each other. An important criterion that was striking in the Büchi experiments was the gas saturation of the deionized water that came to use.

An in-lab deionized water system was used, which showed small differences in gas saturation on some days, meaning the water seemed “clouded” on some days when first filled inside the beaker for weighing. This was caused by tiny gas bubbles inside the water.

Although the reactor was purged 3 times with methane before each experiment, it is assumed that this gas still could influence hydrate formation. It seems that on days where this “clouding” occurred, hydrate formation took longer compared to the days with “clear” water.

This should be investigated in further experimental series.

Figure 40 shows a picture of formed hydrate in a blind experiment. First results indicate that the hydrate formation takes place at the phase boundary between water and gas inside the glass reactor.

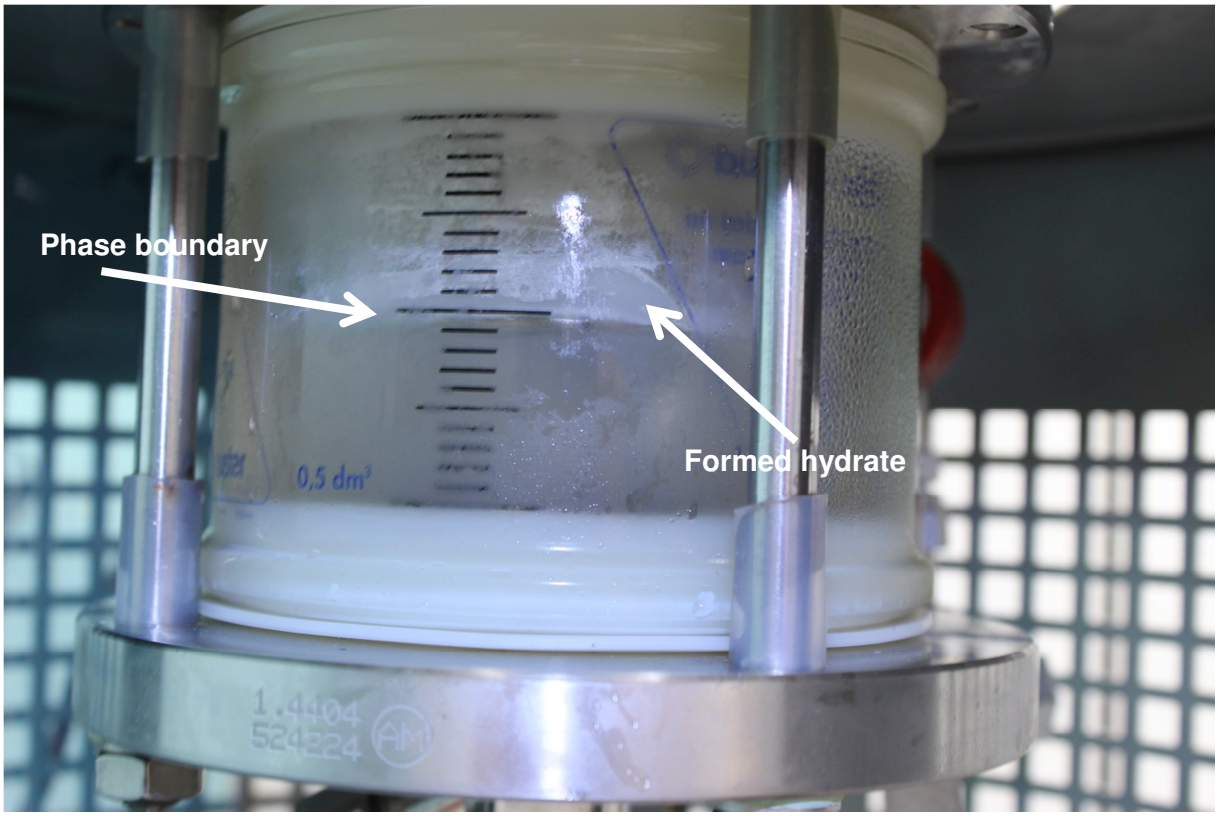

Figure 40: Hydrate formation inside the Büchi Ecoclave reactor; Blind experiment

Also, the picture shows that the hydrates seem to grow into the gas phase. This could be caused by differences in density between water and hydrates (hydrates “swim up”, density is around 0.94 g / cm³ for *s I* hydrates [2] and 0.99 g / cm³ for the water-THF-mixture, see also chapter 10.2 and [90]).

However, since the hydrates should have some kind of adhesion to the glass walls and therefore be hindered from swimming up, this could be an indication that reinforces the “nucleation at the interface hypothesis”, which is also supported by the strong impact that an additional gas phase stirrer had on induction times in both the IKA and the Parr reactor.

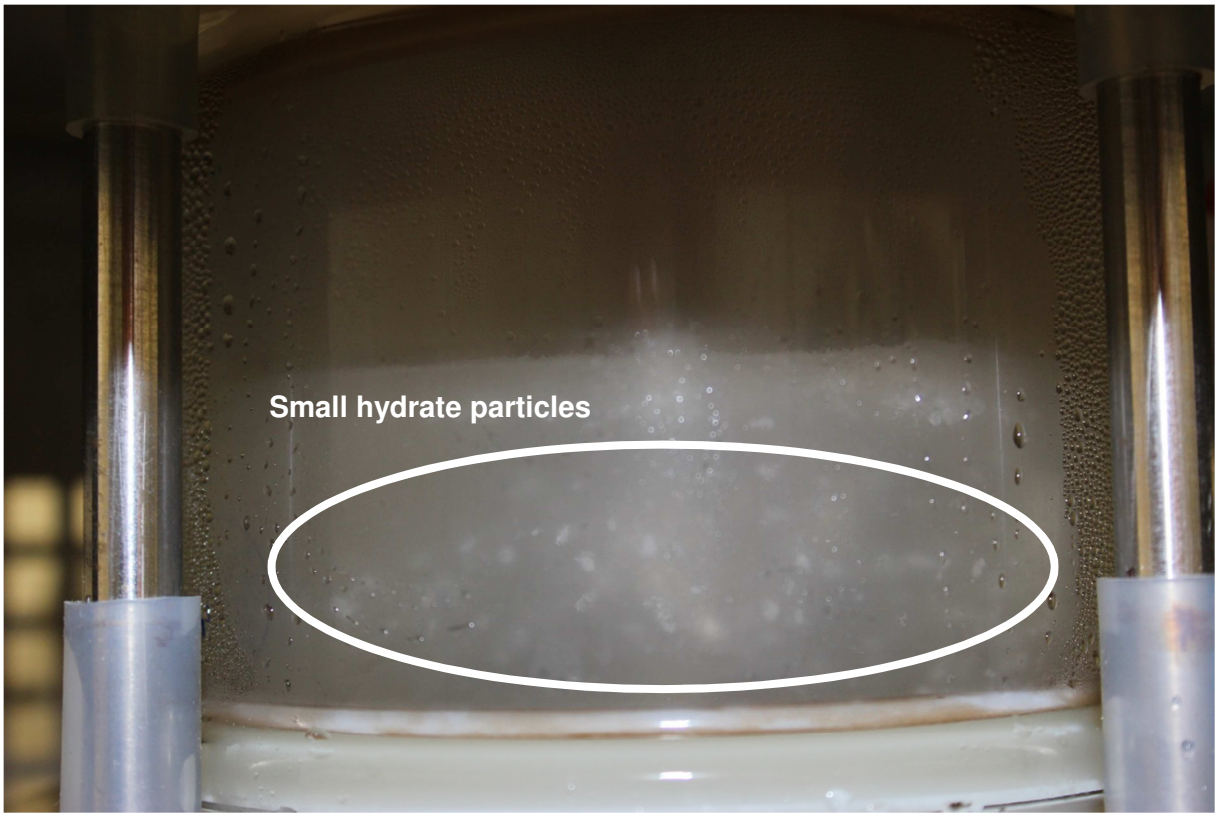

Figure 41: Small hydrate particles in Büchi reaction system

Another phenomenon occurred during hydrate formation: Figure 41 shows an early stage of the hydrate formation experiment. There are small hydrate particles “floating around” inside the reactor. These particles only occurred in some of the experiments before the above-shown “growing into the gas phase”. They were perhaps formed at the interface between water and gas and then “stirred in” below the surface.
Also, it is possible that in some experiments, hydrates were formed in the bulk phase and then swam up to the surface simply because of density effects (see above).

In any case it is recommended to conduct further “blind” experiments inside the glass reactor, e. g. with a high-speed camera, to gain deeper insight into the exact starting point of the macroscopic growth phase and hence draw conclusions regarding the mechanism of hydrate formation.

After the blind experiments, [G1.0]-OH was tested inside the Büchi reactor as first of the custom-tailored inhibitor candidates. With one exception in experiment 3, [G1.0]-OH showed almost no difference in induction times compared to the blind experiments. Nonetheless, further experiments, e. g. with degassing the water before experiments to avoid the above-mentioned problem, are needed to see if the lower or higher induction times are the “true” ones in the long run.

During weighing, there seemed to be some kind of “reaction” with [G1.0]-OH, water and THF. Water was filled into the beaker, then THF was added, after that, [G1.0]-OH. When [G1.0]-OH was added, the beaker showed warming on the outside. This was not observed for [G2.0]-ene or [G2.0]-OH. This phenomenon could be caused by [G1.0]-OH having a higher value for the enthalpy of mixing. In principle, no reaction between THF and [G1.0]-OH should occur, a reaction with water also seems unlikely. In which way the phenomenon influences hydrate formation still has to be further investigated.

Again, the influence of gas saturation in the deionized water seemed to influence hydrate formation. During the third experiment, the deionized water was taken from a storage vessel, where it had the time to “calm down”. This was done since the in-lab deionized water system was in maintenance and hence, the water was filled into storage vessels beforehand. The “calming down” of the water resulted in the highest induction time of the whole measurement series. Experiments after this one, where the maintenance was over, showed very short induction times on the other hand. This could have been caused by after-effects of the maintenance procedure, since all of the water piping had been drained of water during maintenance and there was air inside. Although the water was left on before experiments to remove this residual air, there were still some “gas bubbles” inside the water during experiment 5 with [G1.0]-OH and some of the following experiments.

It is strongly recommended to investigate the effect of residual air inside the water in further experimental series, maybe together with the effect of gas phase turbulence mentioned earlier, to fully clarify this.

After tests with [G1.0]-OH were completed, [G2.0]-ene was tested. Induction times were in the range of the “higher” blind experiments with very low standard deviation. During weighing, it was observed that [G2.0]-ene was not soluble in the water-THF mixture, but rather formed some kind of emulsion. There was no warming as mentioned with [G1.0]-OH. All in all, the influence of [G2.0]-ene on hydrate formation in presence of THF seems to be quite low.

After experiments with [G2.0]-ene, the last of the custom-tailored inhibitor candidates, [G2.0]-OH, was tested. The first experiment showed a slightly higher induction time. Experiment 2 and 3, however, showed a significantly increased induction time. It has to be mentioned, though, that again the above-mentioned phenomenon of gas saturation inside the deionized water could have contributed to this effect. In the last two experiments, the water was very “clear” and there were no gas bubbles at all. This could correlate with the effect that occurred in the 4th experiment with [G1.0]-OH. Hence, not all of the “inhibiting effect” may have been caused by [G2.0]-OH. Nonetheless, the results are promising.

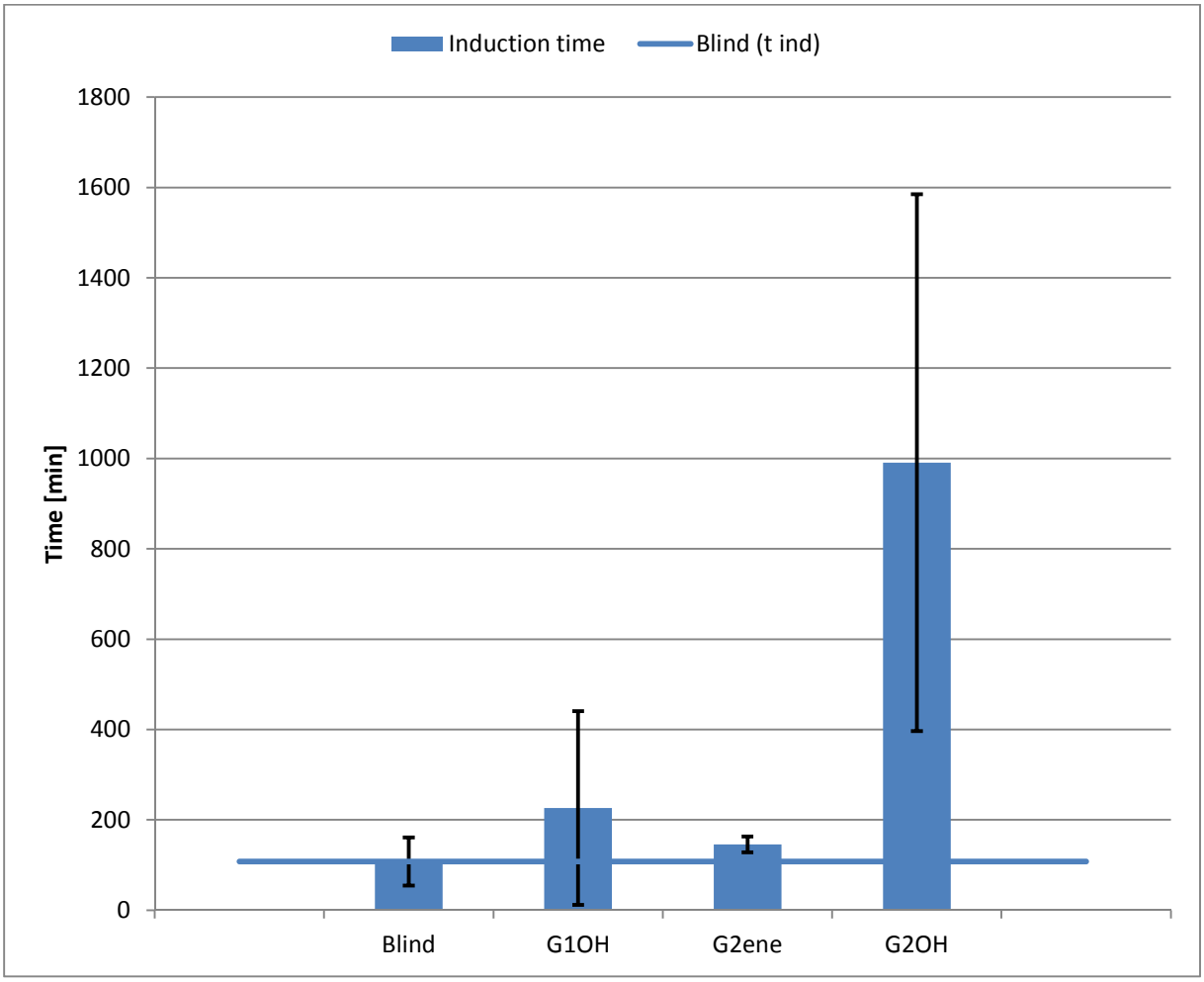

Figure 42: Comparison of t_{ind}; Büchi ecoclave; Custom-tailored inhibitor candidates

Figure 42 shows the graphical comparison of all custom-tailored inhibitors against blind experiments. Again, it can be seen that the influence of [G1.0]-OH and [G2.0]-ene seems small. Nonetheless, the very low standard deviation of experiments with [G2.0]-ene seems worth mentioning.

Experiments with [G2.0]-OH show very high induction times in 2 out of 3 experiments and hence can be regarded as promising first results.

11 Method development

In this chapter, the development of methods as an integral part of this thesis is described in detail. The chapter is divided in three parts.
The first part is focused on the development of the experimental methods and aspects of data analysis, since method development was an integral aspect of this work. Recommendations for future experiments and experimental design as well as methods of data evaluation, which were deduced in the course of this work, are explained in detail in the second part. A detailed error analysis is given in chapter 11.3.

11.1 Modifications and effects

This chapter shows the modifications that have been carried out in equipment, methods and methods of data analysis so far. Also, the effects of those changes will be described.

11.1.1 s II

Since in the screening for determining *s II* inhibition suitability the time for each experiment had to be short to ensure a fast overall screening process, tetrahydrofuran (THF) was used as promoter in each experiment. The "optimal" ratio of water and tetrahydrofuran was taken from literature. "Optimal" in this case means the ideal stoichiometric ratio, where water-THF hydrate formation is favored [2].

The pressure of 5 bar(g) was chosen due to technical reasons: the reactor is designed for pressures up to 8 bar(g). The rupture disk, however, is designed to give way at a pressure of 8 bar(g) ± 15 %, which results in 8 ± 1.2 bar(g). In addition, a safety reserve is added to account for possible pressure increases due to temperature fluctuations. So, conducting the experiments at 5 bar(g) ensures the highest possible driving force for hydrate formation in the IKA LR 2000 system and thus is again important for the number of experiments that could be concluded in the same period of time.

The purging with methane before each experiment was done to reach a minimum dilution of 1:90 (3 times purging with at least 4,5 bar difference in pressure each, see also [57]) and thus to ensure that there is no residual air inside the reactor during hydrate formation.

The stirring frequency of 50 min^{-1} was chosen due to technical reasons: tests at higher stirring frequencies showed that vortex formation occurred and interfered with temperature measurements; the resistance thermometer was measuring the temperature of the liquid

phase and gas phase alternately. To prevent this from happening, there were two possible approaches. The first one was to choose a higher total amount of liquid inside the reactor; the second one was to reduce the stirring frequency.
The higher amount of liquid would have had two major disadvantages: the ratio of liquid to gas would have been changed so that at the same pressure of 5 bar(g), there would have been less methane inside the reactor. Also, higher amounts of liquids would have caused higher costs as well as higher amounts of organic waste than necessary.
Therefore, it was chosen to set the stirring frequency at 50 min^{-1}.

Because the reactor only allows for the measurement of pressure and temperature and has no accurate stirrer torque measurement or visual observation possibilities, induction times are determined based on a decrease in pressure with increase in temperature (see also chapter 4.1). To compensate for the shortcoming of no visual observation possibility, a reactor made of glass and operable at pressures of up to 12 bar(g) (“Büchi Ecoclave type 2”, see also chapter 11.1.6) was purchased.

Due to technical reasons, the IKA reactor’s inner temperature cannot be controlled. Tempering was done by setting the thermostats temperature to a fixed value. The thermostat pumped the cooling liquid through the reactor’s double shell and tempered like this. Therefore, slight temperature fluctuations occurred inside the reactor, which made determination of the induction times based on temperature difficult in some experiments. It is recommended to realize a control of the reactor’s inner temperature in future experiments to further optimize the screening process.

11.1.2 s l

This chapter focuses on the development of an investigation method as well as optimization measures carried out on the Parr 4568 reactor. It is to be noted that for each change that affected the conditions inside the reactor, new reference / “blind” experiments had to be run. Therefore, the modifications consumed quite an amount of experimental time, which may not follow out of the short description that can be given in this chapter.

The first step to develop an investigation method for possible inhibitor candidates was to determine the optimal pressure, temperature, stirrer type and stirrer frequency to use in the experiments. For this, two different stirrers were tested at different pressures and temperatures [84]. The procedure is described in detail in chapter 5.

Optimization of reactor and equipment was done in parallel to the experimental progress:
At first, the reactor was linked to the above-mentioned coriolis-type mass-flow meter to accurately measure the amount of gas that came to use in the experiments.

The next step was to equip the reactor with duplicate valves at all inputs and exits to meet the state of the art for high-pressure devices. Also, in this revision, a pressure transducer with a much higher accuracy (Emerson Rosemount 2088) was equipped. These steps were taken after determination of the “optimal” parameters for *s l* inhibition suitability screenings. After these modifications, another series of “blind” experiments was conducted to account for possible changes of the reactor’s interior and hence for different influencing factors on hydrate formation.

In the course of experiments, the flexible tube for tempering the reactor showed wear and stress. Therefore, in the course of maintenance work, the reactor was equipped with metal tubing for tempering, the principle was developed in-house.

Also, for reasons of safety, the reactor was connected to fixed metal tubing for connecting to the methane bottle, so that the methane bottle could remain inside the fire-resistant locker for gas bottles. Figure 43 shows the reactor after completion of all modifications.

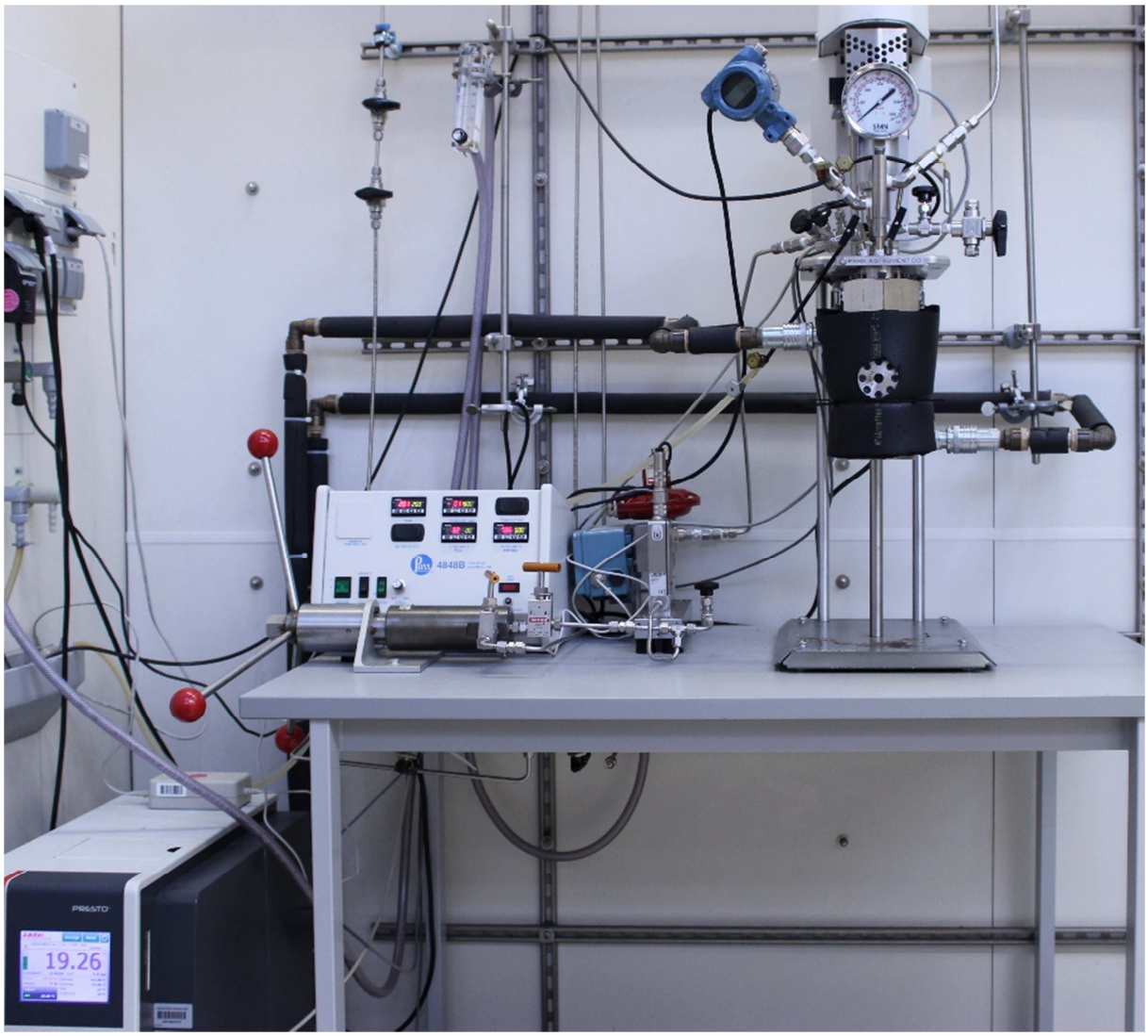

Figure 43: Parr reactor after completion of modifications

Experiments at both the IKA and Parr reactor showed that turbulence in the gas phase is also critical for hydrate formation (kinetics). Because of this new finding, the Parr reactor's hollow shaft stirrer was equipped with an additional oblique blade agitator in the gas phase (see also Figure 44 and Figure 18). The effect on gas phase turbulence is explained by calculating the Reynolds numbers with and without gas phase stirrer (see equations [11.1] and [11.2]). The type of stirrer that was used in the respective experiment is indicated in the related chapters above. Since the installation of the additional stirrer took place in parallel to the exchange of the pressure transducer (see above), no additional series of reference experiments has been conducted.

Figure 44: Hollow shaft stirrer (left); with additional gas phase stirrer (right)

The turbulence in the gas phase is characterized via determination of the Reynolds number, case A is without any additional gas phase stirrer (see equation [11.1]), the diameter of the stirrer shaft ($9.54*10^{-3}$m) is taken as value for *d*.

$$Re_{R,G} = \frac{n * d^2 * \rho}{\eta} = \frac{\frac{200}{60s} * (9.54 * 10^{-3}m)^2 * 148.06 \frac{kg}{m^3}}{1.79 * 10^{-5} \frac{kg}{m * s}} \approx 2509 \quad [11.1]$$

Case B shows gas phase turbulence with the additional oblique blade agitator (see equation [11.2]), diameter of the stirrer was $d = 3.3*10^{-2}$m*:*

$$Re_{R,G,OB} = \frac{n * d^2 * \rho}{\eta} = \frac{\frac{200}{60s} * (3,3 * 10^{-2}m)^2 * 148.06 \frac{kg}{m^3}}{1,79 * 10^{-5} \frac{kg}{m * s}} \approx 30025 \quad [11.2]$$

The values for density and viscosity of methane at 4 °C and 160 bar(g) were taken from [118].

The oblique blade agitator has a critical Reynolds number Re_{cr} of 500 and a turbulent Reynolds number Re_{turb} of 20.000 [119]. This means that in case A, the stirrer in the gas phase operates in the transition area with slight turbulence. In case B, however, the gas phase is fully turbulent. The effect on gas hydrate formation is discussed in the related chapters above. These “gas phase Reynolds numbers” were calculated in addition to the

Reynolds numbers in the liquid / bulk phase that are shown in chapter 5.1 and only describe the difference in gas phase turbulence which were caused by modification of the stirrer.

A phenomenon arose throughout the different experimental series that could not be finally resolved to this day:
In some of the experiments, really huge differences in standard deviation of the hydrate formation times occurred, meaning that there were some experiments that took up to 10 times longer to form hydrates than the others of the same series of experiments (under the same conditions). This even occurred in the “blind” experiments, where no inhibiting substance was added.

The phenomenon first occurred after a reactor standstill, where the reaction water had been left inside; all the valves had been closed off. After a time of 2-3 weeks, the hydrate experiment was run by first tempering to 20 °C, then proceeding according to the experimental procedure detailed in chapter 5.1. The first assumption was that due to the long standstill, the water somehow interacted with the reactor’s wall and maybe iron ions got “washed out”. Therefore, two different analyses were carried out: first, water was left inside the reactor and tested after several days to find out, if iron had actually been washed out. So far, no significant increase in iron concentration could be found by manganometric titration. Results of these investigations are shown in [99]. However, it is recommended to validate those results using different methods of examination, e. g. atomic absorption spectroscopy (AAS) or mass spectrometry. Also, additional titration experiments should be conducted to validate these findings.
In parallel, iron was investigated regarding its inhibition potential. For this, the substance *Iron(II) sulfate heptahydrate* was chosen. Results are shown in chapter 6.2, where also experiments with *potassium thiocyanate* as other ionic possible inhibitor candidate are discussed.

The phenomenon later also occurred after reactor standstill (without water being inside the reactor during standstill times), e. g. due to maintenance. There were many considerations for the cause of this. One thought was that microorganisms formed inside the reactor and caused some kind of fouling. Due to intensive research on the formation of *E. coli* in the system as part of an internal project [98], it can be said that the possibility for formation of microorganisms is very low to non-existent.

Another assumption was that the reactor somehow interacted with the laboratory air or got in any way contaminated in the times of standstill. However, due to the extensive purging before each of the experiments, this possibility also is very low.

Also, the purified water that came to use in the experiments could be the cause. Before each experiment, conductivity of the purified (Milli-Q) water was measured. However, conductivity measurements only detect electrically active substances (mainly ions in the water). Contaminations that are electrically neutral (e. g. parts of the membrane of the water treatment system / ion exchanger) are not detected.
To reduce the possibility of abrasion of membranes etc., the maintenance / exchange intervals of the ion exchanger cartridges used in the Milli-Q system could be shortened.

Also, things like the TOC (total amount of organic carbon) are not measured, since the TOC measurement carried out in-house is done with the same Milli-Q water as a reference and hence, TOC cannot be measured in-house.
However, the possibility that there is organic carbon content in the water phase is very low, because the water which is purified inside the Milli-Q system is taken from the drinking water network of the city of Krefeld (TOC already < 1 mg / L, December 2014, [120]), then purified via reverse osmosis and only then purified in the Milli-Q system.
Nevertheless, to further reduce the risk of TOC having an influence on hydrate formation processes, a water purification system with TOC control could be used.

However, from our current knowledge, the most likely reason for the high standard deviations maybe was the “thermal pretreatment” of the reactor, meaning that an experiment starting after a “pause” due to inspection of the reactor or similar causes could have a longer induction time compared to an experiment starting right after another experiment was finished (in this case, the pause was at approx. 1 h for cleaning of the reactor etc.). Maybe the residual cold inside the reactor walls had some kind of effect on induction times, although all of the experiments were brought to the same starting temperature of 20 °C after filling and closing off the reactor.

The problems arising from thermal pretreatment could be reduced, for example by adding a completely defined thermal pretreating program. This program should include a preheating up to a temperature, where all of the preformed nuclei in the water phase would be destroyed (e. g. 60 °C), then a systematic cool down with a defined cooling rate (e. g. 1 °C / min) to the starting temperature of 20 °C could be done. This should be taken into consideration for further experimental series.

Also, cooling to the target temperature of e. g. 4 °C could be done with a defined cooling rate to reduce irregularities. However, in this work the focus was put on the development of inhibitors. Since in a pipeline the cooling would never occur with a defined cooling rate, because cooling in pipelines occurs due to natural processes, experiments were designed to have more resemblance with the actual application case.

For some of the tested substances that caused an increase in viscosity of the bulk phase, it was considered to test the viscosity and its influence on hydrate formation behavior. A test was carried out in a related project [50] and showed increase in viscosity for the water-inhibitor mixture.
However, the effect that methane at pressures of above 100 bar has on viscosity of this fluid could not be determined due to technical limitations.

Also, it was considered that for the pipeline case a substance that inhibits hydrate formation by increasing viscosity of the water phase and thereby reducing turbulence would also show this behavior inside a pipeline without significantly reducing the flow of the gas phase.

Somehow finding a correlation for the viscosity under influence of methane directly inside the reactor, e. g. by using the stirrer torque and calculating via shear forces, is also not recommended since the formation of solid hydrate particles causes increases in stirrer torque that are a lot higher than any increase in fluid viscosity and also since it cannot be clearly determined what part of a rising stirrer torque is caused by simple viscosity increase and which part is caused by formation of hydrate nuclei of any kind.

Another important aspect which still has to be fully explored is the effect that solubility of methane, or rather the influence of experimental setup (like the HSS stirrer) and the tested substances on solubility of methane, do have on hydrate formation.
Some substances showed inhibiting behavior with higher pressure in the beginning of an experiment than should be expected from cooling and “normal” dissolution. This could be an indicator that the substances reduce the solubility of methane, either by directly influencing the solubility equilibrium or by somehow “repelling” the methane and drive it out to the gas phase, perhaps by somehow influencing the gas-water interface. This would not seem surprising, since surfactants are in general known to influence gas hydrate formation [7, 73].

A method to determine solubility of methane under experimental conditions should be developed to quantify the possible changes in solubility. However, determining the solubility at higher pressures is extremely difficult to realize experimentally, especially since the system would enter the hydrate stability zone at a certain point and it would be very hard to distinguish between the effects of hydrate nucleation and solubility.

Also, it could be important to somehow distinguish between methane and other gases in solution, e. g. to quantify in what way and amount residual air is left in the water, even after purging the reactor. Quantifying this during the process seems to be very difficult from an experimental point of view, though. Another approach hence could be degassing the water before the process. However, since in the case of a pipeline the water would never be degassed and an inhibitor has to work at field conditions, this seems of minor priority compared to the solubility of methane and its influence on hydrate formation.

11.1.3 Data analysis

The method of data analysis also had to be developed, since induction times were not easy to determine in some of the experiments.
Two phenomena occurred, mainly during high-pressure experiments: often, there was a rise in temperature without significant decrease of pressure and without significant changes in stirrer torque. This was interpreted as the *induction time*, which was then defined as the earliest point of exothermic hydrate processes, probably being caused by the formation of “tiny” hydrate nuclei throughout the whole system or at least throughout the whole site of hydrate formation (bulk or phase boundary, whichever formation theory is more suited at given conditions). Temperature rises due to the exothermic nature of hydrate formation, but there is no plugging yet, because no critical nucleus size is reached.

Secondly, the so-called *plug formation time* was defined to determine the point where a pipeline would completely be blocked in an industrial process. It is characterized by a strong increase in temperature, while pressure drops drastically due to “consumption” of methane and stirrer torque also rises significantly, because macroscopic, “hard” hydrates are formed.

It is to be noted, that rises in stirrer torque were only moderate in the first few experimental series. This changed drastically, when the additional gas phase stirrer was installed, which is again a strong indicator for the importance of gas phase turbulence in hydrate experiments.

Because of the major differences in stirrer torque of the experiments with and without additional gas phase stirrer, the criteria for the plug formation time are defined differently in both cases.
When the stirrer torque stays below a value of 30 Ncm throughout the experiment, the plug formation time is characterized through a simultaneous change in all 3 above-mentioned parameters with stirrer torque rising above 15 Ncm in the course of this parameter change.

When “hard” hydrates are formed and hence stirrer torque rises above 30 Ncm through the course of an experiment, plug formation time is characterized by a simultaneous change of the 3 above-mentioned parameters with stirrer torque rising above 25 Ncm in the course of this change.

It has to be mentioned that the *plug formation time* was first introduced after the determination of “optimal” parameters for the high-pressure experiments (→ chapter 5). This was done since the huge differences that made the phenomenon so noticeable occurred mostly in later experiments. The “optimal” parameters had already been established by that time and also proven to be a “good choice”, so that no changes were made in hindsight. Before / during determination of the optimal parameters, the important criterion therefore was the *induction time*, defined in those cases as an increase in temperature by at least 0.1 °C during one minute.

One important thing to mention is that in experiments with no gas hydrate formation (which also means ***good inhibition potential***), the induction and plug formation times were set as 4000 minutes. This value was set as *maximum experimental time* because it is a good “target time” for an inhibitor regarding pipeline conditions: it was calculated for a hold-up time in a pipeline of two days (2880 min), with a “safety reserve” of 40 % (2880 min + 1152 min = 4032 min) and then rounded down to 4000 min as simplification.

11.1.4 Prototype experiments

During the “prototype experiments”, only two “optimizations” were carried out in comparison to the other high-pressure experimental series. First of all, the prototype was fixed inside the reactor by using two pieces of flexible tube which were cut and clamped between prototype and reactor inner wall. The tube pieces did not come into contact with the bulk phase, because they only had contact to the “outside” of the prototype walls. To make sure the prototype was not moved by the stirrer, in addition to the clamping the prototype was marked at two characteristic points to visually control if any movement had occurred after the

experiment. These steps were taken to ensure that the prototype was not moved by the stirrer and hence that the relative movement of the fluid compared to the reactor / prototype wall was the same in all experiments.

Also, the driving belt of the stirrer was changed to a more flexible one that would come off in case of high stirrer torques. This was done to prevent mechanical damage to the prototype.

Figure 45 shows a picture of the prototype inside the reactor.

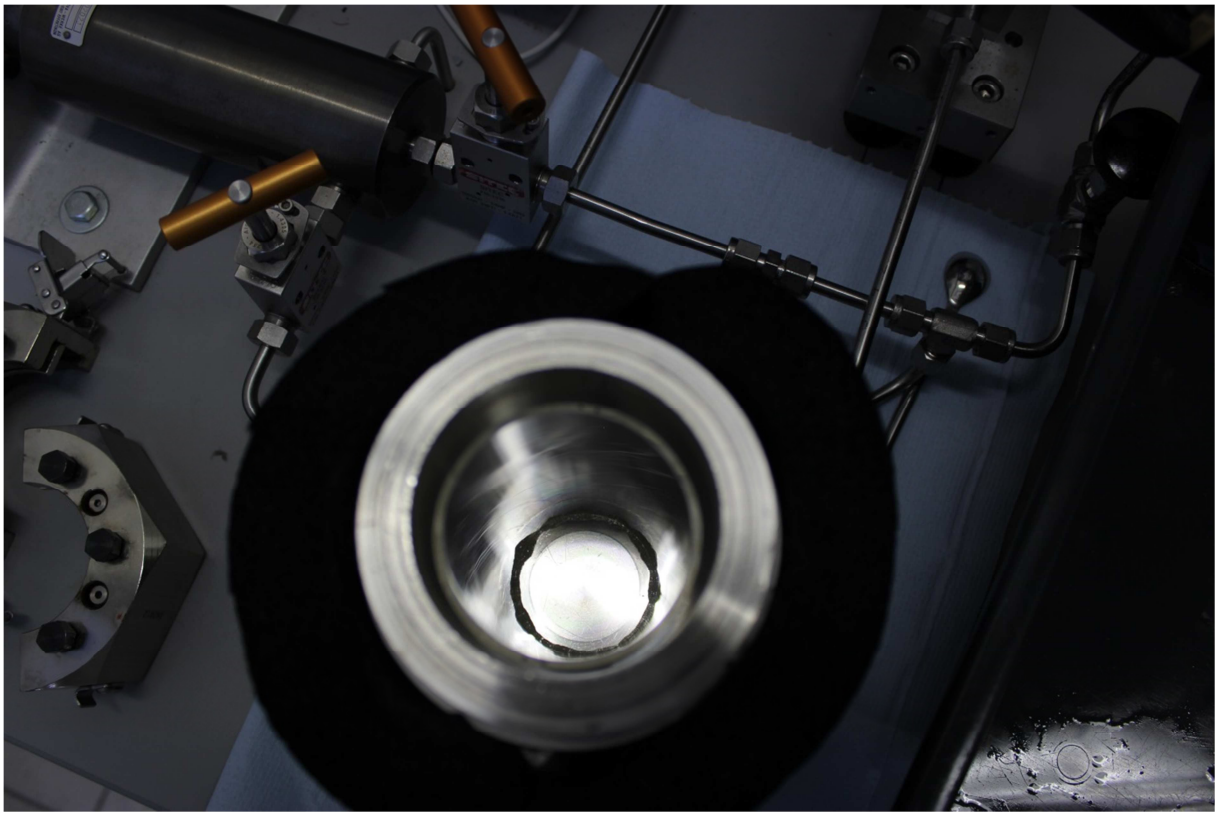

Figure 45: Prototype mounted inside the Parr 4568 reactor

11.1.5 Kinetics

Extensive work was done on developing a kinetic model (see also chapter 9) for transient conditions with pressure gradient and changing driving force for hydrate formation. Although it would be easier to develop a kinetic model based on a constant driving force, which would equal a constant pressure in the *s l* experiments, it was decided not to use constant pressure to have more resemblance to the pipeline case, where there are also gradients in pressure. Also, it was decided not to use temperature "ramps" as form of process control and to temper to the target temperatures, because in a pipeline the tempering occurs irregularly.
Those facts make the development of a kinetic model more difficult, since terms for the irregular behavior have to be included.
Due to these reasons, the focus in this work was on determining parameters in an empirical way just for the system "Parr 4568" and sorted experiments. The gained parameters can be seen as a first start of developing a model in the system used.

11.1.6 New reactor / glass

The "new" glass reactor was purchased because experiments showed, that to draw concrete conclusions to how new inhibitors have to be designed "perfectly", the mechanism of hydrate formation has to be further mapped out. To reach this goal, hydrate formation experiments have been conducted in a reactor made of glass to determine if one of the postulated mechanisms can describe the hydrate formation better than the others or if a completely new model has to be derived.
The reactor was connected to an "Emerson DeltaV" process control system. To use the system with the Büchi reactor, all of the sensors and instruments were connected to the DeltaV system and extensive work was done to generate and test a customized user interface. [121]

After the first series of experiments, the reactor was modified and a mechanism to directly control the reactor's inner temperature was implemented [122]. This was done since the induction time was very hard to determine beforehand because of only small fluctuations in the temperature that made it difficult to detect the first temperature increase due to hydrate formation (as also mentioned in the screening experiments in the IKA reactor).

After the control mechanism was installed, the custom-made possible inhibitors (see chapter 10.1) were investigated inside the glass reactor. Results are discussed in chapter 10.3.

An important criterion which was striking in the Büchi experiments, was the gas saturation of the deionized water that came to use.
An in-lab deionized water system was used, which showed small differences in gas saturation on some days, meaning the water seemed “clouded” on some days when first filled inside the beaker for weighing. This was caused by tiny gas bubbles inside the water.
Although the reactor was purged 3 times with methane before each experiment, it is assumed that this gas still could influence hydrate formation. It seems that on days were this “clouding” occurred, hydrate formation took longer compared to the days with “clear” water.
This should be investigated in further experimental series.

11.2 Recommendations for future experiments

In this chapter, based on the experiences gained from the extensive series of experiments conducted so far, recommendations for future works are given.

First of all, to better understand phenomena like “fluctuations” in the temperature curves (also mentioned in chapters 5, 6 and 7), it is recommended to use further methods of investigation to validate temperature measurements / determination of induction and plug formation times.

For this, RAMAN spectroscopy seems to be the first choice. As already shown in [50], RAMAN measurements of gas hydrates that were formed inside the Parr 4568 reactor, showed a shift in the methane peak. This specific signal could, with an appropriate RAMAN probe head, be measured directly in the reactor. With this, hydrate formation / induction time could be directly detected. With correct calibration, the RAMAN probe could even measure the distribution of nucleation centers throughout the water phase.
A second thermometer to verify hydrate formation could be an easier step to realize in the near future. This second thermometer could be installed at the opposite “side” of the reactor or in another height to gain insight if hydrate formation has a favorite starting area inside the reactor.

The high-speed camera endoscope system, which can already be used for measurements with the Büchi Ecoclave system, could also be used inside the Parr 4568 reactor. To realize this, some kind of bushing, that shields the endoscope from the pressure inside the reactor, has to be built. After this has been realized, the high-speed camera could help in gaining valuable insights into the process. So, the height of temperature peaks could correlate with the amount of hydrate formed per time. This seems logical, but with visual observation in combination with a second point of measuring temperature, the phenomenon could be quantified.

Experiments often showed different hydrate morphologies depending on the height inside the reactor. This will be further discussed in the following chapters. However, from a methodic point of view, in one of the last experimental series an interesting phenomenon showed. Hydrates were not flammable on the “outer side” of the formed hydrates (where they usually are flammable, if they are at all), but on the “inner side”.
To further clarify this and get the most out of flammability testing, which can be correlated to gas saturation inside the hydrate cages, it is recommended to develop a defined “grid” with specific points at which a test for flammability or some other measurement for gas saturation,

is conducted. In the end, a procedure to give an overview over saturation levels at all important parts of formed hydrates should be the goal.

The recommendations that resulted from the experiments conducted so far can be summarized as follows (not sorted by relevance):

- the problems arising from thermal pretreatment could be reduced in all experiments, e. g. by implementing a completely defined thermal pretreating program, consisting of preheating and cool down to target temperatures with defined heating and cooling rates;
- for the *s II* screening inside the IKA reactor, it is recommended to realize a control of the reactor's inner temperature in future experiments;
- a method to determine the solubility of methane under experimental conditions should be developed for all experiments;
- further methods to determine induction times (like second resistance thermometer at a different position inside the reactor, turbidity measurement or RAMAN spectroscopy) should be added to substantiate the measured induction times;
- visual observation, e. g. with a high-speed camera system should be added in all reactors to draw conclusions on the distribution of hydrate nuclei / the starting points of macroscopic hydrate formation inside the reactors;
- measurements of gas saturation should be conducted inside the hydrate phase, in addition to the defined grid for flammability tests mentioned above, to quantify the amount of gas stored inside the formed hydrates.

11.3 Error analysis

In this chapter, the error analysis for the conducted measurements is done. Since for determination of the induction and plug formation times temperature is the most important parameter, the uncertainty of measurement is calculated based on temperature measurement. The measurement of time itself is not considered more closely, since its influence was deemed negligible on the overall accuracy.

A conservative approach for determination is taken to determine the worst case, meaning the highest possible deviation between measured value and true value. The resolution of measurements is considered negligible in all calculations. Accuracy classes of resistance thermometers are defined in [83].

First, calculation is done for temperature measurement inside the IKA LR 2000 system. Temperature is measured with a PT100 resistance thermometer with accuracy class “A”. From there, the signal is transported to a Hitec-Zang ® LabBox and from there, the signal is transported to a measuring computer.
Accuracy of the PT100 is:

$$acc(PT100) = \pm(0.15\,°C + 0.002 * |T|) \quad [11.3]$$

with $|T|$ being the value of the current temperature.
At the given conditions of 8 to 10 °C in the system during experiments, but with a starting temperature of 20 °C, the worst possible error accounts to:

$$acc(PT100) = \pm(0.15\,°C + 0.002 * 20\,°C) = \pm(0.15 + 0.04)°C = \pm 0.19\,°C \quad [11.4]$$

The conversion of the signal, that takes place in the LabBox before transport to the computer, has an error of 0.2 °C [123].
The total error in of temperature measurement hence accounts to:

$$acc(T, IKA) = (0.19 + 0.2)°C = 0.39\,°C \quad [11.5]$$

In consideration of error through environmental effects, signal losses in the transporting cables, etc., the amount is rounded to a total value of

acc (T,IKA) = ± 0.4 °C

In the Parr 4568 system, a PT100 resistance thermometer with accuracy class “1/3 B” is used. At 20 °C the accuracy amounts to *± 0.134 K* [83].
The thermometer is connected directly to the Julabo Presto A40 thermostat; therefore the error of signal detection of the thermostat has to be taken into account. It has a value of ± 0.2 K [124].

The thermostat sends an analog signal to the Parr 4848B controller by means of a 0-10 V signal; the controller then sends the signal to the measuring computer. The signal conversion inside the thermostat (via Julabo analogue module 8900105 with connected „REG+EPROG-connector 8980136”) is done with an accuracy of *± 20 mV* [125]. The signal range of 0 to 10 V equals a temperature range of 50 °C (which was adjusted in all of the experiments). Hence, the error of 20 mV equals an error of *± 0.1 °C* or *± 0.1 K*.

The controller’s input has a range accuracy of 0.2 %, which has to be added to the cumulated error in the end. The total error of measurement is then calculated as follows:

$$acc(Parr) = (0.134 + 0.2 + 0.1)K + ((0.134 + 0.2 + 0.1) * 0.2\%)K$$
$$= (0.434 + 0.000868)K = \pm 0.434868\,K \qquad [11.6]$$

In consideration of error through environmental effects, signal losses in the transporting cables, etc., the amount is rounded to a total value of
acc (T,Parr) = ± 0.45 K.

In the Büchi ecoclave system, a PT100 resistance thermometer with accuracy class “A” is used. From there, the signal is transported to an “Emerson DeltaV” process control system, where it is converted and sent to the measuring computer.
Accuracy of the PT100 is:

$$acc(PT100) = \pm(0.15\,°C + 0.002 * |T|) \qquad [11.7]$$

with /*T*/ being the value of the current temperature.
At the given conditions of 4 °C in the system during experiments, but with a starting temperature of 20 °C, the worst possible error accounts to:

$$acc(PT100) = \pm(0.15\,°C + 0.002 * 20\,°C) = \pm(0.15 + 0.04)°C = \pm 0.19\,°C \qquad [11.8]$$

The conversion of the signal, that takes place in the DeltaV system before transport to the computer, has an error of 0.5 °C [126].

The total error in of temperature measurement hence accounts to:

$$acc(T, B\ddot{u}chi) = (0.19 + 0.5)°C = 0.69\ °C \quad [11.9]$$

In consideration of error through environmental effects, signal losses in the transporting cables, etc., the amount is rounded to a total value of

acc (T,Büchi) = ± 0.7 °C

All of the errors seem to be quite large. Since the errors are only with regard to the absolute measured value, tendencies or changes in the values (like the temperature increase during induction times) can still be detected. However, the systems in their current state should not be used for measuring phase equilibria of hydrate formation, where the measurements have to be very precise.

In any case, as already mentioned above, a second method to validate temperature measurements (like RAMAN spectroscopy) is recommended to gain a higher certainty for the determination of induction and plug formation times.

12 Conclusion and outlook

During the course of this work, extensive series of measurements have been conducted to develop standardized methods for testing substances regarding their potential to inhibit the formation of gas hydrates, namely gas hydrate structures *s I* and *s II*.

Several substances were tested with the developed methods to evaluate their inhibition potential and find connections between chemical structure and influence on hydrate formation. Results showed that promising inhibitors for one hydrate structure are not necessarily good inhibitors for the other structure. Also, there were often major differences in influence on hydrate formation when the same substance came to use at varying concentrations [35]. To further clarify these phenomena and find a way to predict the influence of certain functional groups or whole molecules on gas hydrate formation, further experiments have to be carried out at more concentrations, while also using additional methods, like RAMAN spectroscopy, to figure out in which way the tested substances influence the formed hydrate structures. Also, further methods to verify induction and plug formation times and increase accuracy of measurements, e. g. turbidity measurements, could be implemented to optimize determination of hydrate formation times. Nonetheless, it seems that substances with ionic character, like KSCN or Iron(II) sulfate-heptahydrate, show strong influence on gas hydrate formation.

The influence of functional molecular groups on gas hydrate formation was investigated with a focus on a “homologous series of OH-groups”. Interesting effects were observed and indications were found that there seems to be an “optimal concentration” of OH-groups per volume element. Further investigations, e g. with addition of spectroscopic methods, have to be conducted to further clarify this.

A method to evaluate functional coatings in a specifically designed “measurement prototype” was developed and a first functional coating was investigated regarding its inhibition potential. With this it was proven for the first time that it is feasible to fixate a promising inhibitor permanently on a substrate. The next steps should be the improvement of the “surface density” of the inhibitor in the system, after that it is recommended to optimize the chain length of the polymer molecule or to further test the coating process with other promising inhibitors, like PVA.
In parallel, a method to quantify the amount of inhibitor that has been linked to the surface, has to be developed to allow detailed calculations of the effective surface area.

Also, a method to test the “abrasion” of the inhibitive coating as well as its longevity has to be established.

Extensive work has been done on developing investigation methods (→ chapter 11.1) in the different reactors that were used in the course of this work. Also, important recommendations for further experiments were given (→ chapter 11.2) to optimize experiments in the future.

In addition, kinetic studies on s I-hydrate formation in high-pressure experiments have been carried out. It was found out that the Englezos-Bishnoi model as well as the differential method, which both describe a period in the beginning of hydrate formation experiments, yielded good results in the reaction system that was used, while the fractional life method, which was applied to describe the whole hydrate formation experiment, still needs to be optimized.
All in all it can be said that tendencies in the process can already be described, but for a complete mathematical model of the process, the hydrate formation mechanism has to be further elucidated.

Experiments in a glass reactor showed that gas hydrate formation took place at the gas-water interface in this system and hydrates seemed to grow into the gas phase. This, in addition to the strong effect that an additional gas phase stirrer had on *s I* formation and additional “wiper blades” on *s II* formation, seems a strong indication that underpins the “nucleation at the interface” theory. Further experiments at varying conditions have to be conducted to first prove this without inhibiting substances and later determine the influence of inhibitors on the process. For this, a high-speed camera could be used to investigate the macroscopic hydrate formation. After determining the “rough” area where macroscopic hydrate formation starts, this camera could be equipped with a microscopic objective to gain further and more detailed insights.

Custom-tailored inhibitor candidates (dendrimers) have been synthesized and tested in a first screening. The results were promising for [G2.0]-OH. In parallel, indication has been found that “air saturation” of the water used in experiments seems to have a strong influence on hydrate formation, even though the reactor was extensively “purified” with methane before each experiment.

Although the focus of this work was on *inhibiting* gas hydrate formation, promising substances which could act as *promoters* had been found during the studies. These substances should be further investigated, e. g. regarding their ability to facilitate and

accelerate the formation of hydrogen gas hydrates to contribute to solving the storage problems that hydrogen causes and hence to contribute to solving the energy crisis.

In conclusion it can be said that the experiments are a good starting point for further research, especially regarding the optimization of the developed inhibitive coating, but also, that a lot of work still has to be done to realize the concept in the field.

13 References

[1] Kvenvolden, K. A., Methane hydrate — A major reservoir of carbon in the shallow geosphere? *Chemical Geology* 1988, *71*, 41–51, DOI: 10.1016/0009-2541(88)90104-0.
[2] Sloan, E. D., Koh, C. A., *Clathrate hydrates of natural gases,* 3rd edn., CRC Press, Boca Raton, FL, 2008.
[3] Hammerschmidt, E. G., Formation of Gas Hydrates in Natural Gas Transmission Lines. *Ind. Eng. Chem.* 1934, *26*, 851–855, DOI: 10.1021/ie50296a010.
[4] Merkel, F. S., Schmuck, C., Schultz, H. J., Investigation of the influence of hydroxyl groups on gas hydrate formation at pipeline-like conditions. *Energy Fuels* 2016, DOI: 10.1021/acs.energyfuels.6b01795.
[5] Rojas, Y., Lou, X., Instrumental analysis of gas hydrates properties. *Asia-Pacific Jrnl of Chem. Eng* 2010, *5*, 310–323, DOI: 10.1002/apj.293.
[6] Sloan, E. D., *Natural gas hydrates in flow assurance*, Gulf Professional Pub./Elsevier, Burlington, MA, 2011.
[7] Kelland, M. A., *Production chemicals for the oil and gas industry*, CRC Press, Boca Raton, 2009.
[8] Kelland, M. A., History of the Development of Low Dosage Hydrate Inhibitors. *Energy Fuels* 2006, *20*, 825–847, DOI: 10.1021/ef050427x.
[9] Jeffrey, G. A., McMullan, R. K., The Clathrate Hydrates, in: Cotton, F. A. (Ed.). *Progress in Inorganic Chemistry*, John Wiley & Sons, Inc, Hoboken, NJ, USA, pp. 43–108.
[10] Schultz, H. J., *Zum Gashydratabbau mittels Mammut-Pumpen-Prinzip*, Fraunhofer-IRB-Verl., Stuttgart, 2004.
[11] Jeffrey, G. A., Inclusion Compounds. *Academic Press*, *1984*.
[12] Davidson, D. W., Garg, S. K., Gough, S. R., Handa, Y. P. *et al.*, Some structural and thermodynamic studies of clathrate hydrates. *Journal of inclusion phenomena*, *2*, 231–238, DOI: 10.1007/BF00663261.
[13] Cotton, F. A., *Progress in Inorganic Chemistry*, John Wiley & Sons, Inc, Hoboken, NJ, USA, 1967.
[14] http://naturalgas.org/overview/background/; 2016-04-12, 09:22.
[15] https://www.uniongas.com/about-us/about-natural-gas/Chemical-Composition-of-Natural-Gas; 2016-04-12, 09:21. https://www.uniongas.com/about-us/about-natural-gas/Chemical-Composition-of-Natural-Gas.
[16] http://www.beg.utexas.edu/energyecon/lng/LNG_introduction_07.php; 2016-04-12, 09:22.
[17] Lee, J.-w., Lu, H., Moudrakovski, I. L., Ratcliffe, C. I. *et al.*, n-Pentane and n-hexane as coguests in structure-H hydrates in mixtures of 2,2-dimethylbutane and methane.

Angewandte Chemie (International ed. in English) 2006, *45*, 2456–2459, DOI: 10.1002/anie.200504366.
[18] Deaton, W. M., Frost, E. M., *Gas hydrates and their relation to the operation of natural-gas pipe lines: U.S. Bureau of Mines Monograph*, [n. p., 8, 1946.
[19] Rodger, P. M., Stability of gas hydrates. *J. Phys. Chem.* 1990, *94*, 6080–6089, DOI: 10.1021/j100378a082.
[20] Rodger, P. M., Mechanisms for Stabilising Water Clathrates. *Molecular Simulation* 1990, *5*, 315–328, DOI: 10.1080/08927029008022417.
[21] Bernal, J. D., Fowler, R. H., A Theory of Water and Ionic Solution, with Particular Reference to Hydrogen and Hydroxyl Ions. *J. Chem. Phys.* 1933, *1*, 515, DOI: 10.1063/1.1749327.
[22] Bjerrum, N., Structure and Properties of Ice. *Science* 1952, *115*, 385–390.
[23] Frank, H. S., The Structure of Ordinary Water. *Science* 1970, *169*, 635–641.
[24] Pauling, L., The Structure and Entropy of Ice and of Other Crystals with Some Randomness of Atomic Arrangement. *J. Am. Chem. Soc.* 1935, *57*, 2680–2684, DOI: 10.1021/ja01315a102.
[25] STILLINGER, F. H., Thermal Properties of Water in Restrictive Geometries, in: Rowland, S. P. (Ed.). *Water in Polymers*, AMERICAN CHEMICAL SOCIETY, WASHINGTON, D. C., pp. 11–21.
[26] Frenier, W. W., Ziauddin, M., *Formation, removal, and inhibition of inorganic scale in the oilfield environment*, Society of Petroleum Engineers, [Richardson, Tex.?], 2008.
[27] Cowan, J. C., Weintritt, D. J., *Water-formed scale deposits*, Gulf Pub. Co., Book Division, Houston, Tex., 1976.
[28] Masoudi, R., Tohidi, B., Danesh, A., Todd, A. C. *et al.*, Measurement and Prediction of Salt Solubility in the Presence of Hydrate Organic Inhibitors. *SPE Production & Operations* 2013, *21*, 182–187, DOI: 10.2118/87468-PA.
[29] Tomson, M. B., Kan, A. T., Fu, G., Inhibition Of Barite Scale In The Presence Of Hydrate Inhibitors. *SPE Journal* 2013, *10*, 256–266, DOI: 10.2118/87437-PA.
[30] Ostwald, W., Wilhelm Ostwald: Über die vermeintliche Isomerie des roten und gelben Quecksilberoxyds und die Oberflächenspannung fester Körper. *Zeitschrift für Physikalische Chemie* 1900, 495–503.
[31] Miers, H. A., Isaac, F., The Spontaneous Crystallisation of Binary Mixtures. Experiments on Salol and Betol. *Proceedings of the Royal Society A: Mathematical, Physical and Engineering Sciences* 1907, *79*, 322–351, DOI: 10.1098/rspa.1907.0045.
[32] Kashchiev, D., Firoozabadi, A., Nucleation of gas hydrates. *Journal of Crystal Growth* 2002, *243*, 476–489, DOI: 10.1016/S0022-0248(02)01576-2.

[33] Merkel, F. S., Schultz, H. J., Methane Extraction from Natural Gas Hydrate Reservoirs with Simultaneous Storage of Carbon Dioxide. *Chemie Ingenieur Technik* 2015, 475–483, DOI: 10.1002/cite.201300164.
[34] Schultz, H. J., Merkel, F. S., Bliem, V., Gas hydrates: Feasibility of CO2-sequestration and related natural gas production. *gas for energy* 2013, 64–70.
[35] Merkel, F. S., Schmuck, C., Schultz, H. J., RESEARCH ON INHIBITION OF GAS HYDRATE FORMATION IN PIPELINES AND ARMATURES USING SURFACE ACTIVE SUBSTANCES, in: Royal Society of Chemistry, Speciality Chemicals Sector, European Oilfield Speciality Chemicals Association (Ed.). *Proceedings of the Chemistry in the Oil Industry XIV; Chemistry: Challenges and Responsibilities Conference*, pp. 297–309.
[36] CHRISTIANSEN, R. L., Sloan, E. D., Mechanisms and Kinetics of Hydrate Formation. *Ann NY Acad Sci* 1994, *715*, 283–305, DOI: 10.1111/j.1749-6632.1994.tb38841.x.
[37] Sloan, E. D., Fleyfel, F., A molecular mechanism for gas hydrate nucleation from ice. *AIChE J.* 1991, *37*, 1281–1292, DOI: 10.1002/aic.690370902.
[38] Muller-Bongartz, B., Wildeman, T. R., Sloan, E. D., jr., A hypothesis for hydrate nucleation phenomena, in: *Offshore and polar engineering: 2nd International conference Selected papers*, ISOPE, pp. 628–635.
[39] Long, J., *Gas Hydrate Formation Mechanism and Kinetic Inhibition*, Colerado School of Mines, 1994.
[40] Radhakrishnan, R., Trout, B. L., A new approach for studying nucleation phenomena using molecular simulations: Application to CO[sub 2] hydrate clathrates. *J. Chem. Phys.* 2002, *117*, 1786, DOI: 10.1063/1.1485962.
[41] Moon, C., Taylor, P. C., Rodger, P. M., Molecular dynamics study of gas hydrate formation. *Journal of the American Chemical Society* 2003, *125*, 4706–4707, DOI: 10.1021/ja028537v.
[42] Jacobson, L. C., Hujo, W., Molinero, V., Amorphous Precursors in the Nucleation of Clathrate Hydrates. *J. Am. Chem. Soc.* 2010, *132*, 11806–11811, DOI: 10.1021/ja1051445.
[43] Jacobson, L. C., *Molecular mechanisms of nucleation and growth of clathrate hydrates*.
[44] Jacobson, L. C., Hujo, W., Molinero, V., Nucleation Pathways of Clathrate Hydrates: Effect of Guest Size and Solubility. *J. Phys. Chem. B* 2010, *114*, 13796–13807, DOI: 10.1021/jp107269q.
[45] Jacobson, L. C., Matsumoto, M., Molinero, V., Order parameters for the multistep crystallization of clathrate hydrates. *J. Chem. Phys.* 2011, *135*, 074501, DOI: 10.1063/1.3613667.
[46] Jacobson, L. C., Molinero, V., A Methane–Water Model for Coarse-Grained Simulations of Solutions and Clathrate Hydrates. *J. Phys. Chem. B* 2010, *114*, 7302–7311, DOI: 10.1021/jp1013576.

[47] Nguyen, A. H., Jacobson, L. C., Molinero, V., Structure of the Clathrate/Solution Interface and Mechanism of Cross-Nucleation of Clathrate Hydrates. *J. Phys. Chem. C* 2012, *116*, 19828–19838, DOI: 10.1021/jp305468s.
[48] Nixdorf, J., *Experimentelle und theoretische Untersuchung der Hydratbildung von Erdgasen unter Betriebsbedingungen*. Dissertation, Karlsruhe, 1996.
[49] Chandragupthan, B., An Insight to Inhibitors. *PetroMin* 2011, 50–58.
[50] Kemper, S. D., *Hochdruckuntersuchungen zur Kinetik der Gashydratbildung unter Einfluss verschiedener Inhibitoren*. Masterthesis, Krefeld, 2014.
[51] Bollavaram, P., Sloan, E. D., Hydrate Plug Dissociation by Method of Depressurization, in: *Offshore Technology Conference*.
[52] Eberhardt, E., Meyn, V., Rahimian, I., *Inhibierung von Erdgashydraten durch kinetische Inhibitoren: Literaturstudie ; DGMK-Forschungsbericht 523,1*, DGMK, Hamburg, 2000.
[53] Sloan, E. D., Koh, C. A., Sum, A. K., Ballard, A. L. *et al.*, Hydrates: State of the Art Inside and Outside Flowlines. Distinguished Author Series. *JPT* 2009, 89–94.
[54] Huo, Z., Freer, E., Lamar, M., Sannigrahi, B. *et al.*, Hydrate plug prevention by anti-agglomeration. *Chemical Engineering Science* 2001, *56*, 4979–4991, DOI: 10.1016/S0009-2509(01)00188-9.
[55] Parmar, A. A., *PVCap as kinetic hydrate inhibitor in gas-water system*. Master thesis, Bergen, 2009.
[56] Pakulski, M., Szymczak, S., TWELVE YEARS OF LABORATORY AND FIELD EXPERIENCE FOR POLYETHER POLYAMINE GAS HYDRATE INHIBITORS, in: *Proceedings of the 6th International Conference on Gas Hydrates (ICGH 2008),*
[57] Abay, H. K., *Kinetics of Gas Hydrate Nucleation and Growth*. Dissertation, 2011.
[58] Fu, B., The development of advanced kinetic hydrate inhibitors, in: Frampton, H., Craddock, H. A., Dunlop, J., Reid, P., Payne, G., Balson, T. (Ed.). *Chemistry in the Oil Industry VII*, Royal Society of Chemistry, Cambridge, pp. 264–276.
[59] Cohen, J. M., Wolf, P. F., Young, W. D., Method for preventing or retarding the formation of gas hydrates, Google Patents, 1998. http://www.google.com/patents/US5723524.
[60] Holtrup, F. D., Klug, P. D., Additive zur Inhibierung der Gashydratbildung, Google Patents, 1999. https://www.google.com/patents/EP0933415A2?cl=en29.
[61] Meier, I. K., Goddard, R. J., Ford, M. E., Amine-based gas hydrate inhibitors, Google Patents, 2008. http://www.google.com/patents/US7452848.
[62] Makogon, T. Y., Larsen, R., Knight, C. A., Dendy Sloan, E., Melt growth of tetrahydrofuran clathrate hydrate and its inhibition: method and first results. *Journal of Crystal Growth* 1997, *179*, 258–262, DOI: 10.1016/S0022-0248(97)00118-8.

[63] King, H. E., Hutter, J. L., Lin, M. Y., Sun, T., Polymer conformations of gas-hydrate kinetic inhibitors: A small-angle neutron scattering study. *J. Chem. Phys.* 2000, *112*, 2523, DOI: 10.1063/1.480892.
[64] Anderson, B. J., Tester, J. W., Borghi, G. P., Trout, B. L., Properties of inhibitors of methane hydrate formation via molecular dynamics simulations. *Journal of the American Chemical Society* 2005, *127*, 17852–17862, DOI: 10.1021/ja0554965.
[65] Cruz-Torres, A., Romero-Martínez, A., Galano, A., Computational study on the antifreeze glycoproteins as inhibitors of clathrate-hydrate formation. *Chemphyschem a European journal of chemical physics and physical chemistry* 2008, *9*, 1630–1635, DOI: 10.1002/cphc.200800241.
[66] Carver, T. J., Drew, Michael G. B., Rodger, P. M., Inhibition of crystal growth in methane hydrate. *Faraday Trans.* 1995, *91*, 3449, DOI: 10.1039/ft9959103449.
[67] GomezGualdron, D. A., Balbuena, P. B., Classical Molecular Dynamics of Clathrate-Methane-Water-Kinetic Inhibitor Composite Systems. *J. Phys. Chem. C* 2007, *111*, 15554–15564, DOI: 10.1021/jp071959c.
[68] Hawtin, R. W., Quigley, D., Rodger, P. M., Gas hydrate nucleation and cage formation at a water/methane interface. *Physical chemistry chemical physics PCCP* 2008, *10*, 4853–4864, DOI: 10.1039/b807455k.
[69] Varma-Nair, M., Costello, C. A., Colle, K. S., King, H. E., Thermal analysis of polymer–water interactions and their relation to gas hydrate inhibition. *J. Appl. Polym. Sci.* 2007, *103*, 2642–2653, DOI: 10.1002/app.25414.
[70] Kelland, M. A., SVARTAAS, T. M., ØVSTHUS, J., NAMBA, T., A New Class of Kinetic Hydrate Inhibitor. *Annals of the New York Academy of Sciences* 2000, *912*, 281–293, DOI: 10.1111/j.1749-6632.2000.tb06782.x.
[71] Delgado-Linares, J. G., Majid, Ahmad A. A., Sloan, E. D., Koh, C. A. *et al.*, Model Water-in-Oil Emulsions for Gas Hydrate Studies in Oil Continuous Systems. *Energy Fuels* 2013, *27*, 4564–4573, DOI: 10.1021/ef4004768.
[72] Klomp, U. C., Kruka, V. R., Reijnhart, R., Weisenborn, A. J., A method for inhibiting the plugging of conduits by gas hydrates, Google Patents, 1995. http://www.google.com/patents/WO1995017579A1?cl=ko.
[73] Karaaslan, U., Parlaktuna, M., Surfactants as Hydrate Promoters? *Energy Fuels* 2000, *14*, 1103–1107, DOI: 10.1021/ef000069s.
[74] Smith, J. D., *Hydrate-phobic Surfaces*. Masterarbeit, Cambridge, MA, 2011.
[75] Smith, J. D., Meuler, A. J., Bralower, H. L., Venkatesan, R. *et al.*, Hydrate-phobic surfaces: fundamental studies in clathrate hydrate adhesion reduction. *Physical chemistry chemical physics PCCP* 2012, *14*, 6013–6020, DOI: 10.1039/c2cp40581d.

[76] Fang, B., Samudrala, O., Kulkarni, A. J., Hall, D. B., Lusted, R. M., Butts, M. D., Sivaramakrishnan, S., Wilson, P. R., Giammattei, M. H., Wolfe, C. E., Articles comprising a hydrate-inhibiting silicone coating, Google Patents, 2014. http://www.google.ch/patents/US8728599.
[77] Stenzel, V., Rehfeld, N., *Funktionelle Beschichtungen*, Vincentz Network, Hannover, 2013.
[78] Stenzel, V., Rehfeld, N., Vogt, K., http://www.ifam.fraunhofer.de/de/themen/Oberflaechentechnik/Anti-Eis.html. Accessed 3 February 2016.
[79] Franke-Jordan, S., Uhlmann, P., http://tu-dresden.de/die_tu_dresden/fakultaeten/fakultaet_maschinenwesen/cimtt/projekte/eisab/eisab. Accessed 3 February 2016.
[80] SHAPIRO, S. S., WILK, M. B., An analysis of variance test for normality (complete samples). *Biometrika* 1965, *52*, 591–611, DOI: 10.1093/biomet/52.3-4.591.
[81] Royston, P., Remark AS R94: A Remark on Algorithm AS 181: The W-test for Normality. *Applied Statistics* 1995, *44*, 547, DOI: 10.2307/2986146.
[82] Dean, R. B., Dixon, W. J., Simplified Statistics for Small Numbers of Observations. *Anal. Chem.* 1951, *23*, 636–638, DOI: 10.1021/ac60052a025.
[83] Deutsches Institut für Normung, Industrielle Platin-Widerstandsthermometer und Platin-Temperatursensoren (IEC 60751:2008)(DIN EN 60751:2009-05).
[84] Merkel, F. S., Schmuck, C., Schultz, H. J., Scholz, T. A. *et al.*, Research on Gas Hydrate Plug Formation under Pipeline-Like Conditions. *International Journal of Chemical Engineering* 2015, *2015*, 1–5, DOI: 10.1155/2015/214638.
[85] Kemper, S. D., Jährling, K., *Untersuchung des Einflusses verschiedener Rührertypen auf die Gashydratbildung und Analyse der Eignung von Tylose als Inhibitor*. Projektarbeit, Krefeld, 2014.
[86] Hirsch, D., Karner, S., Sieben, M., Volkmer, J., *Projektstudie zur Ermittlung der Induktionszeit der Gashydratbildung unter Zusatz inhibierender Substanzen*. Projektarbeit, Krefeld, 2014.
[87] Lewandowska, K. A., Porsani, N. K., Skibiszewska, S. A., *Inhibition of methane hydrate in pipelines*. Projektarbeit, Krefeld, 2014.
[88] Neufeld, K., Lewandowski, B., *Projektstudie zur Ermittlung der Induktionszeit der Gashydratbildung unter Zusatz inhibierender Substanzen*. Projektarbeit, Krefeld, 2015.
[89] Neufeld, K., *Projektarbeit zur verfahrenstechnischen Betrachtung der Gashydratbildung im Labormaßstab*. Projektarbeit, Krefeld, 2015.

[90] Das, B., Roy, M. N., Hazra, D. K., Densities and viscosities of the binary aqueous mixtures of tetrahydrofuran and 1,2.dimethoxyethane at 298, 308 and 318 K. *Indian Journal of Chemical Technology* 1994, *Vol. 1*, 93–97.
[91] Vauck, Wilhelm R. A, Müller, H. A., *Grundoperationen chemischer Verfahrenstechnik,* 11th edn., Dt. Verl. für Grundstoffindustrie, Stuttgart, 2000.
[92] Jensen, L., Thomsen, K., Solms, N. von, Propane hydrate nucleation: Experimental investigation and correlation. *Chemical Engineering Science* 2008, *63*, 3069–3080, DOI: 10.1016/j.ces.2008.03.006.
[93] TT Technologies, http://www.tttechnologies.com/job_stories/pipe_ramming_stories/ready_for_ramming_murphy.html. Accessed 23 June 2013.
[94] http://www.interconnector.com/PhysicalOps/IUKSystem.htm. Accessed 23 June 2013.
[95] Scholz, T., *Untersuchung zur Bildung von Gashydrat-Plugs unter Pipeline-ähnlichen Bedingungen*. Bachelorarbeit, Krefeld, 2014.
[96] Atkins, P. W., Paula, J. de, *Physikalische Chemie,* 4th edn., Wiley-VCH, Weinheim, 2006.
[97] Dean, J. A., Lange, N. A., *Lange's handbook of chemistry,* 15th edn., McGraw-Hill, New York, 1999.
[98] Scholz, T. A., Wolinski, S., Ingenfeld, S. G., Banczyk, C., *Gashydrate*. Projektarbeit, Krefeld, 2015.
[99] Scholz, T. A., *Entwicklung von Inhibierungskonzepten zur Vermeidung der Bildung von Methanhydraten in pipeline-ähnlichen Systemen*. Masterarbeit, Krefeld, 2016.
[100] Wolinski, S., *Untersuchung der Einflussfaktoren der Induktionszeit bei der Methanhydratbildung unter Pipeline-ähnlichen Bedingungen*. Bachelorarbeit, Krefeld, 2013.
[101] Englezos, P., Kalogerakis, N., Dholabhai, P. D., Bishnoi, P. R., Kinetics of formation of methane and ethane gas hydrates. *Chemical Engineering Science* 1987, *42*, 2647–2658, DOI: 10.1016/0009-2509(87)87015-X.
[102] Englezos, P., Kalogerakis, N., Dholabhai, P. D., Bishnoi, P. R., Kinetics of gas hydrate formation from mixtures of methane and ethane. *Chemical Engineering Science* 1987, *42*, 2659–2666, DOI: 10.1016/0009-2509(87)87016-1.
[103] Takahata, M., Kashiwaya, Y., Ishii, K., Kinetics of Methane Hydrate Formation Catalyzed by Iron Oxide and Carbon under Intense Stirring Conditions. *MATERIALS TRANSACTIONS* 2010, *51*, 727–734, DOI: 10.2320/matertrans.M2009369.
[104] Skovborg, P., Rasmussen, P., A mass transport limited model for the growth of methane and ethane gas hydrates. *Chemical Engineering Science* 1994, *49*, 1131–1143, DOI: 10.1016/0009-2509(94)85085-2.

[105] Helle, H., *Kinetische Messdatenanalyse der Gashydratbildung unter pipelineähnlichen Bedingungen*. Projektarbeit, Krefeld, 2014.
[106] A. Zielesny, *Vorlesung Laborinformatik*, Standort Recklinghausen.
[107] Naderwitz, P., *Vorlesung Physikalische Chemie*, Krefeld.
[108] Steel, C., Naqvi, K. R., Differential method in chemical kinetics. *J. Phys. Chem.* 1991, *95*, 10713–10718, DOI: 10.1021/j100179a037.
[109] Hill, C. G., Root, T. W., *Introduction to Chemical Engineering Kinetics and Reactor Design, 2nd Editi*, John Wiley & Sons, 2014.
[110] Eberhart, J. G., Levin, E., SIMPLIFIED HALF-LIFE METHODS FOR THE ANALYSIS OF KINETIC DATA. *Journal of Chemical Education* 1988.
[111] Levenspiel, O., *Chemical reaction engineering,* 3rd edn., Wiley, New York, 1999.
[112] Cowan, G., *Statistical data analysis*, Clarendon Press; Oxford University Press, Oxford, New York, 1998.
[113] Schlittgen, R., *Einführung in die Statistik: Analyse und Modellierung von Daten,* 12th edn., Oldenbourg, München, 2012.
[114] Blobel, V., Lohrmann, E., *Statistische und numerische Methoden der Datenanalyse*, Teubner, Stuttgart, Leipzig, 1998.
[115] Atkins, P. W., Paula, J. de, *Physikalische Chemie,* 5th edn., Wiley-VCH, Weinheim, 2013.
[116] Wyszogrodzka, M., Haag, R., A Convergent Approach to Biocompatible Polyglycerol “Click” Dendrons for the Synthesis of Modular Core-Shell Architectures and Their Transport Behavior. *Chem. Eur. J.* 2008, *14*, 9202–9214, DOI: 10.1002/chem.200800892.
[117] Haag, R., Stumbé,, Jean-François, Sunder, A., Frey, H. *et al.*, An Approach to Core–Shell-Type Architectures in Hyperbranched Polyglycerols by Selective Chemical Differentiation. *Macromolecules* 2000, *33*, 8158–8166, DOI: 10.1021/ma000831p.
[118] E.W. Lemmon, M.O. McLinden and D.G. Friend, *Thermophysical Properties of Fluid Systems: NIST Chemistry WebBook, NIST Standard Reference Database Number 69*, National Institute of Standards and Technology, Gaithersburg MD, 20899, http://webbook.nist.gov, retreived July 16, 2014.
[119] Krekel, G., *Vorlesung Mechanische Verfahrenstechnik*, Krefeld.
[120] Analysis of drinking water quality, Krefeld, https://www.swk.de/privatkunden/wasser/trinkwasser/analyse-qualitaet. Accessed 19 January 2016.
[121] Thumulla, M., *Inbetriebnahme eines Versuchsreaktors zur Erzeugung von Gashydraten mit Überwachung durch ein Prozessleitsystem*. Bachelorarbeit, Krefeld, SS 2015.

[122] Maaßen, J., *Optimierung der Messdatenaufzeichnung, Implementierung einer Temperaturregelung und Regelkreisoptimierung für einen Laborreaktor im Prozessleitsystem DeltaV*. Projektarbeit, Krefeld, 2016.
[123] HiTec Zang GmbH, Katalogauszug: Laborautomatisierung Hardware, 2015.
[124] Herrling, F., Genauigkeit Temperaturmessung - Presto A40. E-Mail, 2015.
[125] Julabo, AW: Genauigkeit Temperaturmessung - Presto A40. E-Mail, 2015.
[126] Emerson Process Management, DeltaV (TM) M-Series Traditional I/O: DeltaV Product Data Sheet, 2014.

Permalink to cited ACS publication [4]:
http://pubs.acs.org/doi/full/10.1021/acs.energyfuels.6b01795

14 Appendix

Due to the enormous amount of created data during experiments, the appendix is retained in digital form on a storage medium. It includes the following:

- accuracy data sheets of measurements instruments (as reference for the error analysis in chapter 11.3);
- the experimental data (raw data and completed analyses);
- the gas-chromatographic proof for the existence of methanol after a successful coating (see also chapter 8);
- the spectrometric analyses of the custom-tailored inhibitor candidates (see also chapter 10).

14.1 Symbols and abbreviations

14.1.1 Abbreviations

AA	anti-agglomerate
AAS	atomic absorption spectroscopy
AFM	atomic force microscopy
EDX	energy dispersive x-ray spectroscopy
KHI	kinetic hydrate inhibitor
LDHI	low dosage hydrate inhibitor
LT	leakage testing
MD	molecular dynamics (simulation)
OPEX	operational expenditure
s H	hexagonal gas hydrate structure H
s I	cubic gas hydrate structure I
s II	cubic gas hydrate structure II
SEM	scanning electron microscopy
THI	thermodynamic hydrate inhibitor
TOC	total amount of organic carbon

14.1.2 Abbreviated chemical substances

B_2O_3	Diboron trioxide
CH_4	Methane
DGluc	D(+)-Glucose
EG	ethylene glycol
Gly	Glycerol
Ino	myo-Inositol
Iron	Iron(II) sulfate heptahydrate
PEG	Polyethylene glycol
PMMA	poly methyl methacrylate
PVA	Polyvinyl alcohol
PVAc	Polyvinyl acetate
PVP	Polyvinylpyrrolidone

14.1.3 Symbols

a	combined estimated parameter (K^**A_P)	[mol*cm²*s^{-1}]
a	estimation parameter, differential method	[1]
$A_{(g-l)}$	gas-liquid interface area	[cm²]
acc	accuracy	may vary depending on context
a_i	Shapiro-Wilk weighting factor	[1]
A_P	specific surface area of one hydrate cage at constant pressure and stirrer velocity	[cm²]
b	estimation parameter, differential method	[1]
c_w	dissolubility	[g]
c_{w0}	initial concentration of water	[mol*L^{-1}]
d	diameter of stirrer	[m]
d_D	particle diameter	[mm]
η	dynamic viscosity	[Pa*s]
f	fugacity	[bar]
f	fraction (fractional life method)	[1]
f^{1-l}	fraction (in fractional life method)	[1]
$f_{(eq.)}$	equilibrium fugacity	[bar]
f_i^b	fugacity of component i in „bulk“ phase	[bar]
f_i^{eq}	equilibrium fugacity of component i in the liquid at the hydrate interface	[bar]
j	hydration number	[1]
K^*	hydrate formation growth rate constant	[mol*s^{-1}]
k_d	mass transfer coefficient through phase boundary	[mol*s^{-1}]
k_L	mass transfer coefficient through liquid film	[mol*s-1]

k_r	rate constant	[mol*s-1]
l	order of reaction	[1]
m	mass	[g]
M	Agitator torque	[Ncm]
M_{max}	maximum agitator torque during experiment	[Ncm]
n	molar amount of substance	[mole]
N	stirrer frequency	[min-1]
n_0	molar amount in the beginning of an experiment	[mole]
n_e	ending molar amount	[mole]
p	pressure	[bar] or [bar(g)]
$p_{\_nucleation}$	theoretical initial pressure	[bar]
p_0	theoretical initial pressure	[bar]
$(p_{pl}-p_{ind})$	delay pressure	[bar]
p_{1000}	reference pressure after 1000 minutes experimental time	[bar(g)]
$\Delta p_{\_total}$	total pressure drop	[bar]
p_e	ending pressure	[bar]
ϕ	fugacity coefficient	[1]
p_{ind}	induction pressure	[bar(g)]
p_{pl}	plug formation pressure	[bar(g)]
Q	Dixon-Q test statistic	[1]
r	reaction rate	may vary depending on context
R	universal gas constant	$[J*mol^{-1}*K^{-1}]$
R^2	coefficient of determination	[1]
Re_{cr}	critical Reynolds number	[1]
Re_R	modified Reynolds number (for stirring processes)	[1]
Re_{turb}	turbulent Reynolds number	[1]
RG	reaction rate	may vary depending on context
ρ	density	$[kg*m^{-3}]$ or $[g*cm^{-3}]$
s	standard deviation	may vary depending on context
s [%]	relative standard deviation	[%]
t	time	[min]
T	temperature	[K] or [°C]
t_{ind}	induction time	[min]
t_{pl}	plug formation time	[min]
$(t_{ind}-t_{pl})$	delay time	[min]
t_{St}	stirrer switch-off time	[min]
Δt	time range for which calculation was done (fractional life method)	[min]
V	volume	[m³] or [L]
v	coefficient of variation	may vary depending on context
V_m	molar volume	$[m^3*mol^{-1}]$ or $[L*mol^{-1}]$
$V_{m,ideal}$	molar volume of an ideal gas	$[m^3*mol^{-1}]$ or $[L*mol^{-1}]$

W	Shapiro-Wilk test statistic value	[1]
x_b	bulk liquid mole fraction of the component	[1]
x_i	experimental value in Shapiro-Wilk test	may vary depending on context
x_{int}	initial bulk liquid mole fraction of the component	[1]
$\bar{x}$	arithmetic mean	may vary depending on context
Z	compressibility factor	[1]
z_i	coordination number	[1]
δ	conductivity	[$\mu S*cm^{-1}$]
λ_1	dissolubility coefficient (according to Lange)	[$g*(100\ g\ water)^{-1}*bar^{-1}$]
% wt.	percent of weight	[%]

14.2 List of publications

Peer-reviewed publications

1. Merkel, F. S., Schmuck, C., Schultz, H. J., Investigation of the influence of hydroxyl groups on gas hydrate formation at pipeline-like conditions. Energy Fuels 2016, DOI: 10.1021/acs.energyfuels.6b01795.
2. Merkel, F. S., Schmuck, C., Schultz, H. J., Scholz, T. A. et al., Research on Gas Hydrate Plug Formation under Pipeline-Like Conditions. International Journal of Chemical Engineering 2015, 2015, 1–5, DOI: 10.1155/2015/214638.
3. Merkel, F. S., Schmuck, C., Schultz, H. J.; Research on inhibition of gas hydrate formation in pipelines and armatures using surface active substances; The Proceedings of the Chemistry in the Oil Industry XIV symposium; 02.-04.11.2015, Manchester, United Kingdom
4. Merkel, F. S., Schultz, H. J.; CO_2-sequestration in form of gas hydrates with simultaneous methane extraction; Journal of Energy Challenges and mechanics (ISSN 2056-9386); submitted on 2015-06-26
5. Merkel, F. S., Schultz, H. J., Methane Extraction from Natural Gas Hydrate Reservoirs with Simultaneous Storage of Carbon Dioxide. Chemie Ingenieur Technik 2015, 475–483, DOI: 10.1002/cite.201300164.
6. H. J. Schultz, F. S. Merkel, V. Bliem; Gas hydrates: Feasibility of CO2-sequestration and related natural gas production; gas for energy; 02-2013; ISSN 2192-158X; S. 64-70

Other publications

1. Merkel, F. S., Schultz, H. J., Inhibierung der Gashydratbildung in Rohrleitungen und Armaturen durch Nutzung oberflächenaktiver Materialien - InHydRo. Chemie Ingenieur Technik 2014, 86, 1476, DOI: 10.1002/cite.201450127.

Posters and presentations

Presentations

1. Research on inhibition of gas hydrate formation in pipelines and armatures using surface active substances; Presentation at the Chemistry in the Oil Industry XIV Symposium, 02nd-04th November 2015, Manchester, England, United Kingdom
2. CO2-sequestration in form of gas hydrates with simultaneous methane extraction; Presentation at the 3rd International Symposium on Energy Challenges and Mechanics, 07th-09th July 2015, Aberdeen, Scotland, United Kingdom
3. „Research on inhibition of gas hydrate formation in pipelines and armatures using surface active substances“ - “InHydRo” - "2nd presentation"; Merkel, F. S.; Presentation at workgroup Schmuck, 25.03.2015, University Duisburg-Essen, Essen, Germany
4. Merkel, F. S.; InHydRo - Untersuchungen zur Inhibierung der Gashydratbildung in Rohrleitungen und Armaturen durch Nutzung oberflächenaktiver Materialien; Presentation at "Promovendentag #2 der HS Niederrhein", Promotionskolleg HSNR, 10.11.2014, HSNR, Krefeld, Germany
5. InHydRo – Untersuchungen zur Inhibierung der Gashydratbildung in Rohrleitungen und Armaturen durch Nutzung oberflächenaktiver Materialien; Poster presentation at "ProcessNet-Jahrestagung und 31. DECHEMA-Jahrestagung der Biotechnologen 2014", 30.09.2014, Aachen, Germany
6. „Research on inhibition of gas hydrate formation in pipelines and armatures using surface active substances “ - “InHydRo”; Merkel, F. S.; Presentation at workgroup Schmuck, 19.02.2015, University Duisburg-Essen, Essen, GermanyText

Posters

1. Kinetische Betrachtung der Gashydratbildung unter pipelineähnlichen Bedingungen; Merkel, F. S., Schultz, H. J.; Poster published at "ProcessNet Jahrestreffen der Fachgruppen Computational Fluid Dynamics und Mehrphasenströmungen", 19.-20.03.2015, Lüneburg, Germany
2. Untersuchungen zur Eignung funktionalisierter Oberflächen als Inhibitoren für die Gashydratbildung; Merkel, F. S., Schultz, H. J.; Poster published at "Innovative Werkstoffe in Wissenschaft und Praxis", 06.11.2014, HSNR / ILOC, Krefeld, Germany
3. InHydRo - Methodenentwicklung zur Bewertung der Inhibierungseignung oberflächenaktiver Substanzen in Bezug auf die Gashydratbildung; Merkel, F. S.,

Schmuck, C., Schultz, H. J.; Poster published at "Promovendentag #2 der HS Niederrhein", 10.11.2014, HSNR/ILOC, Krefeld, Germany

4. InHydRo - Untersuchungen zur Inhibierung der Gashydratbildung in Rohrleitungen und Armaturen durch Nutzung oberflächenaktiver Materialien; Merkel, F. S., Schultz, H. J.; Poster published at "ProcessNet-Jahrestagung und 31. DECHEMA-Jahrestagung der Biotechnologen 2014", 30.09.-02.10.2014, Aachen, Germany
5. „InHydRo“ - Untersuchungen zur Inhibierung der Gashydratbildung in Rohrleitungen und Armaturen durch Nutzung oberflächenaktiver Materialien; Merkel, F. S., Schmuck, C., Schultz, H. J.; Poster published at "Promovendentag #1 der HS Niederrhein", 07.11.2013, HSNR/ILOC, Krefeld, Germany
6. „InHydRo“ - Untersuchungen zur Inhibierung der Gashydratbildung in Rohrleitungen und Armaturen durch Nutzung oberflächenaktiver Materialien; Merkel, F. S., Schmuck, C., Schultz, H. J.; Poster published at "Auftaktveranstaltung Promotionskolleg der HS Niederrhein", 06.11.2013, HSNR/ILOC, Mönchengladbach, Germany
7. Influence of weather conditions on the heat transport of corrosion protected transformer tanks; Schultz, H. J., Bliem, V., Merkel, F. S., Loos, W.-D., Cox, K., Dornbusch, M.; Poster published at "Messe Coil Winding", 24.06.-26.06.2014, Berlin, Germany
8. Einfluss von Witterungsbedingungen auf den Wärmetransport korrosionsschutzbeschichteter Trafo-Gehäuse; Schultz, H. J., Bliem, V., Merkel, F. S., Loos, W.-D., Cox, K., Dornbusch, M.; Poster published at "Messe Coil Winding", 24.06.-26.06.2014, Berlin, Germany
9. Investigation of corrosion protective coatings for transformer tanks and calculation of conductive heat transport of coated metal surfaces; Schultz, H. J., Bliem, V., Merkel, F. S., Loos, W.-D., Cox, K., Dornbusch, M.; Poster published at "Messe Coil Winding", 24.06.-26.06.2014, Berlin, Germany
10. Untersuchung von Korrosionsschutzbeschichtungen für Transformatoren-Gehäuse und Simulation der Wärmeleitung von beschichteten Metalloberflächen; Schultz, H. J., Bliem, V., Merkel, F. S., Loos, W.-D., Cox, K., Dornbusch, M.; Poster published at ((Messe Coil Winding, 24.06.-26.06.2014, Berlin, Germany ?))
11. Einfluss von Oberflächenphänomenen auf die Speicherung/ Deponierung von CO 2 in Form von Gashydraten; Schultz, H. J.; Bliem, V.; Merkel, F. S., Poster published at "Chemcologne 2012", 28.11.2012, HSNR/ILOC, Krefeld, Germany
12. Untersuchung des Einflusses von Oberflächenphänomenen auf die kinetische Inhibierung der Gashydratbildung; Schultz, H. J.; Bliem, V.; Merkel, F. S., Poster published at "Chemcologne 2012", 28.11.2012, HSNR/ILOC, Krefeld, Germany

14.3 Curriculum vitae

Der Lebenslauf ist in der Online-Version aus Gründen des Datenschutzes nicht enthalten.

14.4 Declaration

Hiermit versichere ich, dass ich die vorliegende Arbeit mit dem Titel

„Research on inhibition of gas hydrate formation in pipelines and armatures using surface active substances”

selbst verfasst und keine außer den angegebenen Hilfsmitteln und Quellen benutzt habe, und dass die Arbeit in dieser oder ähnlicher Form noch bei keiner anderen Universität eingereicht wurde.

Essen, im Monat Dezember 2016

Florian Stephan Merkel

14.5 Acknowledgement

Mein besonderer Dank gilt Herrn Prof. Dr.-Ing. H. J. Schultz, sowohl für die Bereitschaft, diese Arbeit zu betreuen, als auch für die Anregung des Themas sowie die Freiheit, eigene Ideen zu verwirklichen und dennoch nie ohne wissenschaftlichen Rat dazustehen.

Ebenfalls möchte ich Herrn Prof. Dr. C. Schmuck für die Bereitschaft danken, diese Arbeit zu betreuen, für Geduld und stets wertvolle Ratschläge sowie für die Möglichkeit, die Laboratorien des Instituts für Supramolekulare Chemie zu nutzen.

Herrn Prof. Dr. M. Ulbricht danke ich für die freundliche Übernahme des Disputationsvorsitzes. Weiterhin gilt mein Dank Herrn Prof. Dr. G. Krekel für ein jederzeit offenes Ohr bei Problemen und stets wertvolle Tipps ingenieurstechnischer und chemischer Natur.

Meinen Kollegen D. Kliem, Dr. V. Bliem, H. Sprünken, K. Jährling, A. Stefan, B. Luczak, S. Wolinski, B. Lewandowski, C. Tillmann sowie allen anderen gilt mein Dank für gute Ratschläge und jedwede Unterstützung, ob in experimenteller oder anderer Hinsicht. Des Weiteren gilt mein Dank allen, die diese Arbeit in experimenteller Hinsicht unterstützt haben, unter anderem T. Scholz, H. Helle, S. Kemper, K. Neufeld, D. Hirsch und M. Thumulla.
Frau E. Verheggen gilt mein Dank für wertvolle Unterstützung bei der Synthese der Dendrimere, sowie für die Einführung in den Arbeitskreis Schmuck. Dem Arbeitskreis Schmuck danke ich für die freundliche Aufnahme sowie interessante Konversation.

Meinen Eltern, die mir mein Studium überhaupt erst ermöglicht haben und die immer für mich da waren und an mich geglaubt haben, möchte ich von ganzem Herzen danken. Meinem Bruder danke ich dafür, dass er immer die richtigen Worte fand, mich in schweren Zeiten zu motivieren und für die Hilfe, an mich selbst zu glauben. Allen weiteren Familienmitgliedern und Freunden möchte ich ebenfalls für aufmerksames Zuhören, motivierende Worte und weitere Unterstützung danken.

Allen anderen, die für mich da waren und die an dieser Stelle nicht namentlich erwähnt sind, danke ich ebenfalls von Herzen. Ihr wisst, dass ihr gemeint seid.

Zu guter Letzt danke ich E. S. für die Liebe, das Glück und die Freude, mit der du mein Leben immer wieder aufs Neue bereicherst.